



REPUBLIC OF IRAQ
**MINISTRY OF HIGHER EDUCATION AND SCIENTIFIC
RESEARCH**
AL-FURAT AL-AWSAT TECHNICAL UNIVERSITY
ENGINEERING TECHNICAL COLLEGE- NAJAF

Enhancement of Microstrip Antenna using Fractal Metasurfaces

A THESIS

**SUBMITTED TO THE COMMUNICATION TECHNIQUES
ENGINEERING DEPARTMENT**

**IN PARTIAL FULFILLMENT OF THE REQUIREMENTS FOR
THE TECHNICAL MASTER DEGREE**

IN

COMMUNICATION ENGINEERING

BY

Noor Fadhel Habib

(B. Sc. in Communication Technologies Engineering)

Supervised by

Assist. Prof. Dr. Ahmed Ghanim Wadday

September 2020

بِسْمِ اللَّهِ الرَّحْمَنِ الرَّحِيمِ

عَلَّمَ الْقُرْآنَ
وَهُوَ كَرِيمٌ
۱۴۲۲

Dedication

*To them who left me very early...I miss them at every moment
... my compassionate father and my beloved mother.*

To the soul of the martyr... my older brother

*To all the doctors who done exert so much and supported me
medically and morally so that I could stand again.*

To them, I dedicate my humble dream

Acknowledgements

In the name of ALLAH, the Most Gracious, and the Most Merciful for giving me the determination and will to complete this research work.

*My sincere thanks and greatest gratitude are expressed to my supervisor, **Dr. Ahmed Ghanim Wadday**, for his patience, guidance, fruitful discussions in support of this research.*

*A special word of thanks to **Dr. Ghufraan Mahdi Hatem** for her unlimited scientific support and continuous encouragement throughout my research.*

*I would like to extend my highest gratitude and thanks to **Dr. Nasr Nomas Al-Khafaji** for his generous support, his time, effort, that helped me to complete this research work.*

Finally, I would like to thank my dear brothers and my sister my companions in the most difficult times.

Supervisor Certification

I certify that this thesis titled " **Enhancement of Microstrip Antenna using Fractal Metasurfaces**" which is being submitted by **Noor Fadhel Habib** was prepared under my supervision at Techniques Engineering Department, Engineering Technical College-Najaf, AL-Furat Al-Awsat Technical University, as a partial fulfillment of the requirements for the degree of Master of Technical in Communication Engineering.

Signature:

Name: **Assist. Prof. Dr. Ahmed Ghanim Wadday**

(Supervisor)

Date: / / 2020

In view of the available recommendation, I/we forward this thesis for debate by the examining committee.

Signature:

Name: **Dr. Salim Muhsen Wadi**

(Head of comm. Tech. Eng. Dept.)

Date: / / 2020

Committee Report

We certify that we have read this thesis titled **Enhancement of Microstrip Antenna using Fractal Metasurfaces** " which is being submitted by **Noor Fadhel Habib** and as Examining Committee, examined the student in its contents. In our opinion, the thesis is adequate for award of degree of Master of Technical in Communication Engineering.

Signature:

Name:

Supervisor

Date: / / 2020

Signature:

Name:

(Member)
Date: / / 2020

Signature:

Name:

(Member)
Date: / / 2020

Signature:

Name:

(Chairman)

Date: / / 2020

Approval of the Engineering Technical College- Najaf

Signature:

Name:

Dean of Engineering Technical College-
Najaf

Date: / / 2020

Abstract

A metasurface (MS) is a 2-dimension type of metamaterial (MTM) constructed from periodic structures but with low weight. Metasurface offers exceptional properties such as negative refractive index resulting from a combination of negative permittivity and negative permeability at the same frequency. Materials with these properties are not available in nature but can be artificially engineered.

In this thesis, four antenna designs and three fractal metasurface unit-cells are designed. The dispersion parameters of unit cells are studied employing CST microwave studio package. These designs show the behavior of left-handed (LH) material.

The study of the effect of applying the metasurface layer on the antenna and its effects on the antenna performance can be summarized in three aspects: gain improvement, bandwidth increment and size reduction. A meta-cover of the fractal unit-cells is placed over the proposed designs. The circular fractal shape design is slotted on patch with MS plate offered dual-band frequencies and the results have showed the gain enhanced to reach 8dB. The fractional bandwidth is 3.59%. The second design is modified cross with MS has enhanced the gain by 6dB and the fractional bandwidth is 4.655%. A third design is Minkowski fractal slotted on antenna patch and provides good enhancement in the bandwidth by 32.11% and the gain is improved approximately 3dB. The fourth design is made of the circular fractal shape slotted on the ground plane which achieves multiband design with gain of 6dB and compact size. Finally, this thesis presents the interesting new solutions for high gain and low cost antennas which are very simple compared to arrays for many reasons such as element matching, feeding circuit complexity, large area and high cost.

List of Contents

Subject	Page No.
Acknowledgements	i
Supervisor Certification	ii
Committee Report	iii
Abstract	iv
List of Figures	ix
List of Tables	xiv
List of symbols	xv
List of Abbreviations	xvi
Chapter One: Introduction and Literature Survey	
1-1 Introduction	1
1-2 Some Types of the Antennas	1
1-2-1 Wire Antennas	1
1-2-2 Aperture Antennas	1
1-2-3 Array Antennas	1
1-2-4 Microstrip Antennas	2
1-3 Literature survey	3
1-4 Motivation	7
1-5 Problem statement	8
1-6 Objectives	8
1-7 Contributions	9
1-8 Thesis Layout	9

Chapter Two: The Theory of Fractal Antennas and Metasurface Concepts	
2-1 What is A fractal	16
2-2 Fractal Properties	17
2-2-1 Space-Filling	17
2-2-2 Self-Similarity	18
2-2-3 Fractal Dimensions	19
2-3 Types of Fractal Antennas	19
2-3-1 Koch curve	19
2-3-2 Sierpinski Triangle	20
2-3-3 Sierpinski Carpet	21
2-3-4 Minkowski Fractal	21
2-3-5 Circular Slot Fractal Antenna	22
2-3-6 Cross Shape Fractal Antenna	22
2-4 Introduction to Metasurface	23
2-5 What is Metasurface	23
2-6 Negative Refractive Index	26
2-7 The Important Equations to Calculate ϵ, μ, n	29
2-8 The Usage of Metasurface in Designing Antennas	30
2-8-1 The Radiators Antenna above The Metasurface	30
2-8-2 The Radiators of Antenna Established within The Structure of Metasurface	30
Chapter Three: Design Configuration	
3-1 Introduction	32

3-2 First Proposed Design: Circular Fractal Slot Antenna without and with Metasurface for X and Ku band Applications	33
3-3 Second Proposed Design: Modified Cross Fractal Antenna with MS for X-band Applications	37
3-4 Third Proposed Design: Minkowski Fractal Slot Antenna with Metasurface	40
3.5 Fourth Proposed Design: Multiband Compact Microstrip Circular Slot Fractal MS Antenna for C and S-band Applications	44
Chapter Four: Results and Discussions	
4-1 Introduction	47
4-2 The First Design: The Characteristics of Circular Fractal Slot Antenna without and with Metasurface (CFSMS) for X and Ku - Band Applications.	47
4-2-1 The input reflection coefficient of Circular Fractal Slot Antenna without Metasurface	47
4-2-2 The Gain and Directivity of Circular Fractal Slot Antenna without MS	48
4-2-3 The input reflection coefficient of Circular Fractal Slot Antenna with MS	49
4-2-4 The gain and directivity of (CFSMS) circular fractal slot with MS antenna	50
4-3 The Second Design: The Characteristics of Modified Cross Fractal Shape without and with MS Antenna (MCFMS) for X - Band Applications	59

4-3-1 The input reflection coefficient of the Modified Cross Fractal Shape without MS.	59
4-3-2 The Gain and Directivity of Modified Cross Fractal Shape without MS	60
4-3-3 The input reflection coefficient of the Modified Cross Fractal Shape with Metasurface	61
4-3-4 The Gain and Directivity of Modified Cross Shape Fractal Antenna with MS	62
4-4 The Third Design: The Characteristics of Minkowski Fractal Slot Antenna without and with Metasurface (MFSAMS) for C-Band Applications	70
4-4-1 The input reflection coefficient of Minkowski Fractal Slot antenna without MS	70
4-4-2 The Gain and Directivity of Fractal Shaped Minkowski Slotted without MS	70
4-4-3 The Input Reflection Coefficient of Minkowski Fractal Slot Antenna with MS	71
4-4-4 The Gain and Directivity of Minkowski Fractal Slot Antenna with MS	72
4-5 The Fourth Design: The Characteristics Multiband Compact Microstrip Circular Slot Fractal MS Antenna (MCMCSFMS) for C and S – Band Applications.	80
4-5-1 The input reflection coefficient of Multiband Compact Microstrip Circular Slot Fractal MS Antenna	80

4-5-2 The Gain and Directivity of Fractal Shaped Circular Slot Antenna with MS	81
Chapter Five: Conclusion and Future Works	
5-1 Conclusion	88
5-2 Future Works	90
References	91
Appendix	97

List of Figures

Figures	Page No.
Fig.1.1: Two types of microstrip antenna rectangular and circular	2
Fig.2.1: Natural fractal forms	16
Fig.2.2: Types of mathematical geometry of the fractal antenna (a) Sierpinski- Gasket, (b) Sierpinski- Carpet, (c) Koch- Curve, (d)Minkowski – curve	17
Fig.2.3: Model of space-filling property (a) Third iteration of the Koch curve (b) Third iteration of Minkowski fractal	18
Fig.2.4: Self-similarity property (a) Third iterations of Sierpinski gasket (b) Third iteration of Sierpinski carpet	18
Fig.2.5: The first four steps in the design of the Koch curve	20
Fig.2.6: The first four steps in the design of the Sierpinski gasket	20
Fig.2.7: Design steps of the Sierpinski carpet	21
Fig.2.8: Design steps of Minkowski fractal antenna	22
Fig.2.9: Three steps of designing circular slot fractal antenna	22

Fig.2.10: Design steps of cross shape (a) first iteration (b) second iteration	23
Fig.2.11: Electric – magnetic- surface wave and Poynting vectors of an electromagnetic wave in right-handed and left-handed mediums	24
Fig.2.12: Collection of thin wires and SRR to shape DNG MTM	25
Fig.2.13: The four possible areas of materials and the directions of wave reflection or refraction according to permittivity and permeability signs	25
Fig.2.14: Materials with near-zero refractive index	27
Fig.2.15: The scheme of the Snell's law of normal medium when $n_1 > 0$ and LH medium when $n_2 < 0$	28
Fig.2.16: The antenna geometry with radiator above the metasurface layer	30
Fig.2.17: Side view of the antenna geometry	31
Fig.3.1: Circular fractal slot antenna	33
Fig.3.2: Design circular slot fractal shape a (first iteration) b (two iterations) c (three iterations)	34
Fig.3.3: Design of metasurface plate (a) front view (3×3) unit cell (b) front view (5×5) unit cell (c) side view of the 3×3-unit cell (d) side view of the 5×5-unit cell	33
Fig.3.4: Periodic setup of the one unit cell	34
Fig.3.5: Design modified cross fractal shape	36

Fig.3.6: (a) (4×4) MS layer (b) (5×5) unit cells (c) the dimensions of single cell	37
Fig.3.7: Setup of periodic unit cell using the CST	37
Fig.3.8: Design steps of Minkowski slot fractal shape	39
Fig.3.9: a ((6×6) MS layer) b (the dimension of a single cell)	40
Fig.3.10: (a) 3×3 (b) 4×4 (c)5×5 (d) 6×6 unit cells	40
Fig.3.11: The front view when placed the antenna above the MS layer	41
Fig.3.12: Double layers of MS adding to the proposed antenna	41
Fig.3.13: Double square closed ring of metasurface	42
Fig.3.14: The design steps of the proposed antenna at the front view a (initial state) b (first iteration) c (second iteration) d (third iteration) e (back view)	44
Fig.4.1: The input reflection coefficient of a single circular fractal	48
Fig.4.2: The result of the gain at the frequency (11.18) GHz	48
Fig.4.3: The result of the directivity at the frequency (11.18) GHz	49
Fig.4.4: The input reflection coefficient when using (3×3) order of MS	50
Fig.4.5: The relationship between gain and frequency after adding (3×3) order of MS	50
Fig.4.6: The results of directivity (a) at the (11.2) GHz (b) at the (12.2) GHz	51

Fig.4.7: The input reflection coefficient when used (5×5) cells of MS	52
Fig.4.8: Demonstrates the relationship between gain and frequency when using (5×5) order of MS	52
Fig.4.9: The results of directivity (a) at the (11.14) GHz (b) at the frequency (12.3) GHz	53
Fig.4.10: The input reflection coefficient at each state	53
Fig.4.11: The gain at each gap	54
Fig.4.12: The current distribution a (at 11.4 GHz) b (at 12.3 GHz) c (5×5 MS at 11.14 GHz) d (5×5 MS at 12.3 GHz)	54
Fig.4.13: Radiation patterns of the electric field of the proposed antenna (a) at the (11.14) GHz (b) (at 12.3) GHz	55
Fig.4.14: The negative values of permittivity at the center frequencies.	57
Fig.4.15: The negative values of permeability at the resonance frequencies	57
Fig.4.16: The negative refraction index at the center frequencies	57
Fig.4.17: The input reflection coefficient of modified cross fractal antenna	60
Fig.4.18: Simulated values of (a) The gain at 8.77 GHz, (b) The directivity at 8.77 GHz	60
Fig.4.19: The states of simulated input reflection coefficient	62

Fig.4.20: The gain over the frequency with different numbers of unit cells	63
Fig.4.21: The parametric study to the distance between cells	63
Fig.4.22: The relation between gain and frequency at each distance	64
Fig.4.23: The current distribution at the center frequency 8.9 GHz (a) single fractal without MS (b) the current distribution on the unit cells of MS	64
Fig.4.24: The radiation pattern at the center frequency (a) (x-z) plane (b) (y-z) plane	65
Fig.4.25: The dispersion parameters of MS (a) the real part of ϵ (b) the real part of μ (c) the real part of n	66
Fig.4.26: The input reflection coefficient of the Minkowski fractal slot antenna without MS	70
Fig.4.27: The gain and directivity (a) The gain at (5.1) GHz (b) The directivity at (5.1) GHz	71
Fig.4.28: The input reflection coefficient when adding MS to the proposed antenna	72
Fig.4.29; The gain of the proposed antenna	72
Fig.4.30: The directivity at the (5.25) GHz	73
Fig.4.31: The simulated input reflection coefficient when placing the radiator part above the MS	73
Fig.4.32: The relationship between the gain and frequency when placed the radiator part above MS	74

Fig.4.33: The gain over frequency when using double layers of MS	74
Fig.4.34: The current distribution before and after MS (a) before adding MS (b) after adding MS	75
Fig.4.35: The radiation pattern of the antenna at (5.25) GHz (a) (x-z) plane (b) (y-z) plane	76
Fig.4.36: The permittivity response	77
Fig.4.37: The permeability response	77
Fig.4.38: The refractive index response	77
Fig.4.39: The input reflection coefficient of the proposed antenna at each state	80
Fig.4.40: The 3D values of gain at a (2.62) GHz b (3.92) GHz c (5.92)GHz	81
Fig.4.41: The 3D simulated values of directivity at a (2.62) GHz b (3.92) GHz c (5.92) GHz	82
Fig.4.42: The input reflection coefficient for different widths of the feeding line	83
Fig.4.43: The input reflection coefficient at each thickness	83
Fig.4.44: The 2D radiation patterns of the proposed antenna at a (2.6) GHz b (3.9) GHz c (5.7) GHz	84
Fig.4.45: The current distribution at each frequency a (2.6) GHz b (3.9) GHz c (5.7) GHz	85

List of Tables

Table Title	Page No.
Table 1.1 References of fractal antenna designs associated with metasurface from 2008-2020	10

Table 3.1 Dimensions of Circular Fractal Slot Antenna with MS	36
Table 3.2: The Dimensions of the Modified Cross Fractal Shape with Metasurface	38
Table 3.3: The Dimensions of the Minkowski Slotted Patch Fractal Shaped with Metasurface Antenna	42
Table 3.4: The Dimensions of the Proposed Antenna	45
Table 4.1: Comparison between results at three cases	58
Table 4.2: Present the comparison of all results of the proposed antenna	67
Table 4.3: Comparison between the proposed antenna at four cases	78
Table 4.4: The comparison between (MCMCSFMS) and other References	86
Table 4.5: The comparison among all results obtained from the proposed designs	86

List of Symbols

μ	Permeability of medium (H/m)
D	Directivity (dimensionless quantity)
E	Electric field intensity (V/m)
E total	Total antenna efficiency
ECD	Conduction and dielectric efficiency
er	Reflection efficiency

FD	Fractal dimension
G	Gain (dimensionless quantity)
H	Magnetic field intensity (A/m)
K	Wave vector
N	Number of self-similar objects
n	Refractive index
Pin	Input power (Watt)
Prad	Radiated total power (Watt)
r	Decrease factor
S11	Input reflection coefficient
S21	Transmission coefficient
U	Radiation intensity (Watt/unit solid angle)
Ui	The radiation intensity of the isotropic source
Zin	Input impedance (Ω)
λ	the wavelength of the radiated electromagnetic energy
ϵ	The permittivity of medium (F/m)

List of Abbreviations

Abbreviation	Definition
BW	Bandwidth
DNG	Double negative medium
DPS	Double positive medium
EBG	Electromagnetic Band-Gap

EM	Electromagnetic wave
ENG	Epsilon negative medium
FR-4	Flame resistant 4
FSS	Frequency selective surface
HISs	High Impedance Surfaces
IEEE	Institute of electrical and electronics engineers
LH	Left-handed
LHM	Left-handed material
MNG	Mu negative medium
MS	Metasurface
MTM	Metamaterial
NZI	Near-zero refractive index
PEC	Perfect electric conductor
PMC	Perfect magnetic conductor
RISs	Reactive Impedance Surfaces
SNG	Single negative medium
SRR	Split ring resonator

CHAPTER ONE

INTRODUCTION AND LITERATURE SURVEY

1.1 Introduction

In all wireless telecommunications systems antennas are indispensable components. They are considered as a link between free space and wireless devices. Several limitations accompany antennas like the operation single frequency, low gain and directivity, low efficiency and large physical size.

1.2 Some Types of the Antennas

1.2.1 Wire Antennas

Wire antennas are familiar to the layman because they are seen virtually everywhere on automobiles, buildings, ships, aircraft, spacecraft, and so on. There are various shapes of wire antennas such as a straight wire (dipole), loop, and helix [1].

1.2.2 Aperture Antennas

Aperture antennas may be more familiar to the layman today than in the past because of the increasing demand for more sophisticated forms of antennas and the utilization of higher frequencies. Antennas of this type are very useful for aircraft and spacecraft applications, because they can be very conveniently flush-mounted on the skin of the aircraft or spacecraft.

1.2.3 Array Antennas

Many applications require radiation characteristics that may not be achievable by a single element. It may, however, be possible that an aggregate of radiating elements in an electrical and geometrical arrangement (an array) will result in the desired radiation characteristics. The arrangement of the array may be such that the radiation from the elements adds up to give a radiation maximum in a particular direction or directions, minimum in others, or otherwise as desired.

1.2.4 Microstrip Antennas

The microstrip antenna is one kind of these antennas and it is the most popular type of printed antennas. It can be used in spacecrafts, aircrafts, missile applications and satellites, because of its small size, lightweight, low cost and easy installation. The major drawbacks of microstrip antennas are low power, narrow bandwidth, poor scan performance and poor polarization purity [1]. Figure 1.1 shows two types of the microstrip antenna.

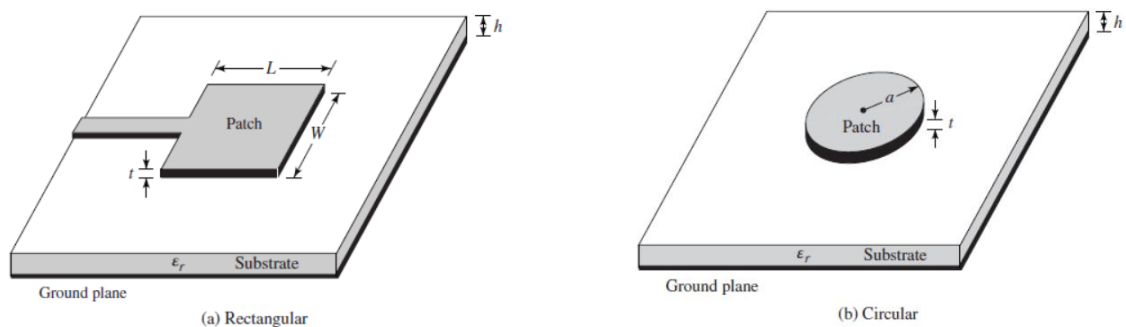


Fig.1.1: Two types of microstrip antenna rectangular and circular [1]

Many techniques have been used to overcome these limitations, including the technique of fractal shapes. This technique has Non-integer dimensions that are different from conventional geometry. The fractal curves have three properties: self-similarity, space-filling and fractal dimension. The property of self-similarity aids to design fractal antenna which are multiband structures. The property of space-filling can be applied to reduce size of the antennas while the property of fractal dimension is widely used to distinguish between the Euclidean and fractal geometries [2] [3].

The second technique that has been used to provide unique properties is the metasurface technology, where this branch is known as metasurface antennas if it is combining with antenna design. The need for designing this type of antennas has raised due to its the radiation characteristics that encourage to be used in many applications [4].

Metamaterials have been the aim of extensive studies over the last two decades for their extraordinary electromagnetic characteristics. They are artificial materials constructed by a periodic arrangement of dielectric or metallic inclusions and it has high flexibility for synthesizing their optical and electromagnetic properties like an effective refractive index according to designer desires [5].

Metasurfaces are a 2-dimensional type of metamaterial, consisting of the periodic arrangement of sub-wavelength scatters. The metasurface is better when compared with metamaterial because it offers advantages such as small physical size and low loss. Since they are constructed from unit cells, repeating themselves in space with smaller than a quarter wavelength, they can be treated as a homogenous material which has effective permittivity and effective permeability [6].

Metasurface has properties not found in nature such as negative permittivity, negative permeability and negative refraction index [7][8]. Metasurfaces can be classified into three types including "Electromagnetic Band-Gap (EBGs) structures, Reactive Impedance Surfaces (RISs), and High Impedance Surfaces (HISs) or Artificial Magnetic Conductors (AMCs) [9]".

1.3 Literature Survey

Much previous work on an enhancement of antennas properties based on metasurface has been published. They are summarized as following:

- **In 2008, Vesna Crnojevic-Bengin, et, al** [10] proposed complementary split-ring resonators (CSRRs) are typically used as negative-permittivity particles in microstrip left-handed structures. It is shown that the application of fractal geometries results in significant miniaturization of the metamaterial unit cell in comparison with conventional and equivalent meander structures. When used in the design of left-handed transmission lines, fractal

complementary split rings improve frequency selectivity in the upper transition band when compared to other nonfractal topologies.

- **In 2012, Riad Yahiaoui, et, al** [11] proposed metasurface design and investigation to enhance the directivity of the microstrip patch antenna by using metasurface as partially reflecting surfaces at microwave frequencies, where two layers of the frequency selective surfaces were used and separated by a small gap.
- **In 2013, He-Xiu Xu, et.al** [12] suggested a design of superlens inspired from fractal geometry based on the concept of Left-Handed material (LHM) to overcome the defects in the lenses. By combining fractal geometry with a concept of Left-Handed material super-three-dimensional lenses were obtained.
- **In 2013, Yongjiu Li, et.al** [13] discussed a design consisting of several layers, where the fractal patches in the upper layers are inductive and fractal slots in the lower layer (on the ground) give a capacitance. The substrate (thin dielectric layer) is considered as a transformer and produces resonant modes. The use of Minkowski fractal in the design of frequency selective surface (FSS) for miniaturization purpose is proposed.
- **In 2013, He-Xiu Xu, et, al** [14] studied combining between the metasurface and meta-resonators that possess space-filling a feature to achieve circular polarization with compact size and a single feed. The artificial metasurface is designed by a slot-loaded on a patch to provide the magnetic response for enhancing antenna performances and miniaturization. Complementary crossbar fractal tree slot (CCFT) and three-turn complementary spiral resonators (TCSRs) with the same gap are used as meta-resonators to make the waves propagating from antennas with Circular Polarization (CP) and to reduce the size of antennas.
- **In 2014, Tanan Hongnara, et, al** [15] studied characteristics of metasurface which consists of the closed ring resonator and fractal fishnet structure. The

fractal fishnet structure uses Minkowski fractal geometry for miniaturization. They have also studied a mechanism to reduce resonance frequency by increasing the number of iterations.

- **In 2015 T. Cai, et, al** [16] proposed a 2D fractal metasurface design to reduce the antenna size and to obtain circular polarization. The shape of the fractal is Wunderlich Reactive Impedance Surface (WRIS) and is implemented to decrease a thickness of the substrate layer without deteriorating the electromagnetic properties. To reduce the antenna size and to make the wave polarization circular, they have used the aperture resonator, Hilbert – Complementary Singular Ring Resonator (HCSRR) and complementary three transitions snail resonator.
- **In 2016 Tanan Hongnara, et, al** [17] suggested fractal design with metasurface which has contradictory rays and can radiate in the forward direction or inversely direction by placing the radiating element correctly according to the metasurface. An array of Minkowski fractal shapes are used in square closed ring resonators (SCRRs) to create metasurface. The main purpose of using the fractal technique is to reduce the size of the unit cell and to get the multiband operation.
- **In 2017 Roman Kubacki, et, al** [18] offered a microstrip antenna depending on the concept of double negative materials and used periodic arrangement to improve characteristics of the antenna. The metamaterial feature was obtained as an effect of the double-fractal layers where the crossbar fractal is used at the upper layer and the Minkowski fractal is used at the bottom layer of the antenna. It was observed through the final design that there was a significant improvement in the antenna performance.
- **In 2018 Gohar Varaminia, et, al** [19] studied and developed microstrip slot antenna with Sierpinski fractal carpet. Afterwards metamaterial loads are added to the antenna. The transmission and reflection method has been applied to get the values of permittivity and permeability of the unit cell of

the metamaterial. The design provides high gain and can cover the WiMAX wireless application with a two-directional pattern.

- **In 2018 Jianxun Su, et, al** [20] suggested ultra-wideband Radar Cross Section (RCS) metasurface design based on irregular layered fractal parts. The suggested metasurface has created from two fractals subwavelength parts with various thicknesses for each layer. Ultra-wideband and RCS reduction can be obtained from the phase deletion through two regional waves generated by those two unit cells.
- **In 2018 M. R. I. Faruque, et, al** [21] proposed a tree fractal-shaped antenna consisting of metal branches connected through a straight metal line combined with a metasurface for use in absorption applications. The same shape (tree fractal) was also used in the design of the unit cell of the metasurface with smaller dimensions.
- **In 2018 Mahsa Ahmadi Rad, et, al** [22] suggested microstrip antenna with circular fractal metasurface with wide bandwidth and low RCS. The slot antenna is one of the best types of antennas which has been used in many applications such as radar, and the metasurface is used to reduce the RCS more than -15dB.
- **In 2019 Diptiranjan Samantaray, et, al** [23] studied a modified rectangular fractal slot antenna design with metasurface placed at the bottom layer in the ground plan to use in dual-band application with high gain. The design of the unit cell is a collection of L and C shapes letter is placed at the center of the unit cell. The metasurface layer consists of (4×5) periodical arrangement of unit cells.
- **In 2019 Paulkani Iyampalam, et, al** [24] proposed Sierpinski Knopp fractal shape with metasurface unit cells. It involves two layers, the first layer is metasurface and placed at the upper side and the second layer is the fractal shape and placed at the lower side. The metasurface layer consists of a (4×6) array of Sierpinski Knop fractal unit cells.

- **In 2019 Si Jia Li, et, al** [25] designed a fractal metasurface with multiband and multifunctional response according to the coupling interaction. The proposed design implements polarization conversion from linear to linear polarization and linear to circular polarization according to the coupling interaction.
- **In 2020 Sandra Costanzo, et, al** [26] a novel fractal-based metamaterial unit cell, useful for ambient power harvesting is proposed to operate within the 2.45 GHz Wi-Fi band. The simulated fractal cell offers very high absorption coefficients, a wide-angle and polarization-insensitive behavior, and very small size.

Table 1.1- attached at the end of the chapter shows the references mentioned in the literature survey and have reviewed in terms of resonance frequency, shape and type of fractals.

The idea of removing slots in the radiator element is inspired from ref. [23] and is used to obtain large bandwidth in the proposed design. As from ref. [24], adding a metasurface layer above an antenna aids to improve the gain and increase the band width of antenna. This process is also adopted in our work to enhance the performance of proposed design. The fourth design was inspired from ref. [19] and [22] but modifications. The antenna gain was improved to 6dB compared with these references. The adopted designs explained and simulated in the chapters 3 and 4 respectively by using software CST.

1.4 Motivation

The focus of this thesis is to design and study a new principle in designing antennas based on metasurface (periodic structure) and using the fractal antenna as a microstrip antenna to improve the gain and bandwidth. The main purpose of the fractal antenna is to get wideband or multiband and it can be used for miniaturization, while the metasurface offers special improvement in gain.

1.5 Problem Statement

The development of modern communication systems needs small size antennas with high bandwidths and good performances so the microstrip antenna is the most popular type of these antennas. Although it has good features, it has a narrow bandwidth. Several techniques have been suggested to address the bandwidth of the antenna in many cases. The suggested solution that can be used was to increase the thickness of the substrate layer and to decrease the permittivity in the same time but when metasurfaces are used, this aids to decrease the value of the dielectric constant to negative value without changing the thickness of the substrate and to improve the overall performance of the antenna especially the gain.

1.6 Objectives

The objective of this thesis is to design and simulate a fractal metasurface by using the program CST microwave studio package to improve the performance of microstrip antenna and get the best results for bandwidth, gain, directivity, matching at different parameters and different states.

1.7 Contributions

This thesis contributes to improve the following parameters:

- 1-The antenna gain has been enhanced by using the metasurface technology a proximally by 6dB at 8.9GHz for the second proposed design.
- 2-Through the use of fractal geometry, the impedance bandwidth has been improved by 35.7% for the third proposed design.
- 3-With the combination of the fractal technique and the metasurface technology, the proposed antennas have been reduced in size.

1.8 Thesis Layout

This thesis consists of five chapters, including this chapter and the content of each chapter is as follows:

Chapter one includes the introduction to the thesis, literature survey, motivation, problem statement, aims of the work, objective, contributions and thesis layout.

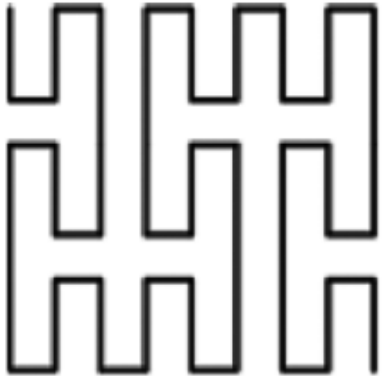
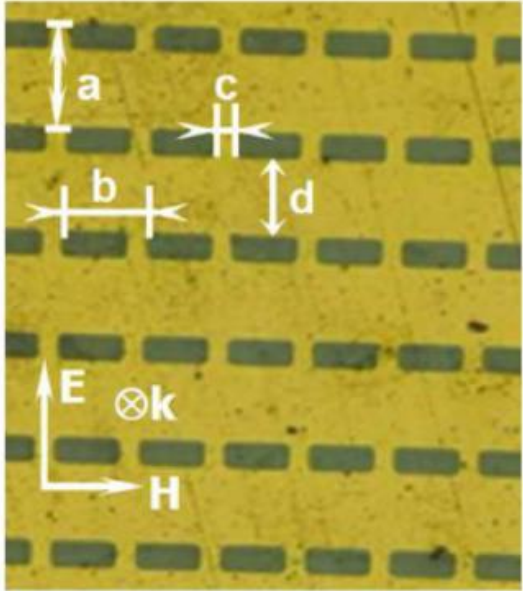
Chapter two provides the theory of the fractal geometry, fractal properties, some types of fractal antennas and the theory of metasurfaces, negative refractive coefficient, the important equations to calculate ϵ, μ and n , applications metasurfaces in designing antennas.

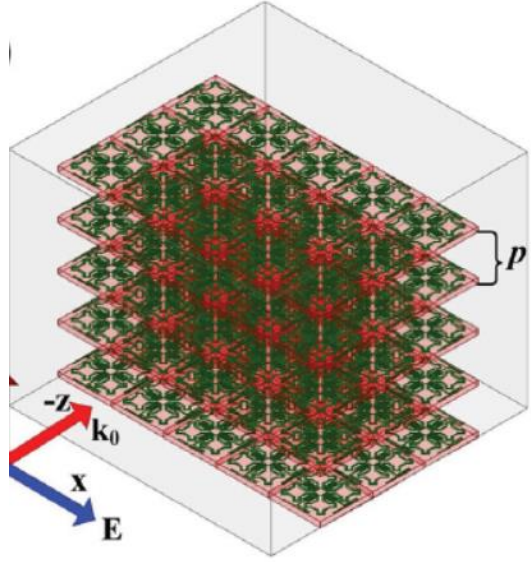
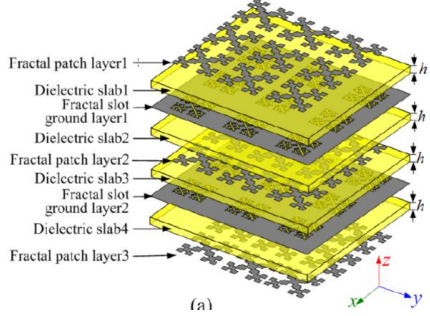
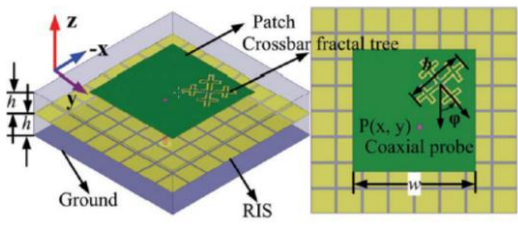
Chapter three shows configurations of the designs that will be implemented in this thesis.

Chapter four offers design, simulation, and results of fractal metasurface antennas with new shapes of unit cells, where simulation results of each single fractal antenna before and after applying the metasurface layer have been compared.

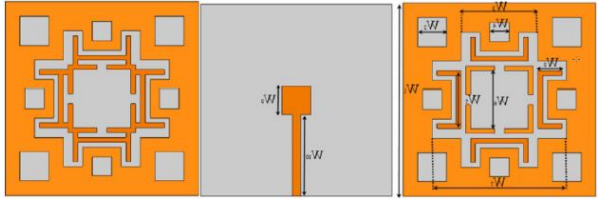
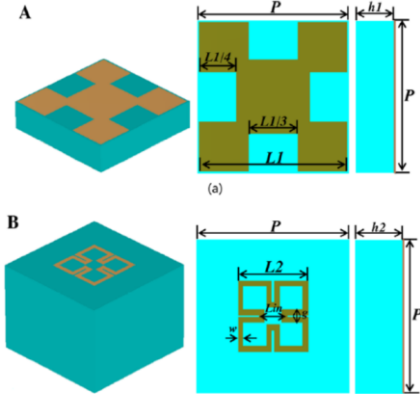
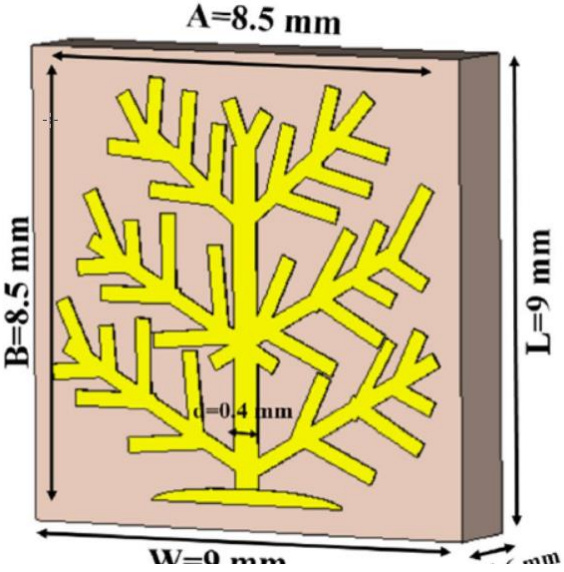
Chapter five provides the main conclusions of the thesis and the future works.

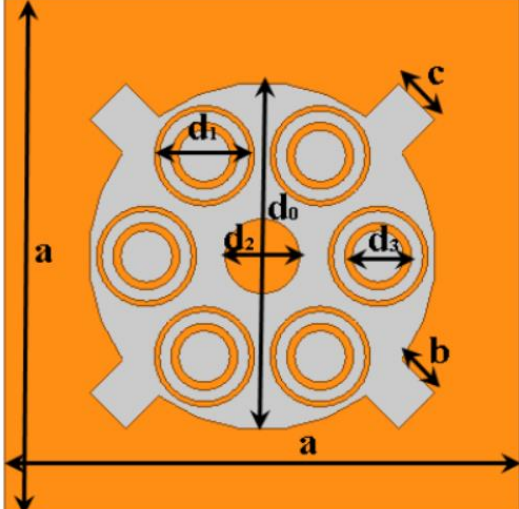
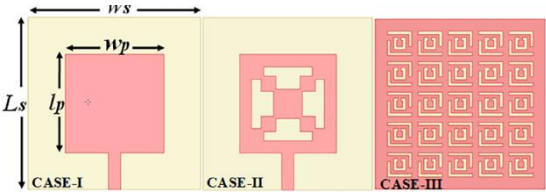
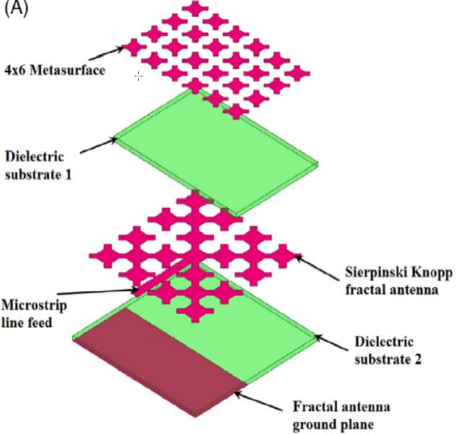
Table-1.1: References of fractal antenna designs associated with metasurface from 2008-2020

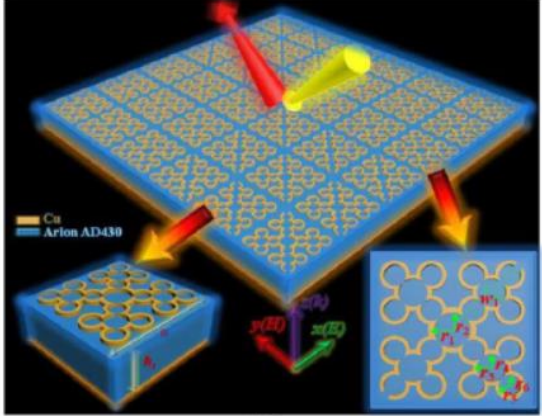
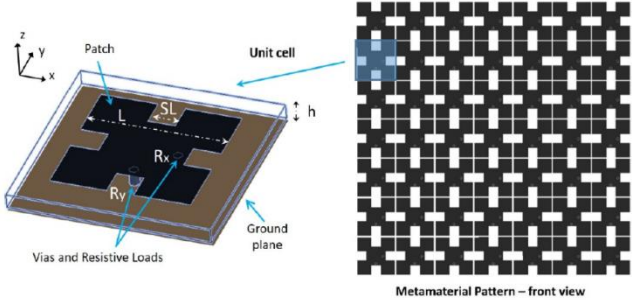
No.	Frequency Band (GHz)	The type of fractal used	Design of Fractal metasurface
1	1-6	Peano	
2	6-12	FSS Used Double Layers of Frequency Selective Surface	

<p>3</p>	<p>4.89 - 5.55</p>	<p>Sierpinski Fractal Curves</p>	
<p>4</p>	<p>7-13</p>	<p>Minkowski Fractal</p>	
<p>5</p>	<p>2.86-3.11</p>	<p>Crossbar Fractal Tree</p>	

<p>6</p>	<p>1.25-9.88</p>	<p>Minkowski Fractal</p>	
<p>7</p>	<p>3-4</p>	<p>Wunderlich Fractal Shape</p>	
<p>8</p>	<p>1-3.5</p>	<p>Minkowski Fractal</p>	
<p>9</p>	<p>0-20</p>	<p>Crossbar and Minkowski Fractal</p>	

<p>10</p>	<p>2-7</p>	<p>Sierpinski Fractal Carpet</p>	
<p>11</p>	<p>6.5-23.9</p>	<p>Minkowski Fractal</p>	
<p>12</p>	<p>4-16</p>	<p>Tree Fractal Shape</p>	

<p>13</p>	<p>1-5</p>	<p>Circular Slot Fractal Shape</p>	
<p>14</p>	<p>2-12</p>	<p>Modified Rectangular Slot Fractal Shape</p>	
<p>15</p>	<p>4-6</p>	<p>Sierpinski Knopp</p>	

<p>16</p>	<p>2-16</p>	<p>Three orders- Split Rings Fractal Shape</p>	
<p>17</p>	<p>2.2-2.8</p>	<p>Minkowski Fractal</p>	

CHAPTER TWO

THE THEORY OF FRACTAL ANTENNAS AND THE METASURFACE CONCEPT

2.1 What is A Fractal?

The fractal term is taken from the Latin word "fractus" which means broken [27]. The fractal antenna is defined by the Mandelbrot in 1975 and can be generated according to a mathematical equation. Fractal geometry can be found in nature such as in clouds, mountains and trees. It can be generated based on dividing the shape into smaller pieces and can repeat this process for any number of iterations. Each small piece is similar to the original structure but with lower size scale. The main objective for using fractal geometry is the agreement with the requirements of the fast development of wireless communication in the multiband, wideband and small size antennas [28][29].

Figures (2.1) and (2.2) illustrate some types of natural fractal and mathematical kinds of fractal antennas.



Fig. 2.1: Natural fractal forms [2]

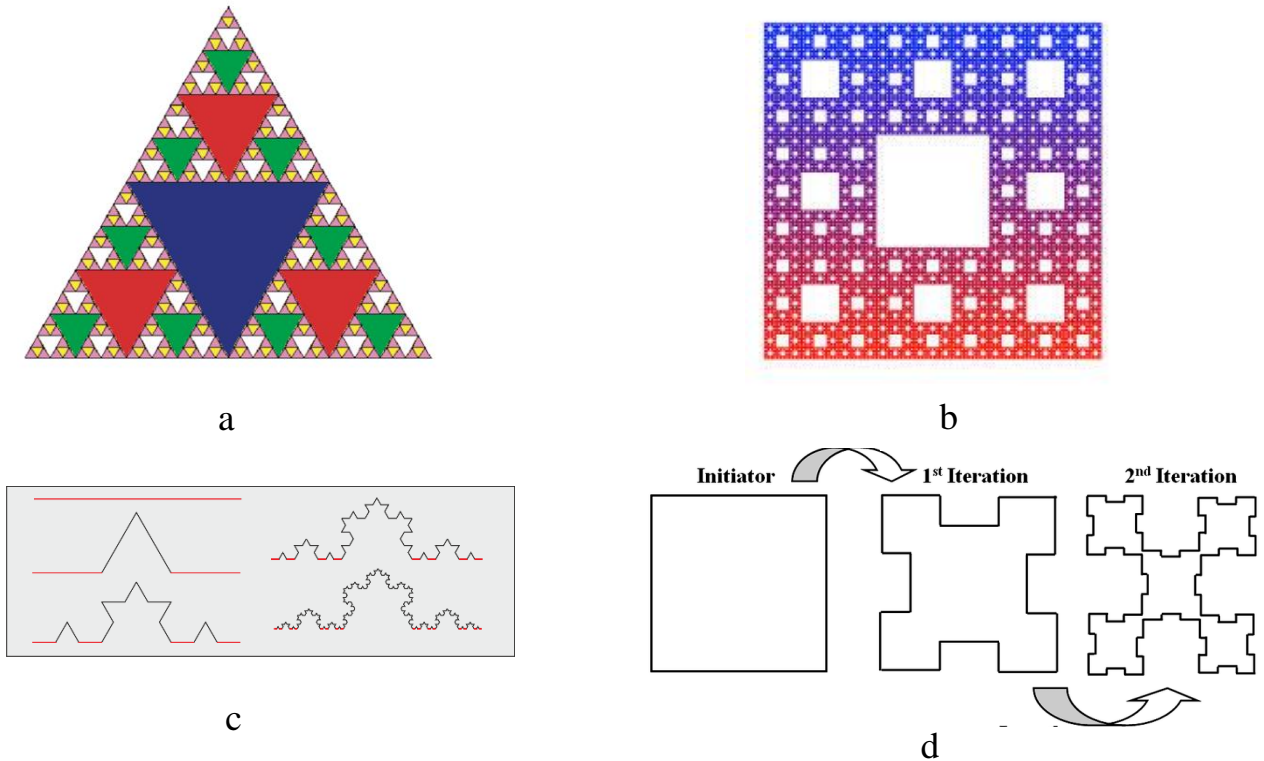


Fig.2.2: Types of mathematical geometry of the fractal antenna (a) Sierpinski- Gasket (b) Sierpinski- Carpet (c) Koch- Curve (d) Minkowski – curve[30]

2.2 Fractal Properties

Fractal shapes are distinguished from others by three common characteristics: space-filling, self-similarity, and non integer dimension [30].

2.2.1 Space-Filling

This feature is one of the most prominent properties of fractal geometry. The fractal geometry enables antennas to have long edge lengths but with small sizes compared to antennas following the Euclidean geometry in their design [31][32]. Figure 2.3 shows a sample following this feature.

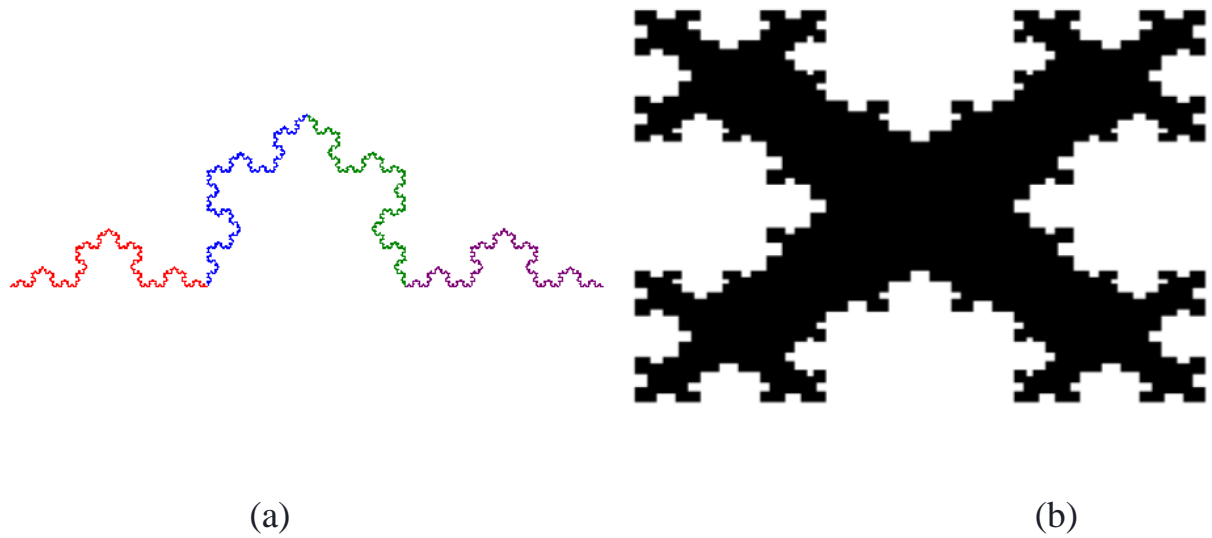


Fig.2.3: Model of space-filling property (a) third iteration of the Koch curve
(b) third iteration of Minkowski fractal patch [30]

2.2.2 Self-Similarity

The object's shape is called self-identical if it is fully formed by copying the replica from it with different scales. This means that the body's shape is repeated according to the reduction factor [31]. Figure 2.4 shows this property.

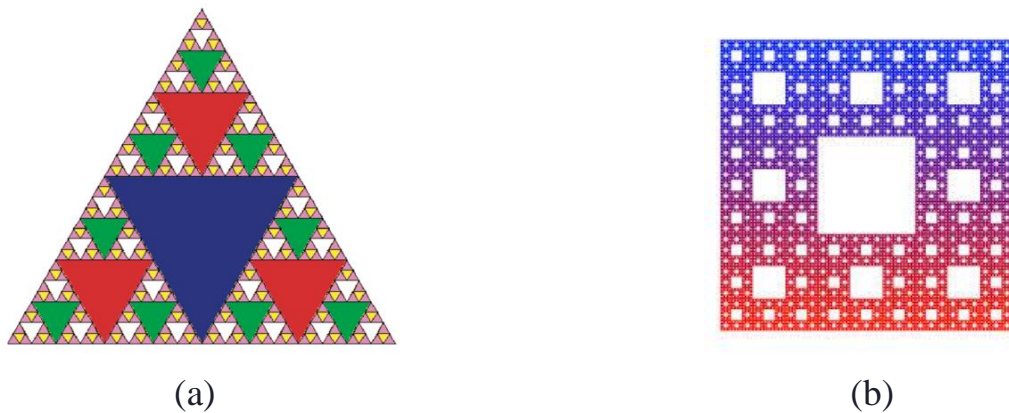


Fig. 2.4: Self-similarity property (a) third iterations of Sierpinski gasket (b)
third iterations of Sierpinski carpet [31]

2.2.3 Fractal Dimensions

The last characteristic of the fractal geometry is the dimensions which distinguish the fractal geometry from the Euclidean geometry whose dimensions are integers numbers, while the fractal dimensions are non-integer numbers.

The fractal dimensions can be expressed as the equation below:

$$FD = \frac{\log_{10}(N)}{\log_{10}\left(\frac{1}{r}\right)} \quad (2.1)$$

N: The overall number of elements

r: Decrease factor

To find fractal dimensions, the shape must first be divided into several parts (N parts) where the size of each part is less in a certain amount than the original part [3].

2.3 Types of Fractal Antennas

2.3.1 Koch Curve

The Koch curve is generated beginning from the initiator. Each unit line has been divided into three lines. After that the middle third line is replaced by two equal lines. Both two lines which form an equilateral triangle, this step is the first iteration. That can be repeated to any number of iterations to produce the Koch curve [2] as displayed in figure 2.5. From the procedure above it can be observed the Koch curve has infinite length. The length of Koch curve of the first three iterations can be calculated as,

$$L1 = L^{\circ} \left(4 \times \frac{1}{3} \right) \quad (2.2)$$

$$L2 = L^{\circ} \left(19 \times \frac{1}{9} \right) \quad (2.3)$$

$$L3 = L^{\circ} \left(64 \times \frac{1}{27} \right) \quad (2.4)$$

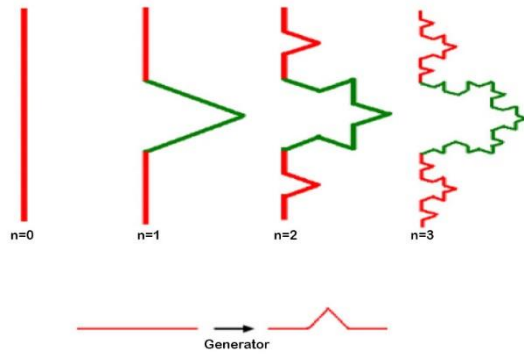


Fig. 2.5: The first four steps in the design of the Koch curve [2]

2.3.2 Sierpinski Triangle

The initial form is patch equilateral triangle. At the first iteration we subtract an upside down small patch triangle with corners located at the middle of the original triangle's arms from the original triangle. Then, the middle triangular sections are removed from the remaining triangular elements and so on. After many iterations, the Sierpinski gasket is constructed. Each iteration in the construction process is composed of three smaller triangles (copies) of the previous stage. Each copy (in each iteration) is scaled down by a reduction factor of a half [2].

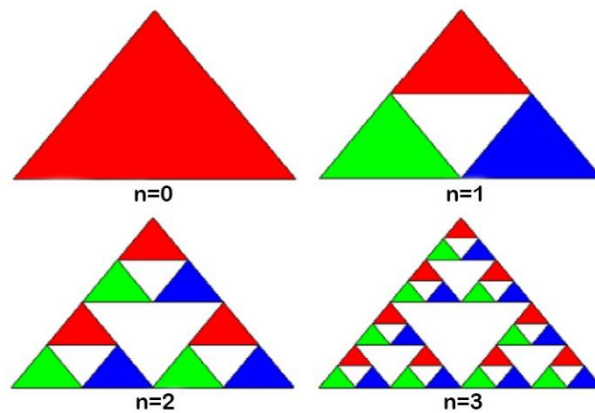


Fig. 2.6: The first four steps in the design of the Sierpinski gasket [3]

2.3.3 Sierpinski Carpet

The Sierpinski carpet is similar to Sierpinski triangle but it consists of squares instead of triangles. To build this type of fractal, take a square patch and then cut it into nine smaller squares equal in size, with removing the central square patch. The remaining squares from the previous process are divided into nine squares again and remove the central square patches. The same procedure could be repeated to complete any iteration [2] as shown in figure 2.7.

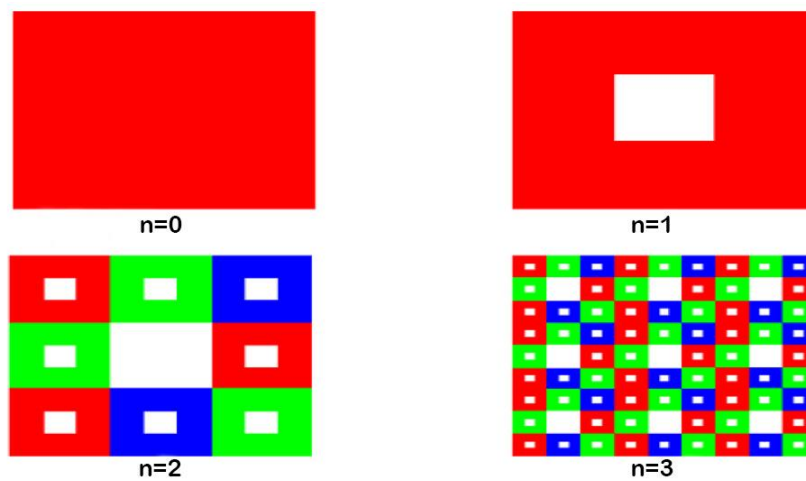


Fig. 2.7: Design steps of the Sierpinski carpet [3]

2.3.4 Minkowski Fractal

Minkowski fractal is evolved from the square. Suppose the side length of the square patch M_0 is L , suppose the square patch M_0 side length is L , each edge is trisected, in each side the middle line segment whose length is $L/3$ is translated h to the inside of the square, then four $L/3 \times h$ rectangular notch are formed. Setting the ratio of the depth and width of the notch for p , $p = 3h/L$ ($0 < p < 1$) indicates the relative size of the notch depth. By changing p can get a different first order Minkowski fractal patch M_1 . All the straight edge of the first-order Minkowski fractal patch is trisected, following the same value p iteration can generate second-order Minkowski fractal patch M_2 . Such infinite iteration can generate high-order Minkowski fractal

curve, the patch surrounded by this curve is Minkowski fractal antenna patch. Those unlimited iterations can generate high-order Minkowski fractal [32] as displayed in figure 2.8.

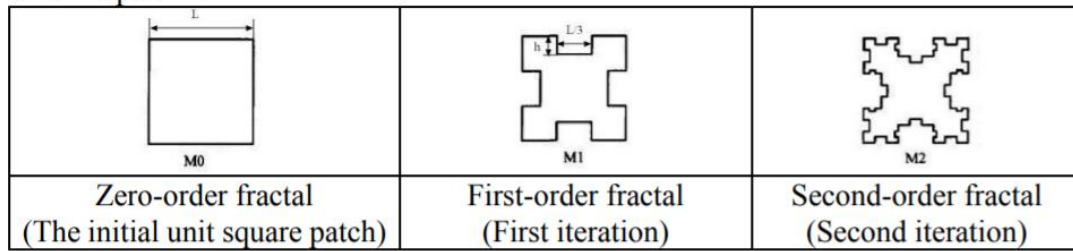


Fig. 2.8: Design steps of Minkowski fractal [32]

2.3.5 Circular Slot Fractal Antenna

The design of circular fractal shape is started from a circle with a radius r . Then add two circles into the main circle with radius $r/2$. After that we subtract the two circles from the main circle that is the first iteration. The same procedure could be repeated for more iterations by halving the radius of the circles [33] as shown in figure 2.9.



Fig. 2.9: Three steps of designing circular slot fractal antenna [33]

2.3.6 Cross Shape Fractal Antenna

The cross fractal is constructed by drawing the cross-sign shape. For each iteration, we change the four arms of the previously constructed cross into smaller crosses. This procedure can be repeated several times to obtain high iteration fractal structures. Figure 2.10 explains the procedure for designing this antenna [34].



Fig. 2.10: Design steps of cross shape (a) first iteration (b) second iteration

2.4 Introduction to Metasurface

Metasurfaces are an important topic of research, since they are used in different applications. They have a unique ability to manipulate electromagnetic waves at microwave and optical frequencies. The features of lightweight, manufacturing ease, and capability to control waves using flat structures make the metasurface preferred over other structures. Metallic or dielectric pins with subwavelength scale arranged in 2D configuration are the basic layouts of metasurfaces. The specific capabilities of various types of metasurfaces have been stressed beginning with the production of frequency-selective surfaces and metamaterials. Surface impedance can be varied and controlled by patterning the unit cells of the metasurface with many applications in surface wave absorber. They also require transmission as well as a reflection to form the beam. Polarizer, cloaking, and modulator are other uses of the metasurfaces. The metasurfaces controlling refractive index can also be used in lenses. Eventually, new imaging technologies appeared by metasurfaces [35].

2.5 What is Metasurface?

It is the 2D type of the metamaterial. Metamaterial (MTM) is known as manmade structure that can be designed to provide the required electromagnetic

response in particular frequency. It is known as a category of the artificial materials constructed from the scattering elements that have negative permeability and permittivity respectively. It can be called a fairly homogeneous material (i.e. the material's physical size is small as compared to the electromagnetic wave's wavelength) and this has a negative refractive index for a provided frequency band [36]. Meta is a Greek word and means "beyond". Walser in 2001 coined term "metamaterial" to be referred to as "artificial materials" which have performance beyond traditional material limitations. In 1968, the propagation of the plane wave through material that has negative permittivity and negative permeability was studied by the V.G. Veselago [37]. The negative permittivity or negative permeability shows that the electrons are moving in the opposite direction according to the utilized electric field. The direction of the vector in the Veselago medium is opposite to the direction of the phase velocity. This is contrary to traditional material wave propagation. This is a cause of called this kind of medium as Left-handed- materials [38]-[40] and is illustrated seen in figure 2.11 and figure 2.12.

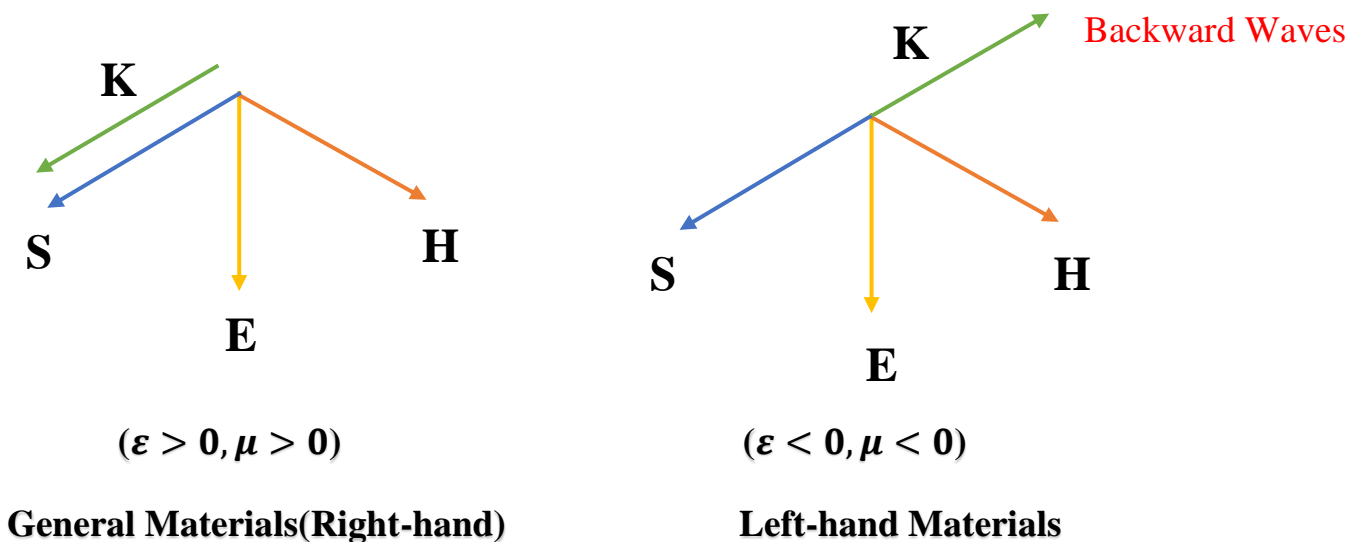


Fig. 2.11: Electric – magnetic- surface wave and Poynting vectors of an electromagnetic wave in RH and LH mediums [36]

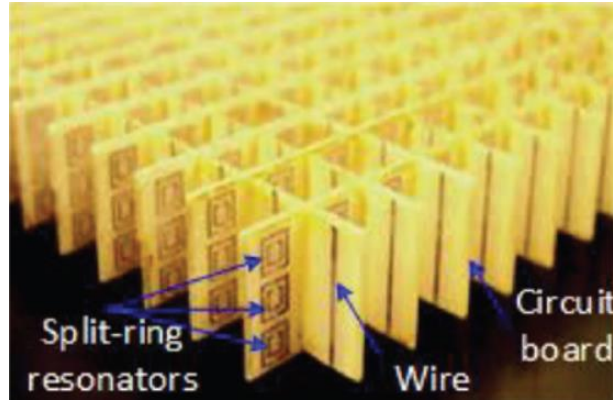


Fig. 2.12: Collection of thin wires and SRR to shape DNG MTM [36]

It is first to establish the permittivity (ϵ) and permeability (μ) of material as the parameters used in the interaction of electromagnetic waves to characterize electric and magnetic response. The permittivity is known as how the electric field can affect the dielectric medium and affected by it. This is an internal test of polarization [41] or known as the ratio of the D (the electric displacement) to the E (the strength of the electric field) of the medium. The permeability of the material is known as the degree of magnetization when the magnet field is applied [42]. The materials may be divided into four divisions, as seen in the fig.2.13.

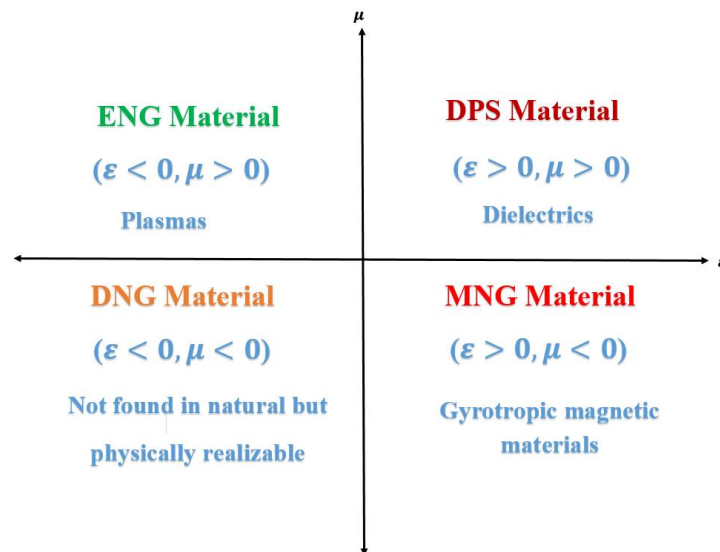


Fig.2.13: The four possible types of materials based on permittivity and permeability signs [43]

most materials have the positive values of permittivity and permeability and thus are referred as "double-positive" (DPS) materials. If all these quantities are negative, it is called "double-negative (DNG)". Epsilon-negative (ENG) is a substance of only negative permittivity. Finally, for types with negative μ is called negative permeability (MNG). Furthermore, there is no substance in nature capable of offering negative permittivity and permeability at the same time. So, they have to be artificially created [43].

2.6 Negative Refractive Index

A large part of research has been recognized by the theory of negative refractive index. This research field has led to the lens or super lens growth [44]. Super lens supports the ability to focus on all propagation modes, and the picture gets without losing information. To establish left-hand actions in mathematics both ϵ and μ should be negative values [45]. As seen below, the refractive index is the square root of the product of permittivity and the permeability:

$$n = \pm \sqrt{\epsilon_r \mu_r} \quad (2.5)$$

In the left-handed medium, the value of n is refractive index and has negative value. The μ_r is magnetic permeability while the ϵ_r is electric permittivity. There shall be four potential states of signs ϵ and μ (+, +) and (-, +) and (-, -) where these lead to double-positive (DPS), single negative (SNG), or double negative (DNG). Although there are negative permittivity and permeability values, the value of the refractive index will not appear negative until now but it is possible to prove that choosing the square root leads to the values of the refractive index close to zero [46]. The value of (n) in a left-handed medium is negative and can drive this from the phase (π) for both μ and ϵ . The values of μ and ϵ in LH medium expressed according to quantity and phase in the complex plane [47].

$$\epsilon r = |\epsilon r| e^{j\varphi\epsilon} \quad (2.6) \quad \text{where } \varphi\epsilon \left(\frac{\pi}{2}, \pi \right)$$

$$\mu r = |\mu r| e^{j\varphi\mu} \quad (2.7) \quad \text{where } \varphi\mu \left(\frac{\pi}{2}, \pi \right)$$

The medium's refractive index can, therefore, be expressed as:

$$n = \sqrt{|\epsilon\mu|} e^{j\varphi n}, \quad (2.8)$$

$$\varphi n = \frac{1}{2}(\varphi\mu + \varphi\epsilon),$$

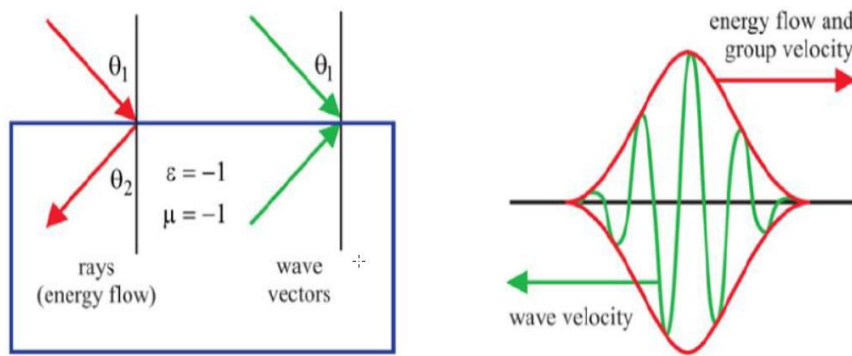


Fig. 2.14: Materials with near-zero refractive index [48]

Figure (2.14) shows the materials with a negative refractive index of refractive, by shifting the incident light rays to the "opposite" side of the standard. The wave vector is in the reverse direction to the flow of energy because of the negative group velocity [49]. It is shown by Snell's law:

$$n_1 \sin \theta_1 = n_2 \sin \theta_2 \quad (2.9)$$

n_1 = is the refractive index of the incidence medium

n_2 = is the refractive index of the refracted medium

θ_1, θ_2 = The angles of incidence and refraction are represented respectively

The index n_1 is from an ordinary medium and another is with negative ϵ and negative μ . Therefore, according to the Snell's law, the refractive angle of θ_2 should have the same sign as the incident angle θ_1 , when $n_2 > 0$, while it will be negative at $n_2 < 0$, as seen in Figure (2.15) [50].

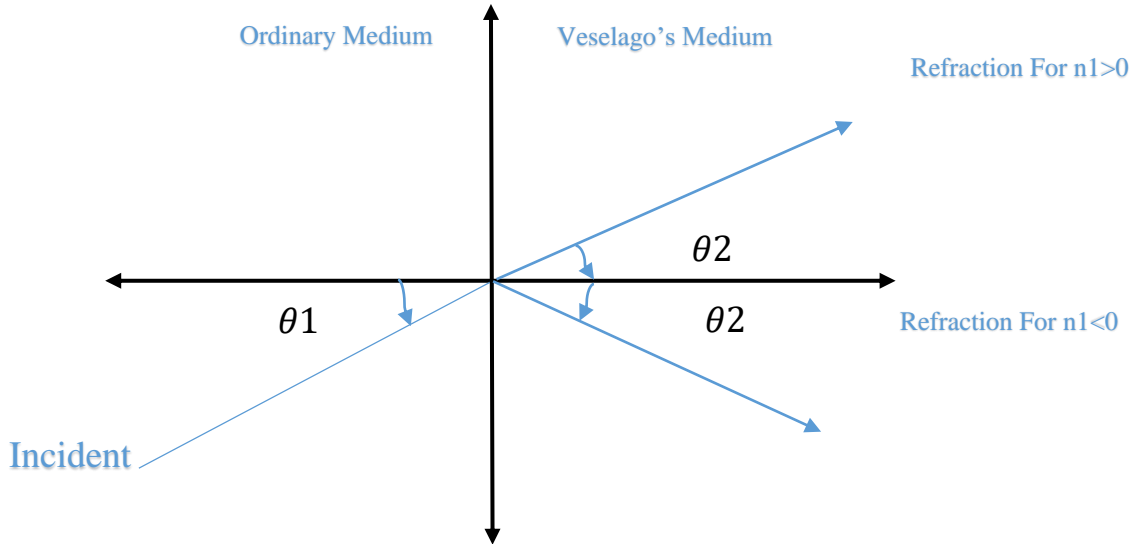


Fig.2.15: The scheme of the Snell's law of normal medium when $n_1 > 0$ and LH medium when $n_2 < 0$ [46]

When the medium is the left-handed medium the Snell's law is:

$$\frac{\sin \theta_1}{\sin \theta_2} = \frac{n_2}{n_1} < 0 \quad (2.10)$$

The conventional material refractive index is positive, $n_1 > 0$, while the left-handed material refractive index is negative, $n_2 < 0$.

2.7 Important Equations to Calculate ϵ, μ, n

The permittivity and permeability describe the characteristics of materials in electromagnetics. Calculating these parameters at various frequencies defines the propagation of substance at this frequency. Single element (one cell) of metasurface with periodic boundary conditions is examined. The boundary conditions are set to be Perfect Electric Conductor (PEC) in y-axes, Perfect Magnetic Conductor (PMC) in x-axes, and open space in z-axes. The response of this system can be expressed as [51]:

$$S_{11} = \frac{R(1 - e^{i2nk^{\circ}h})}{1 - R^2 e^{i2nk^{\circ}h}} \quad (2.11)$$

$$S_{21} = \frac{(1 - R^2)e^{i2nk^{\circ}h}}{1 - R^2 e^{i2nk^{\circ}h}} \quad (2.12)$$

Solving Eq. (11) and (12) gives

$$Z = \pm \sqrt{\frac{(1 + S_{11})^2 - S_{21}^2}{(1 - S_{11})^2 - S_{21}^2}} \quad (2.13)$$

$$e^{ink^{\circ}h} = \frac{S_{21}}{1 - S_{11} \frac{z-1}{z+1}} \quad (2.14)$$

$$n = \frac{1}{k^{\circ}h} [\{[\ln(e^{ink^{\circ}h})]'' + 2m\pi\} - i[\ln(e^{ink^{\circ}h})]'] \quad (2.15)$$

(.)'' refers to complex element, (.)' refers to the real element of the complex number. S11: input reflection coefficient, S21: transmission coefficient. $R = \frac{z-1}{z+1}$

n: refractive index h = the length of unit cell m = the periodicity element

k = wave number z = the impedance H and E: the magnetic & electric field

The (ϵ) and (μ) are related to (n) the refractive index and (z) impedance by the following relations [52].

$$\varepsilon = \frac{n}{z} \quad (2.16)$$

$$\mu = nz \quad (2.17)$$

2.8 The Usage of Metasurfaces in Antenna Design

2.8.1 The Radiators Antennas above A Metasurface

The major problem with a planar antenna placed a top of the metal reflector is that the space between the metal reflector and the radiating elements should be equal to the quarter- wavelength to achieve optimal features of antennas. Instead, the metal reflector as shown in Figure 2.16 can be replaced by a metasurface to solve this problem. The metasurface has been constructed of metal plates on a dielectric substrate. It is interesting that the surface waves that spread over the metasurface produce additional radiation resonances. Such external resonances are useful to improve the antenna bandwidth [53].

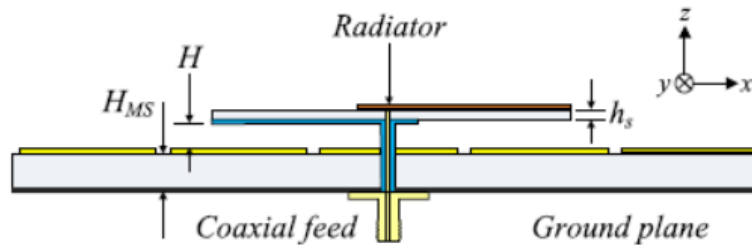


Fig.2.16: The antenna geometry with radiator above the metasurface layer [53]

2.8.2 The Radiators of Antenna Established within the Structure of Metasurface

The antennas that were explained previously have a relative high antenna as their radiating components are situated above the structure of the meta-surface. Their wide bandwidth, short antenna height, polarization conversion, reconfigurable polarization and high efficiency [54] recently received a lot of attention about the radiators below the metasurface. Figure 2.17 displays this type of designs.

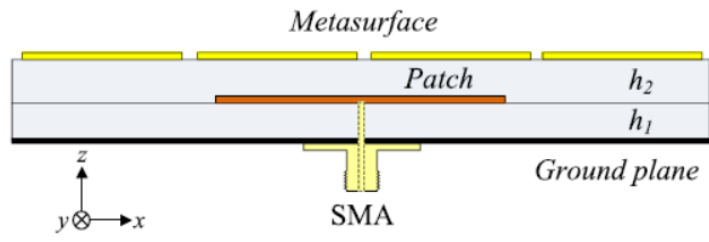


Fig.2.17: Side view of the antenna geometry [53]

CHAPTER THREE

DESIGN CONFIGURATION

3.1 Introduction

This chapter presents four designs for different types of fractal metasurface antennas. The objective is to improve the performance of the microstrip antenna in terms of bandwidth, matching and especially gain as it is the primary function of the inclusion of the metasurface plate in the proposed designs. As for the most important reasons is to choose the fractal antenna due to its high bandwidth and miniaturization purposes. The first design includes a circular fractal antenna with the same shape of the circular fractal used in the design of the unit cell. The second design is a modified cross fractal shape at the third iteration with the same shape for designing the unit cell of the metasurface layer but slightly different. The third design is the Minkowski slot fractal design with closed rectangular rings resonator (RCRRs). The fourth design is compact microstrip antenna of circular fractal shape with MS. Parametric study is carried out to study the effect of the number of unit cells on the design and study the distance between cells. This chapter, also shows the effect of placing the radiator above and below the metasurface layer and finally simulate the performance of the unit cell in each design and obtain the negative value of permittivity and permeability.

3.2 First Proposed Design: Circular Fractal Slot Antenna without and with Metasurface for X and Ku band Applications .

The first proposed design is a circular fractal slot antenna with metasurface. The design consists of several layers, starting from the ground layer and ending with the last layer, which is the metasurface. As for the design steps, they start from a partial ground layer with dimensions of (50×25) mm² made from copper material. The dielectric layer is FR-4 material with dimensions of (50×50) mm² with dielectric constant of (4.3). As for the fractal antenna, it starts from designing a circle with a diameter of 45 mm made from copper material, with a thickness of 0.035 mm. Then make two small circles inside the main circle with a diameter of 22.5 mm and then subtract these two circles from the main circle patch. After that, we draw four small circles inside the previous two, where the diameter of each of these four circles is 11.25 mm, and then the same steps are repeated to make more iterations. The antenna is fed by the microstrip feed line connected to 50 ohms characteristics impedance as shown in figure 3.1.

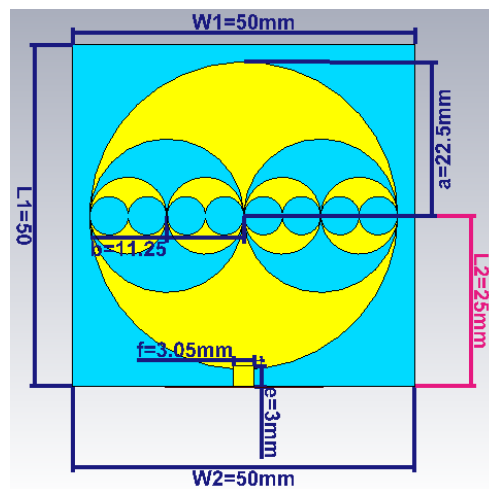


Fig. 3.1: Circular fractal slot antenna

Figure (3.2) explains the design steps of the circular fractal antenna where the same procedure of fractal generation is used to design the unit cells of metasurface.

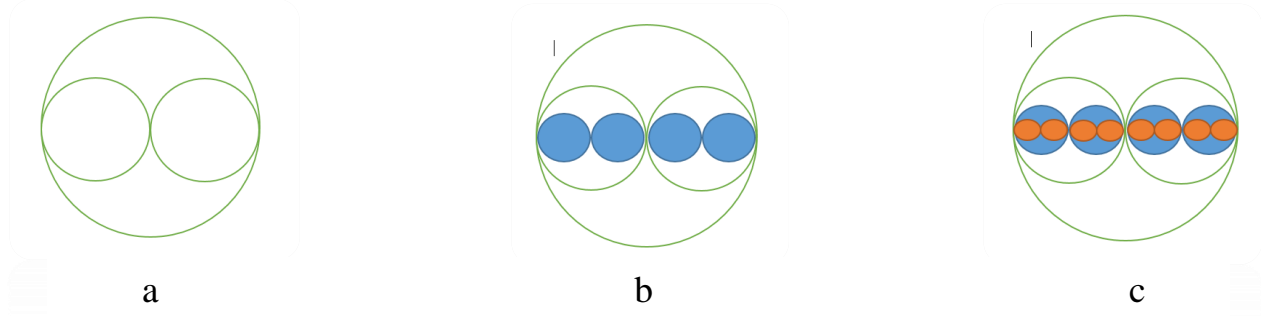
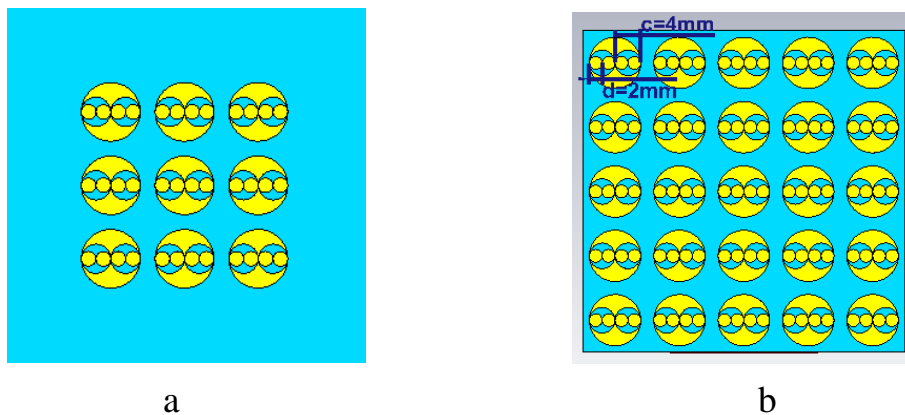


Fig. 3.2: Design of circular slot fractal shape (a) first iteration (b) second iteration (c) third iteration

For the design of the metasurface layer, the same fractal design was used as a unit cell for the metasurface layer with a smaller size because of using fractal forms to design unit cells offers special properties not found in classical patterns. The main circle has a diameter of (8) mm and the two small circles with a diameter of (4) mm in the periodic array. Two different cases have been studied with a different number of cells. It was used in the first case (3×3) of unit cells and in the second case (5×5) of unit cells. The metasurface layer was designed on the same dielectric substrate which is FR-4 that has the same characteristics as mentioned earlier. The three cases of the small gap between the MS and the radiation layer were studied at (1, 2 and 3) mm. Figure 3.3 illustrates the metasurface with a various number of the unit cells.



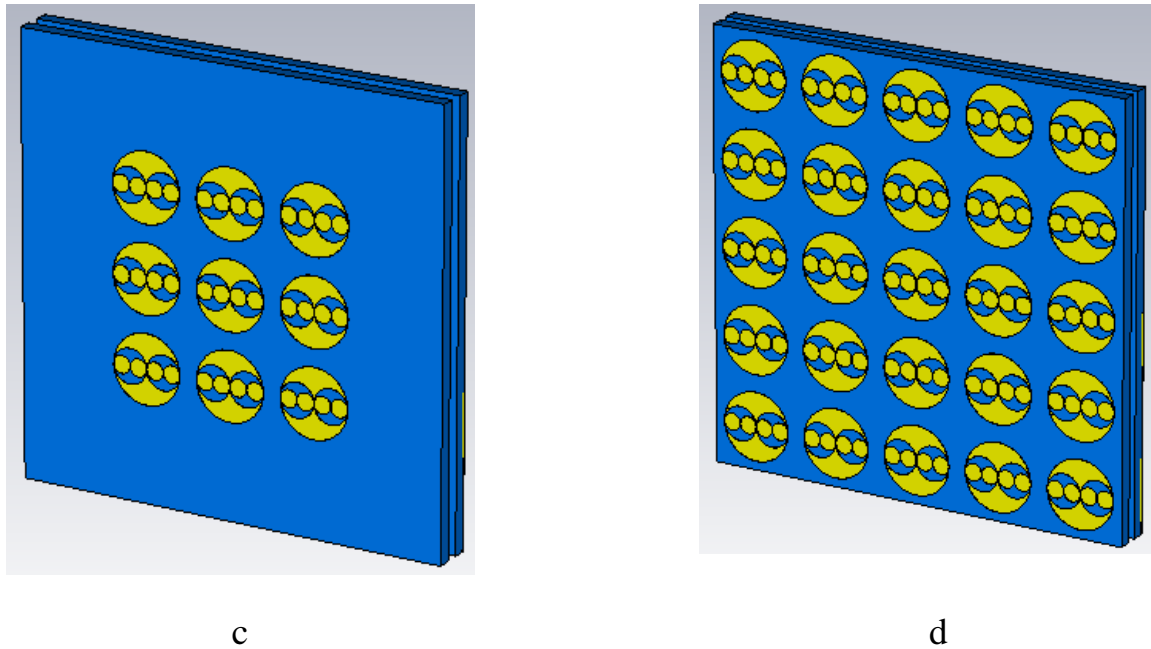


Fig.3.3: Design of metasurface plate (a) front view (3×3) unit cell (b) front view (5×5) unit cell (c) side view of the 3×3-unit cell (d) side view of the 5×5-unit cell

Also, the performance of single-cell from metasurface have been studied and the negative values of permittivity and permeability were obtained. The main circle is presented at a radius of 4mm and the circular slots with a radius of 2mm. The same procedure can be repeated for more iterations. The FR4 substrate with a thickness of 1.6 mm is used as shown in Figure 3.4.

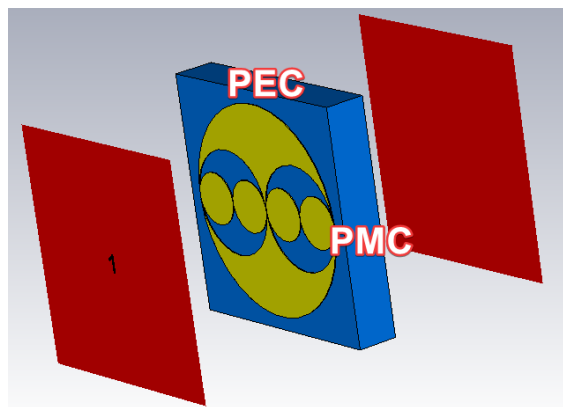


Fig.3.4: Periodic setup of the one unit cell

The performance of the antenna was evaluated in the CST program [55] and has two resonance frequencies at (11.2) and (12.2) GHz. The table below includes all dimensions of the proposed antenna.

Table-3.1: Dimensions of Circular Fractal Slot Antenna with MS

Symbols	Parameter	Dimension(mm)
W1=L1	the width & length of substrate	50
W2	the width of the ground	50
L2	The length of the ground	25
a	The radius of the main circle	22.5
b	The radius of two circles (slots)	11.25
c	The radius of the main circle in MS	4
d	The radius of two circles(slots) in MS	2
e	The length of the feeding line	3
f	The width of the feeding line	3.05
g	The gap between metasurface and fractal antenna	1

3.3 Second Proposed Design: Modified Cross Fractal Antenna with MS for X-band Applications

The second proposed design is the modified cross fractal antenna with a metasurface. The design begins from drawing the cross sign with the length of 30 mm and the width of 1.6 mm. After that we design the figure similar to (L) shape at both ends of the cross sign then take a copy of this structure and rotated by 90° . Figure 3.5 shows the design steps of the cross fractal shape.

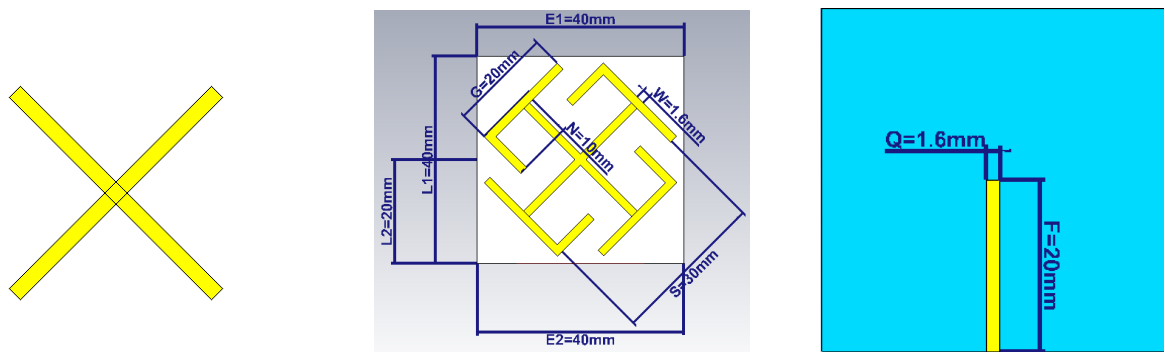


Fig. 3.5: Design modified cross fractal shape

Then, add the metasurface layer to the antenna to improve the overall performance, especially the gain. The MS consists of the same design of cross antenna but with small sizes. Two different layers of metasurface have been utilized, where the first one has (4×4) unit cells and the second one has (5×5) unit cells. As seen in figure 3.6.

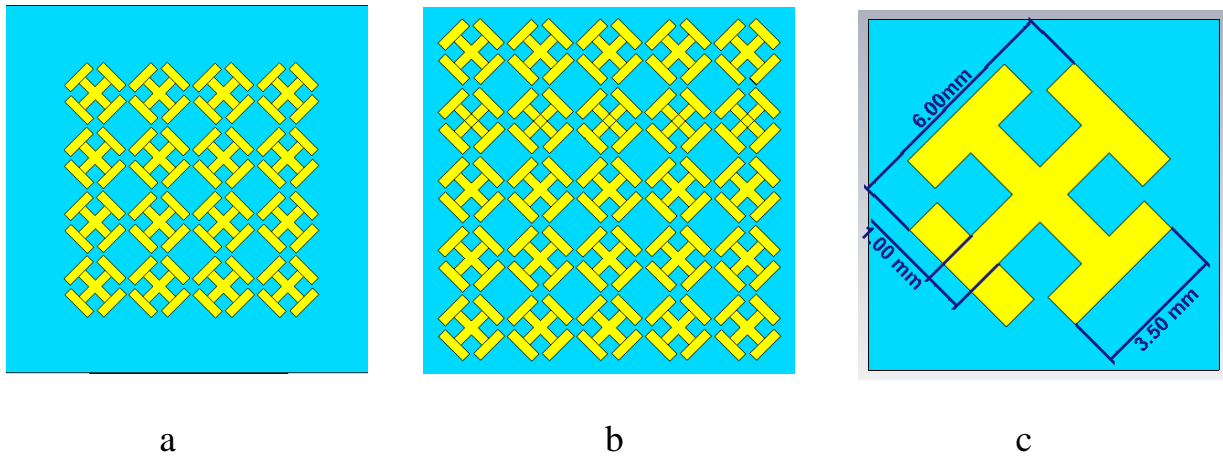


Fig.3.6: (a) (4×4) MS layer (b) (5×5) unit cells (c) dimensions of a single unit cell

The whole structure is designed on the partial ground with dimension of $(40 \times 20) \text{ mm}^2$. The dielectric layer of FR-4 with dimension of $(40 \times 40) \text{ mm}^2$ has dielectric constant of (4.3) and thickness of 0.8mm. The antenna is fed by utilizing waveguide feeding with dimension $(20 \times 1.6) \text{ mm}$ because it has high power and low loss. Fig.3.7 illustrates the structure of one unit cell from the structure shown above to realize negative permittivity and negative permeability as the main goal for using the metasurface.

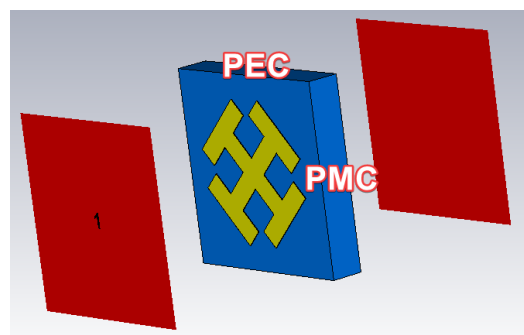


Fig.3.7: Setup of periodic unit cell using the CST

Table-3.2: The Dimensions of the Modified Cross Fractal Shape with Metasurface

Symbols	Parameter	Dimension(mm)
E1=L1	The width &length of substrate	40
E2	The width of the ground	40
L2	The length of the ground	20
S	The length of each side of the cross sign	30
W	The width of each side of the cross sign	1.6
G	The long side of the L shape	20
N	The small side of L shape	10
F	The feeding line length	20
Q	Feeding line width	1.6
D	Distance between metasurface and cross fractal antenna	1.5

3.4 Third Proposed Design: Minkowski Fractal Slot Antenna with Metasurface

The third proposed design is Minkowski fractal slot patch antenna with metasurface layer. The design initially is started from a simple square patch of the copper material at the dimension of (16×16) mm² with a thickness of (0.035) mm. The suggested shape is designed on the substrate layer of FR-4 with the thickness of (1.6) mm. The next step is to cut out a slot in the center of the patch with meandered sides, called Minkowski shapes with the dimensions shown in figure (3.8) (a) and (b).

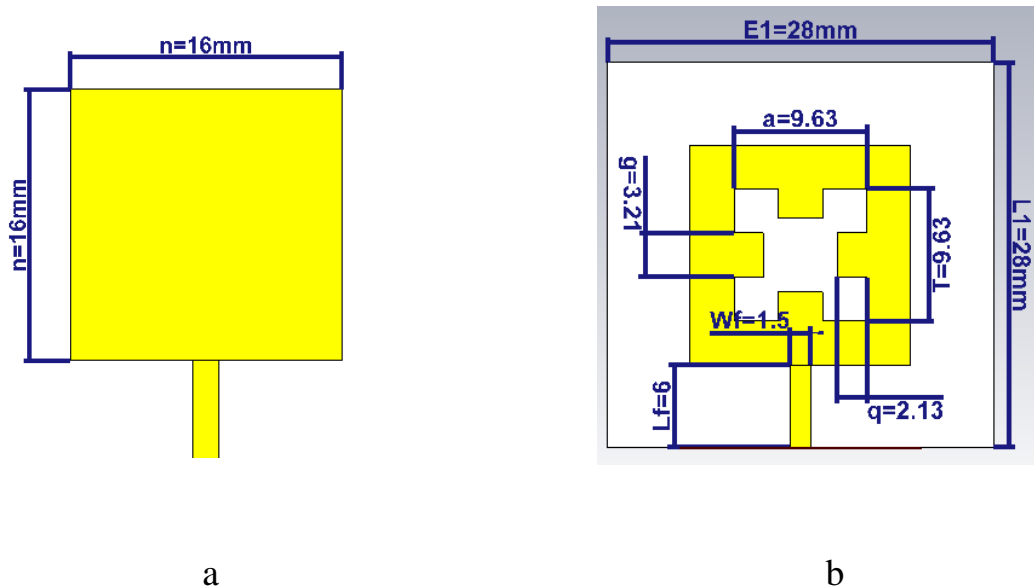


Fig.3.8: Design steps of Minkowski slot fractal shape

Then, add the metasurface layer in front of the radiator layer but leave a small distance between them. A metasurface layer with different unit cells of (3×3) , (4×4) , (5×5) and (6×6) has been used. The design of the unit cell is consisted of the double square closed ring (DSCR) from copper material placed on the dielectric layer with dimension of (28×28) mm² with a dielectric constant is (4.4). The dimensions of a single unit cell in the outer square of (4×4) mm² and the small

inner square is (2×2) mm² with thickness of (0.035). Figure 3.9 shows the entire design of the metasurface layer.

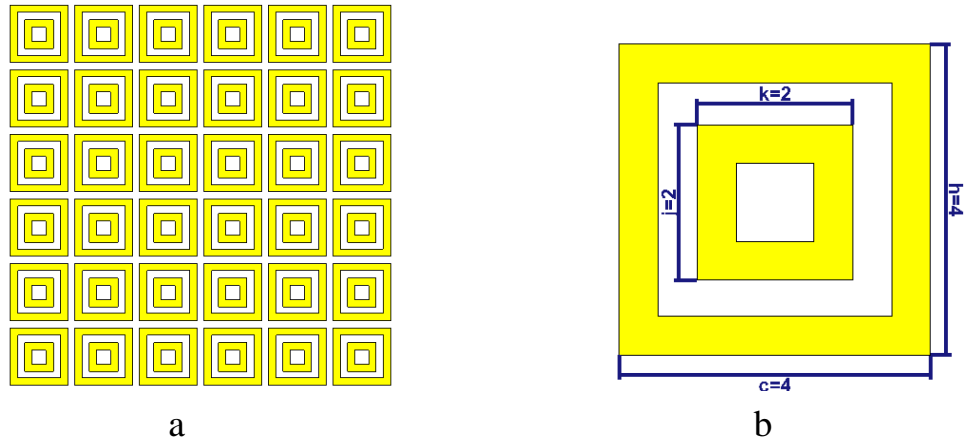


Fig.3.9: a ((6×6) MS layer) b (the dimensions of single cell)

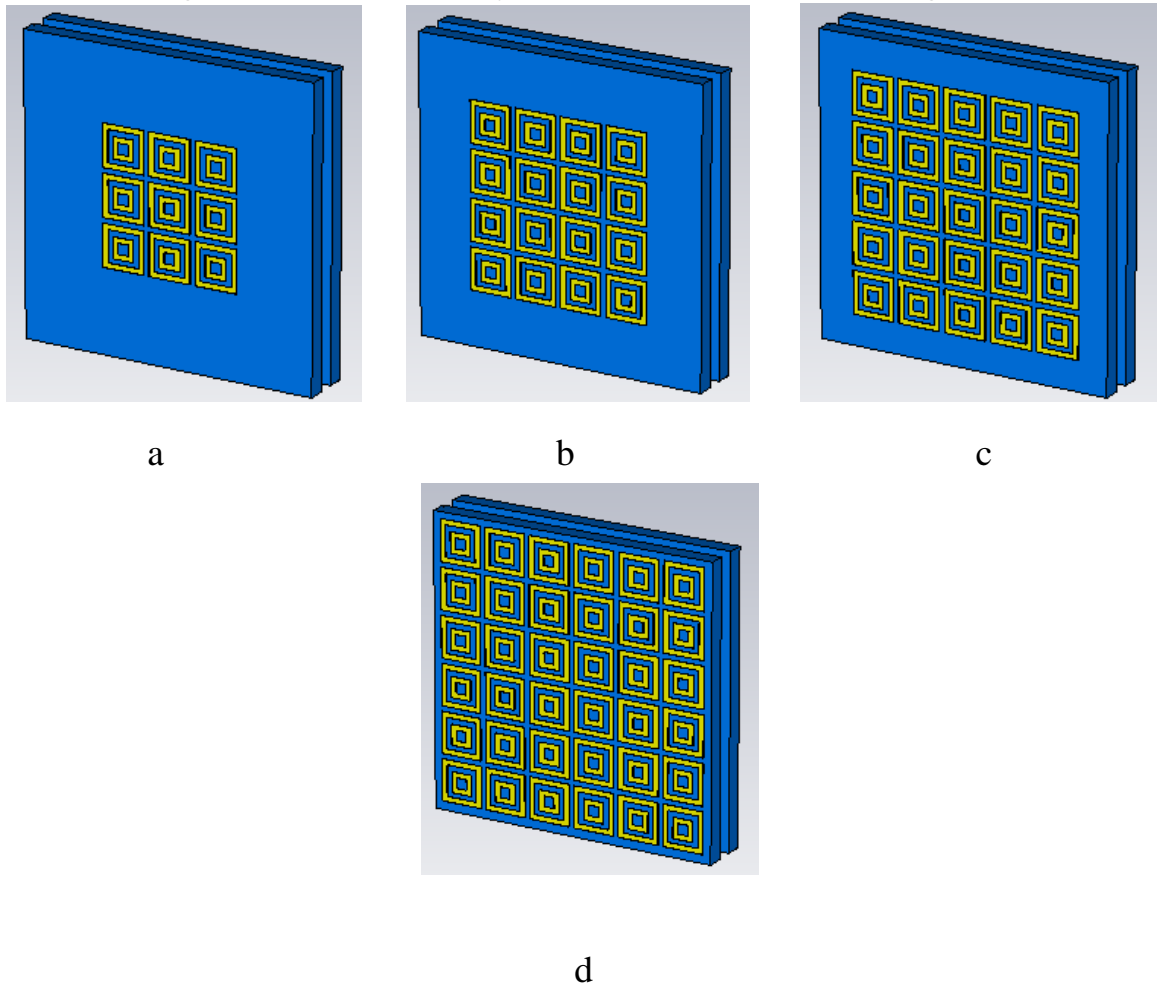


Fig.3.10: (a) 3×3 (b) 4×4 (c) 5×5 (d) 6×6 unit cells

In contrast to the previous procedures, we place the radiating part above the MS layer and study the effect on the performance of the antenna as shown in figure 3.11

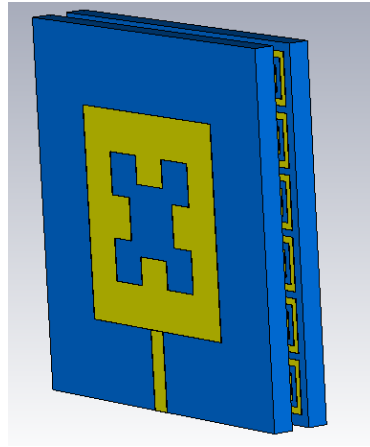


Fig.3.11: The front view when placing the antenna above the MS layer

The next study is adding double MS layers and placing them above the antenna with a small gap between the antenna and the two plates to see their effects on the gain of the proposed antenna. Figure 3.12 illustrates insertion of double MS layers to the design.

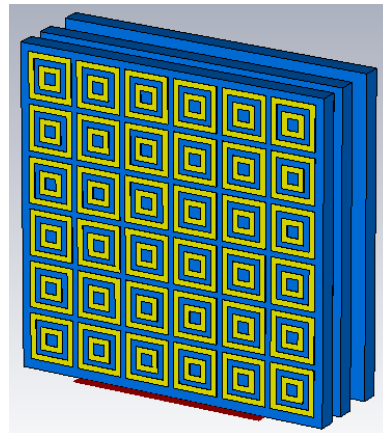


Fig.3.12: Double layers of MS adding to the proposed antenna

Finally, implementation of single-unit cell of metasurface layer was studied and their permittivity, permeability and refractive index were calculated. Figure 3.13 displays the structure of a single unit cell.



Fig.3.13: Double square closed ring of metasurface

Table-3.3: The Dimensions of the Minkowski Fractal Slot Patch with Metasurface Antenna

Symbols	Parameter	Dimension(mm)
$E1=L1$	The width and length of the substrate	28
n	The length and width of the square patch	16
$a=T$	The length and width of the slot	9.63
g	The length of the small rectangle of Minkowski fractal shape	3.21

q	The width of a small rectangle of Minkowski slots	2.13
Lf	The length of the feeding line length	6
Wf	Feeding line width	1.5
h=c	The length and width of the outer rectangle of MS	4
k=j	The length and width of the inner rectangle of MS	2
d	The separator gap between the MS & the patch	1.7

3.5 Fourth Proposed Design: Multiband Compact Microstrip Circular Slot Fractal MS Antenna for C and S-band Applications.

The proposed design consists of the circular fractal slot on the ground plane. When slots are loads over the ground plane this called defected ground structure. Then we add four tilted rectangular slots at the edges of the circle. Each slot is rotated by an angle of 90° . The design of fractal antenna begins from a circular slot with a radius of 4mm. After that we add two small circles with a radius of 2mm removed from the first circle. Finally, design four circles with 1mm where two inside one circular slot and we can repeat these steps for more iterations. At the center of the main circular slot we add disk of a diameter $d= 5.8$ mm. The feeding line has characteristics impedance of 50Ω . Proposed antenna is designed on FR4 substrate

with (40×40) mm², a thickness of 1.6 mm, and $\epsilon = 4.3$. The ground plane is the copper material with a thickness of 0.035 mm. The feeding line length is $e = 20$ mm and the width is $i = 1.6$ mm. Figure 3.14 (a, b, c, d and e) displays the design steps for the proposed antenna. Table 4.4 summarizes dimensions of the antenna.

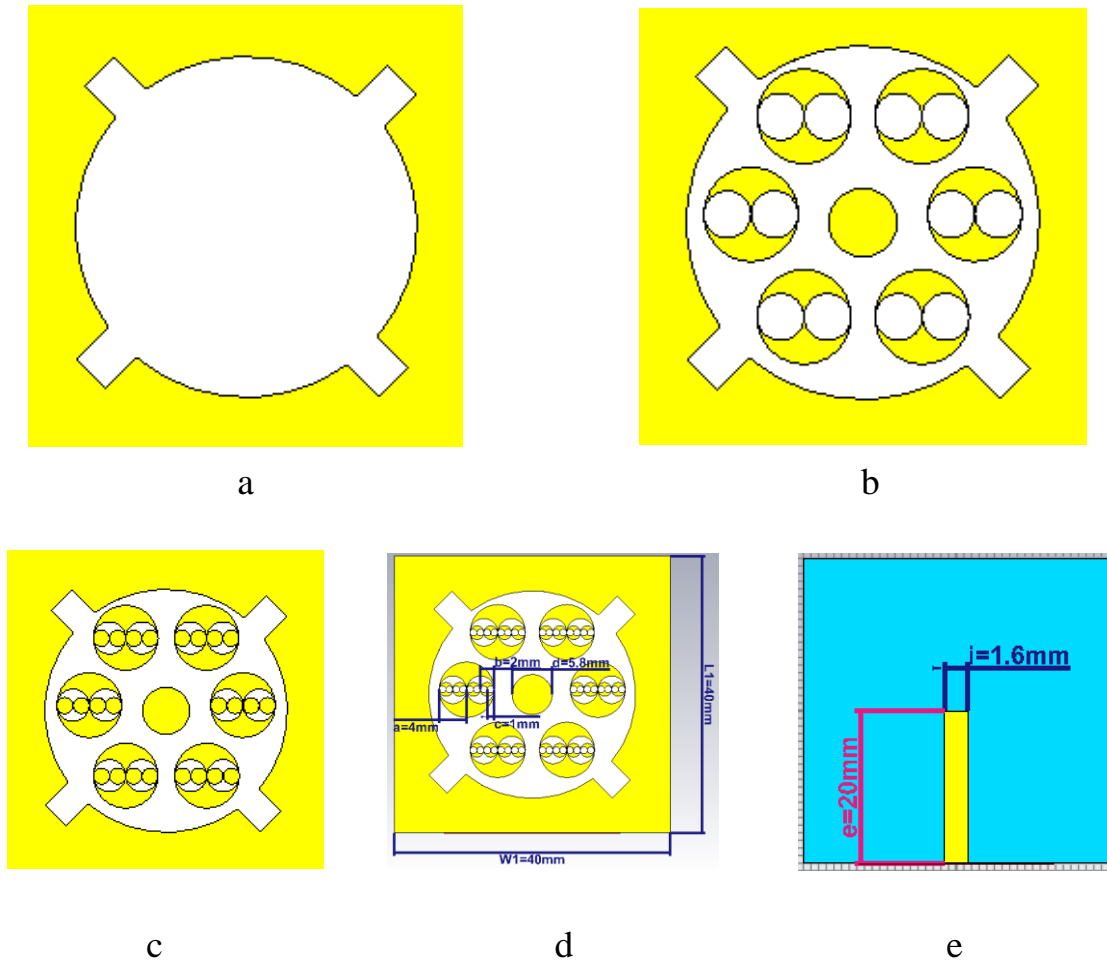


Fig.3.14: The design steps of the proposed antenna at the front view (a) initial state (b) first iteration (c) second iteration (d) third iteration (e) back view

Table-3.4: The Dimensions of the Proposed Antenna

Parameter	Dimensions(mm)	Symbols
The width and length of substrate	40	W1=L1
The width and length of the ground	40	W2=L2
The radius of circular at the 1st iteration	4	a
The radius of a circular slot at the 2nd iteration	2	b
The radius of circular at the 3rd iteration	1	c
The diameter of center desk	5.8	d
The length of the feeding line	20	e
The width of the feeding line	1.6	i

CHAPTER FOUR

RESULTS AND DISCUSSIONS

4.1 Introduction

This chapter will discuss the most important results obtained from the four designs designed in the previous chapter.

It presents a detailed study on each of the proposed fractal antennas for various parameters such as input reflection coefficient, gain, directivity, efficiency and bandwidth. Then a study of adding the metasurface layer to the antenna design to see how to improve the antenna performance and compare the results with ones without metasurface layers.

Also, metasurface unit cells have been analyzed for each proposed antenna to demonstrate that they can offer negative permittivity, permeability, and refractive index at the interesting frequency bands.

4.2 The First Design: The Characteristics of Circular Fractal Slot Antenna without and with Metasurface (CFSAMS) for X and Ku - Band Applications.

4.2.1 The input reflection coefficient of Circular Fractal Slot Antenna without Metasurface

Initially, the fractal antenna was implemented without the metasurface layer as shown in Figure (3.1). Using the CST microwave studio program, the response of this antenna is shown in Figure (4.1), where it is noticed that the resonance frequency is located at (11.18) GHz with the S11 about (-17.82) dB. The bandwidth obtained is (190) MHz ranging from (11.1 to 11.29) GHz.

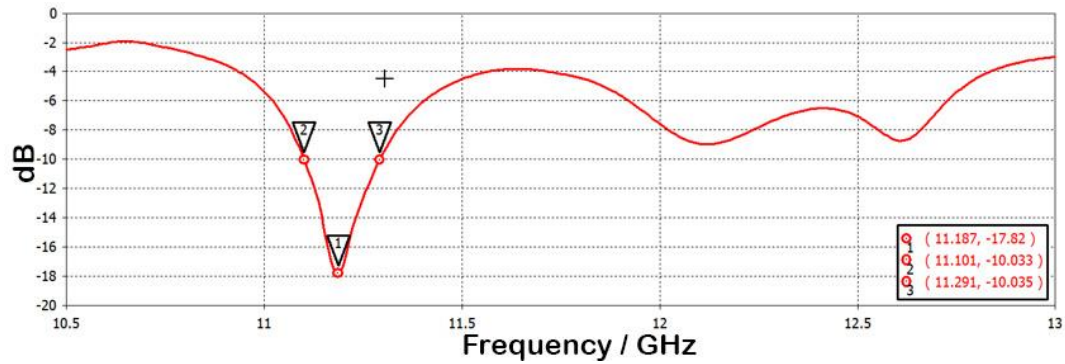


Fig.4.1: The input reflection coefficient of a single circular fractal

4.2.2 The Gain and Directivity of Circular Fractal Slot Antenna without MS

The magnitude of the gain at the resonance frequency is (4.55) dB when implemented separately and before adding the metasurface layer. As for the directivity at the same resonance frequency, it was recorded as (5.76) dBi. Figure 4.2 shows the result of the gain, while Fig.4.3 shows the result of the directivity.

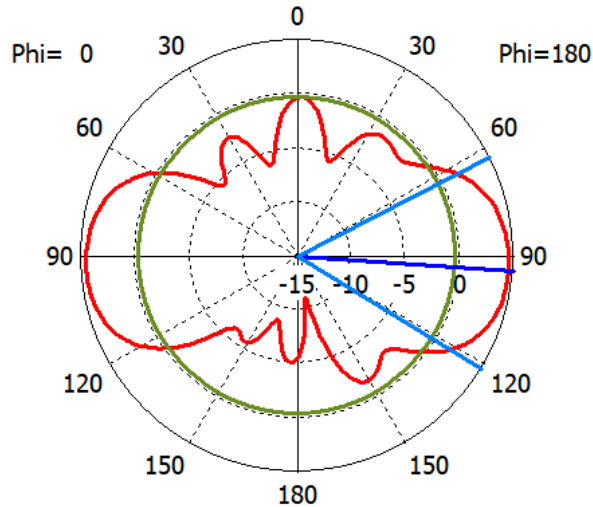


Fig.4.2: The result of the gain at the frequency (11.18) GHz

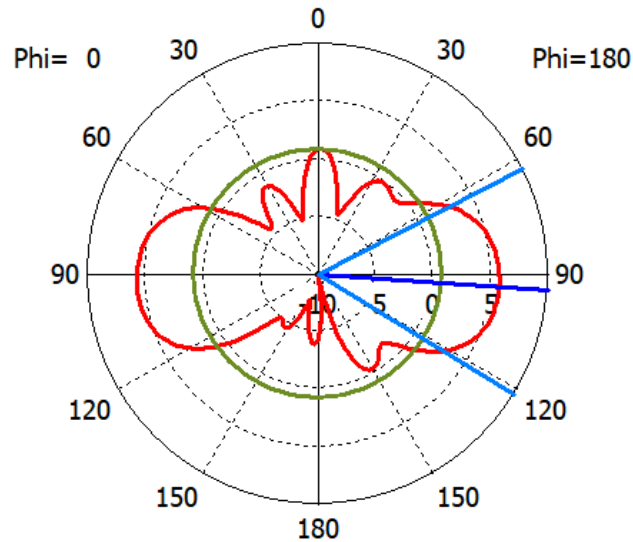


Fig.4.3: The result of the directivity at the frequency (11.18) GHz

4.2.3 The input reflection coefficient of Circular Fractal Slot Antenna with MS

The next step is adding metasurface in front of radiator patch and we observe the changes in the simulated results. A number of unit cells used in each time is changed to check the performance enhancement. As can be seen in figure (4.4) the enhancement is evident in the overall performance and the matching is improved, resulting in dual-band response. The first bandwidth is about (234) MHz at the resonance frequency of (11.23) GHz ranging from (11.1 to 11.3) GHz and the second bandwidth is about of (139) MHz at the frequency of (12.2) GHz ranging from (12.1 to 12.2) GHz. This increment in the bandwidth is attributed to the influence of the air cavity that separates between the MS and the patch antenna.

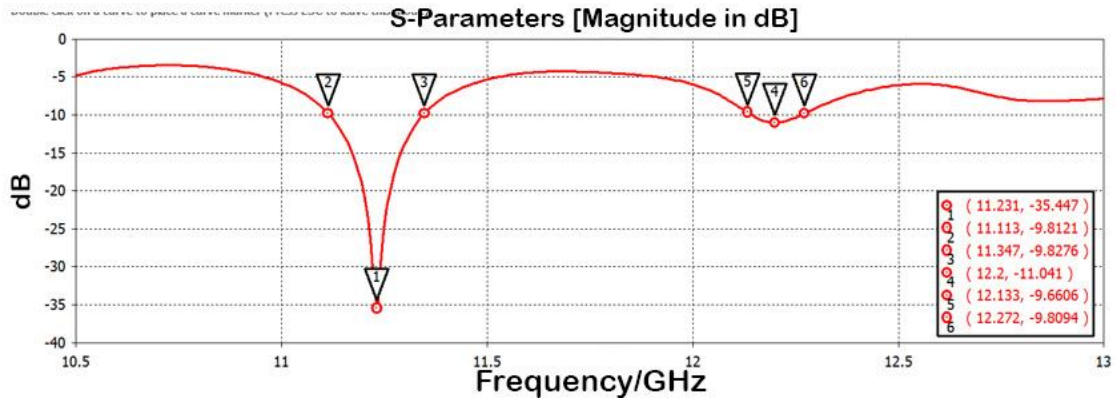


Fig.4.4: The input reflection coefficient when using (3×3) order of MS

4.2.4 The Gain and Directivity of Circular Fractal Slot with Metasurface Antenna (CFSMS)

It is noticed that the gain of the proposed antenna is increased when inserting the metasurface layer with order of (3×3) unit cells to the design. The gain is indicated as (6.05) dB at the resonance frequency of (11.2) GHz while it is about (6.4) dB at (12.2) GHz. Figure 4.5 shows the relation between gain and frequency when using (3×3) unit cells of MS.

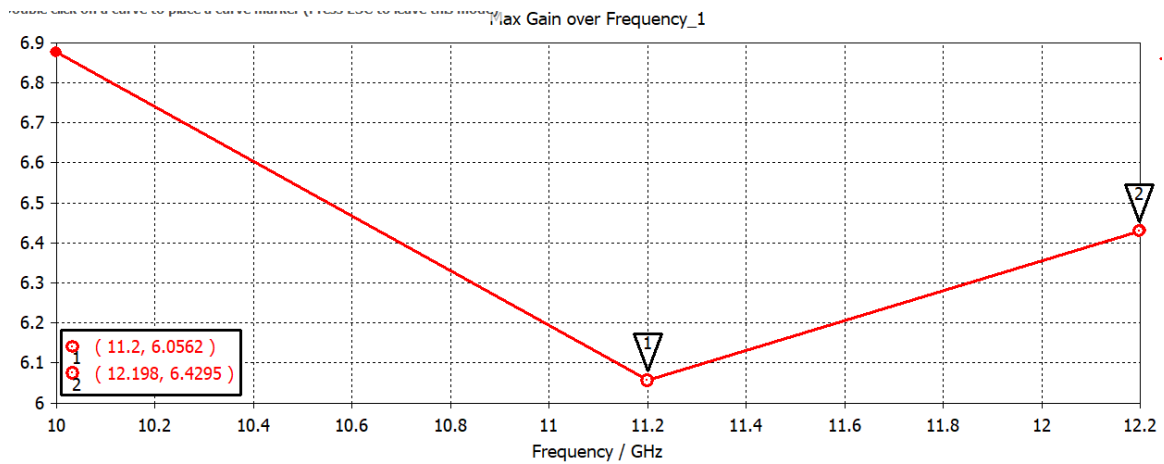


Fig.4.5: The relationship between gain and frequency after adding (3×3) cells of MS

The directivity is also varied where it is about (6.76) dBi at the resonance freq. (11.2) GHz and (6.95) dBi at the freq. (12.2) GHz. Figure 4.6 displays results of the directivity.

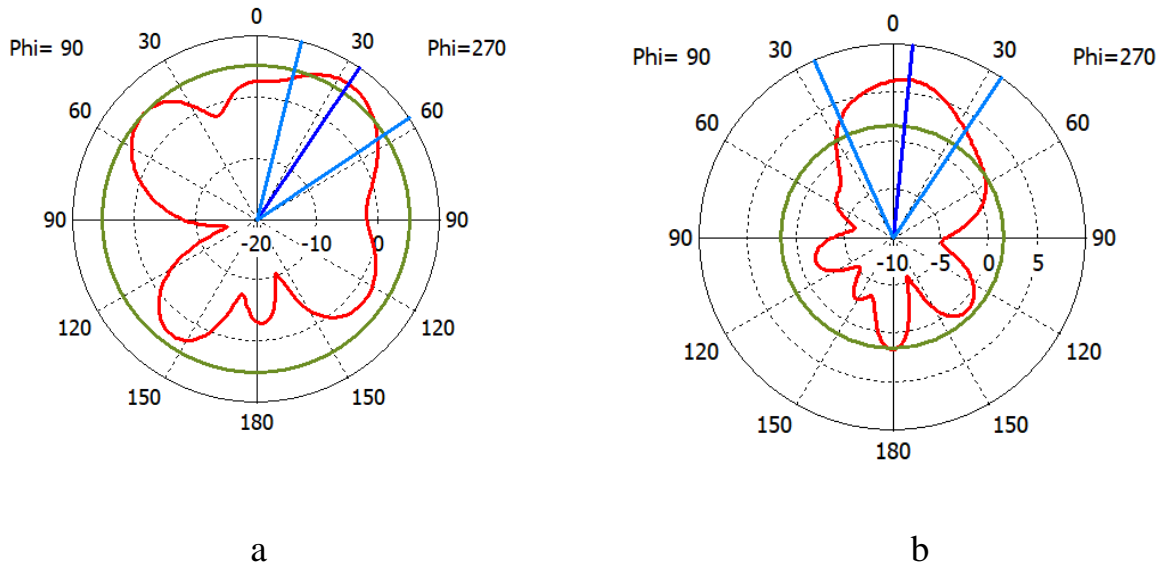


Fig.4.6: The results of directivity (a) at the (11.2) GHz (b) at the (12.2) GHz

Another case was studied in terms of the difference in a number of unit cells. In this time, (5×5) unit cells are used and the results obtained offers dual-bands as well. The first band is at the frequency of (11.14) GHz and the second band is at the frequency of (12.3) GHz. The bandwidth at the first band is (400) MHz ranging from (10.9 to 11.3) GHz while the second band is (300) MHz ranging from (12.1 to 12.4) GHz. Figure 4.7 presents the input reflection coefficient when using (5×5) unit cells.

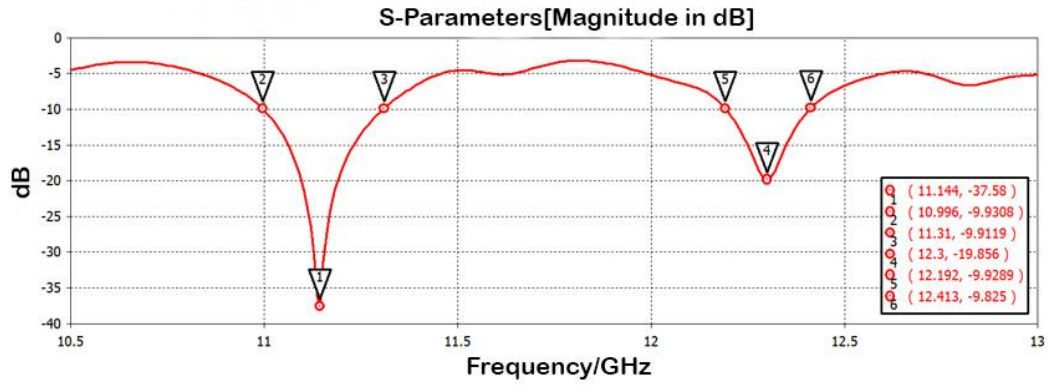


Fig.4.7: The input reflection coefficient when used (5×5) cells of MS

As for the gain, it was noticed that the gain at (11.14) GHz is (7.6) dB while the gain at (12.3) GHz is (8) dB as shown in figure 4.8. The previous results provided a good solution to increase the gain without using arrays. The proposed procedures are very easy compared to arrays especially the complexity of the feeding circuit in arrays.

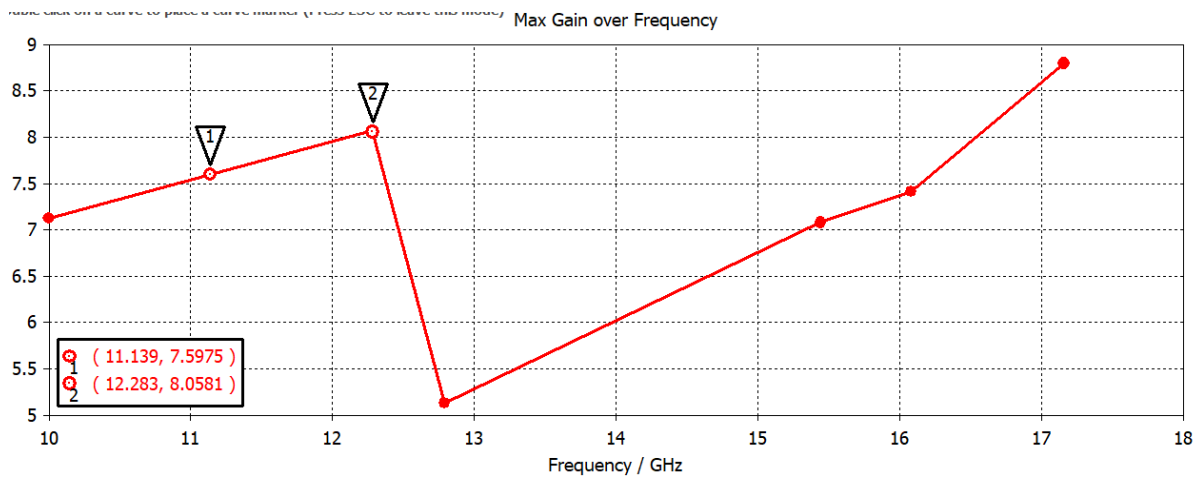


Fig.4.8: Demonstrates the relationship between gain and frequency when using (5×5) cells of MS

The directivity is also varied which is about (8) dBi at the resonance frequency of (11.14) GHz and (8.6) dBi at the frequency of (12.3) GHz. Figure 4.9 displays the results of the directivity. So the efficiency of the antenna is 95% according to (A.4)

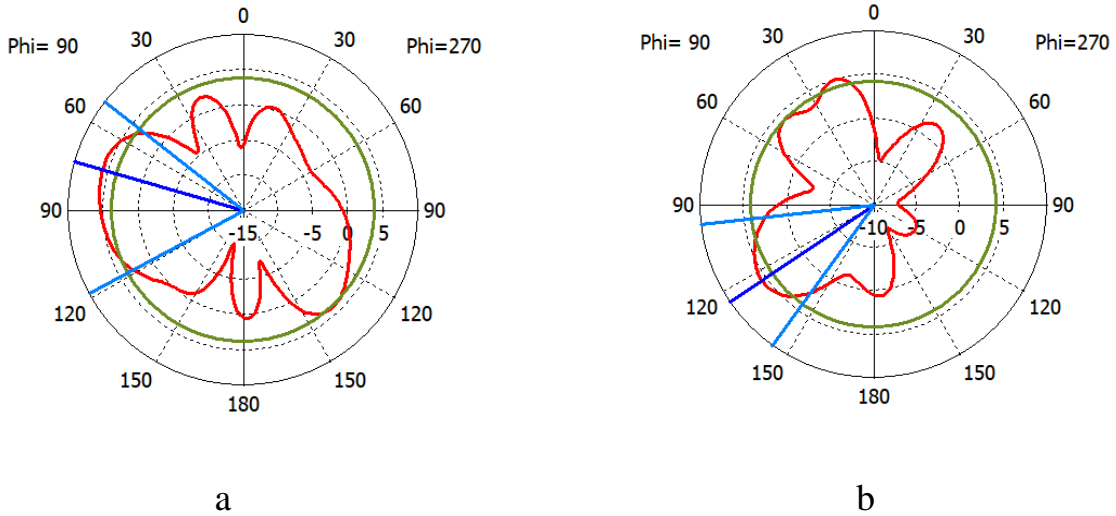


Fig.4.9: The results of directivity (a) at the (11.14) GHz (b) at the frequency (12.3) GHz

After studying the effect of a number of unit cells on the gain and bandwidth of the proposed antenna. Now let us study the influence of the air distance that separates between the circular slot and the MS plate at (1, 2 and 3) mm. Figure 4.10 and figure 4.11 exhibit the bandwidth and gain for each distance.

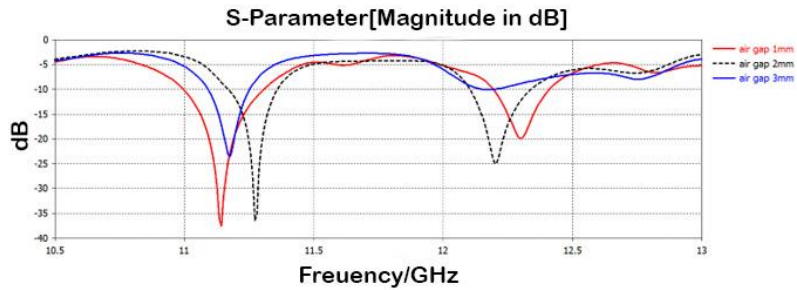


Fig.4.10: The input reflection coefficient at each state

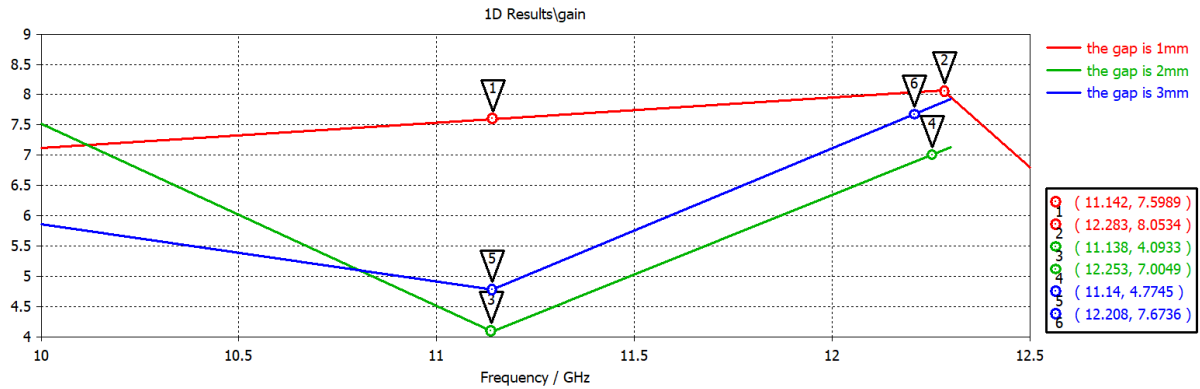
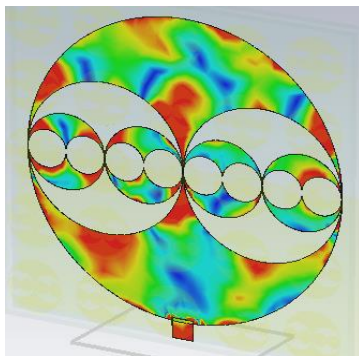


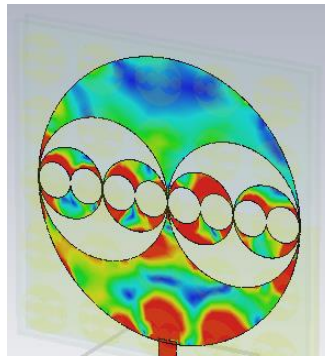
Fig.4.11: The gain at each gap

From the previous results it is observed that the widest bandwidth and highest gain are achieved a gap of 1 mm. The capacitance effects of the gap that separates between the substrate layer hosting the metasurface and the circular slot are decreased at large distances. It is known as the circular fractal antenna has inductance properties so the cancellation process of this effects is reduced at a large distance.

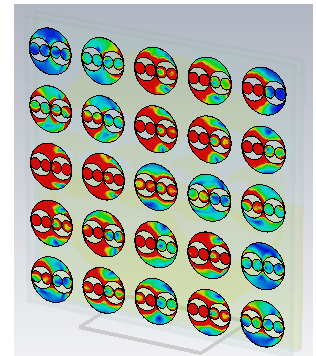
To show our characteristics of the proposed antenna more clearly, figure 4.12 displays the current distribution simulated at (11.14) and (12.3) GHz at different cases. The red color area indicates a higher current density, where it is noticed that the highest current density is distributed around the slot and the feeding line.



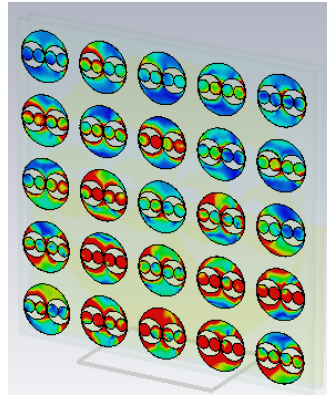
a (11.14) GHz



b (12.3) GHz



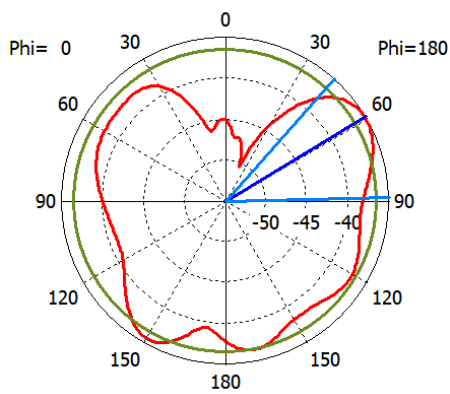
c (11.14) GHz



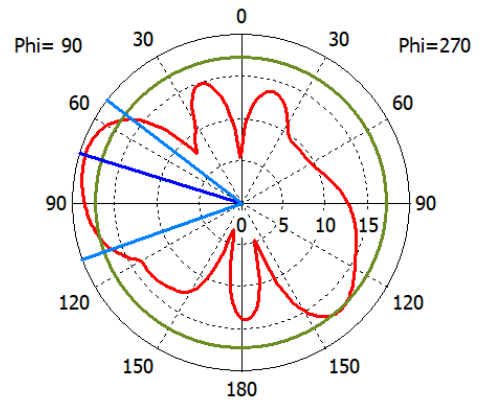
d (12.3) GHz

Fig.4.12: The cases of the current distribution a (at 11.14 GHz) b (at 12.3 GHz) c (5×5 MS at 11.14 GHz) d (5×5 MS at 12.3 GHz)

Figure (4.13) displays the radiation pattern of the overall electric field in (x-z) plane and (y-z) plane at the two center frequencies (11.14) and (12.3) GHz.



(x- z) plane



(y- z) plane

a

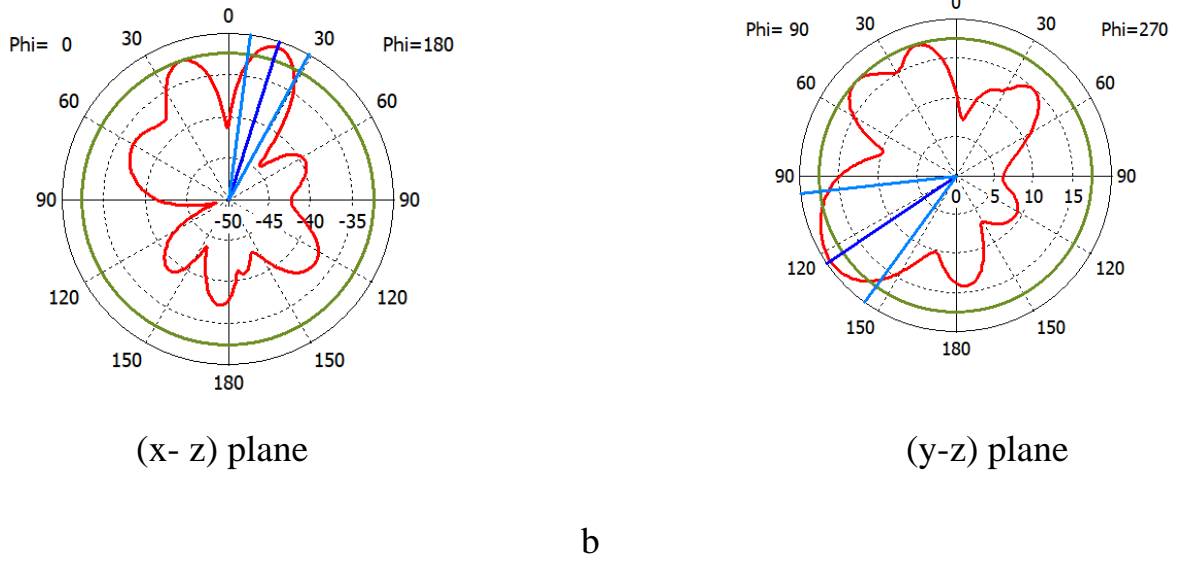


Fig.4.13: Radiation patterns of the electric field of the proposed antenna (a) at the (11.14) GHz (b) (at 12.3) GHz

In this part, the analysis of the metasurface layer is carried out. If using a big number of unit cells, the process will be time-consuming, so a single unit cell with periodic boundary conditions is examined. The boundary conditions are set to be a perfect electric conductor (PEC) in y-axes, perfect magnetic conductor (PMC) in x-axes, and open space in z-axes, as seen in figure 3.4.

From the figures 4.14, 4.15 and 4.16, it can be observed that values of permittivity and permeability are negative at the resonance frequencies (11.14) GHz and (12.3) GHz respectively resulting in that negative refractive index. Negative refraction index is an important parameter, proving that the antenna radiation beam becomes narrower, thereby increasing the gain of the proposed antenna.

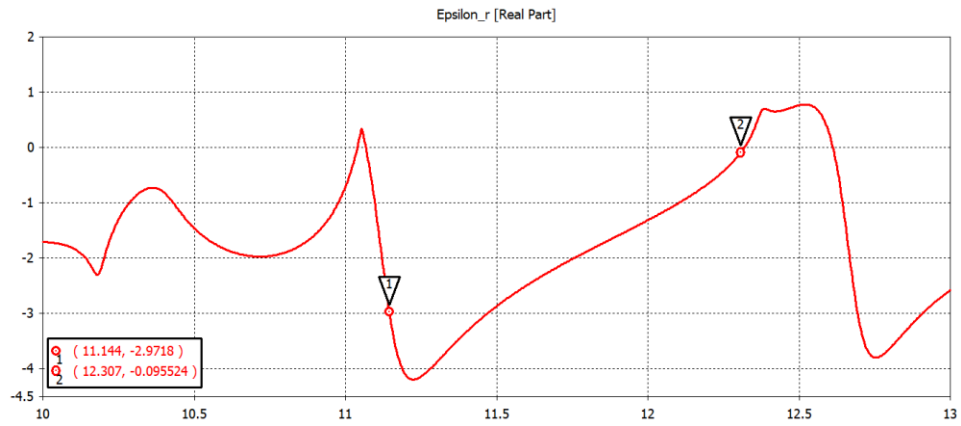


Fig.4.14: The negative values of permittivity at the center frequencies

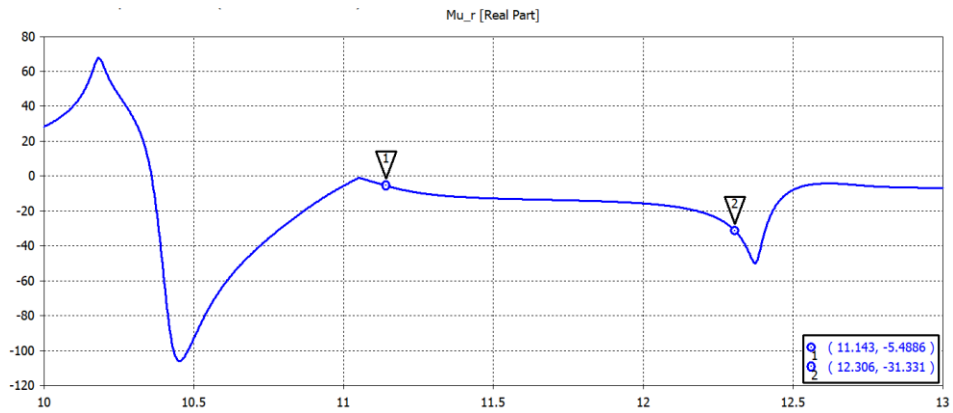


Fig.4.15: The negative values of permeability at the resonance frequencies

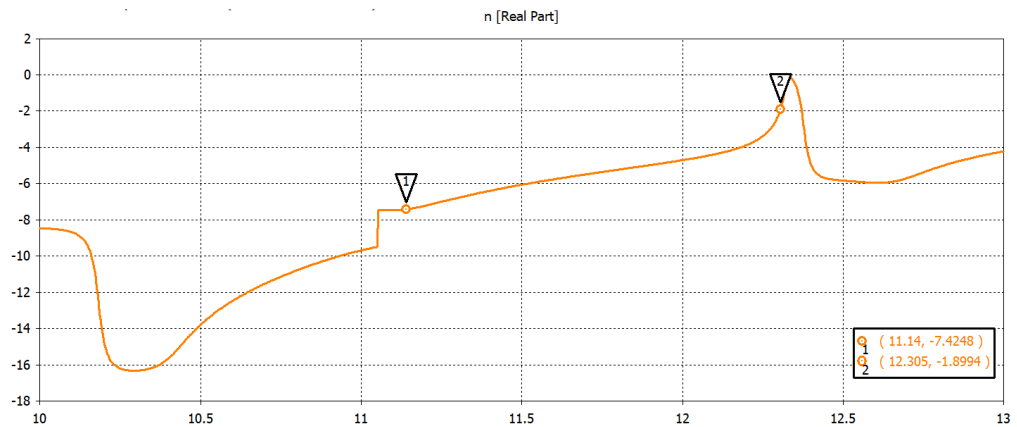
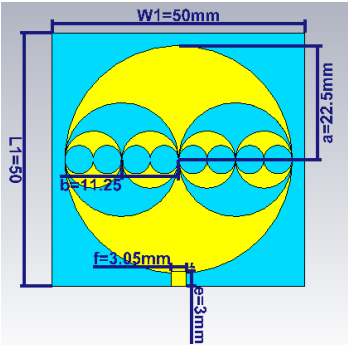
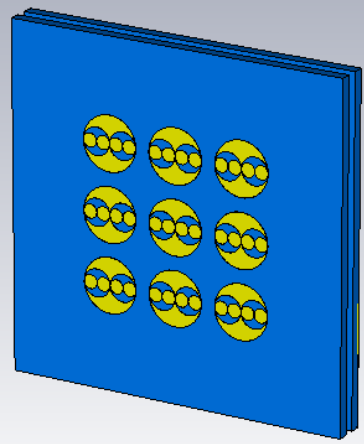
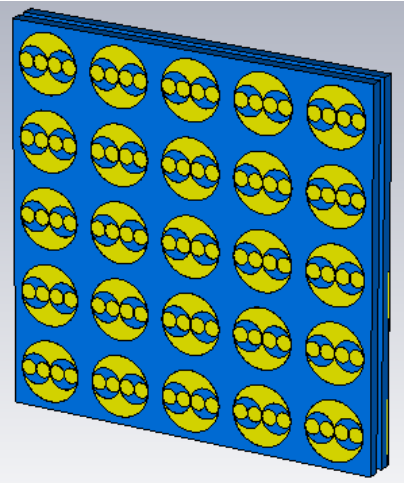


Fig.4.16: The negative refraction index at the center frequencies

Table 4.1 offers the comparison of all parameters at each study of the circular fractal MS antenna.

Table-4.1: Comparison between Results of Three Cases

	Directivity	gain	Resonance frequency	BW(MHz)	S11 dB
 <p>Without metasurface</p>	5.76 dBi	4.55 dB	11.18 GHz	190	-17.8
 <p>3×3 unit cell</p>	6.76 dBi 6.95 dBi	6.05 dB 6.4 dB	11.23 GHz 12.2 GHz	234 139	-35 -11

 <p>5×5 unit cells</p>	8 dBi	7.6	11.14 GHz	400	-37
	8.6 dBi	dB	12.3 GHz	300	-19
		8 dB			

4.3 The Second Design: The Characteristics of Modified Cross Fractal Antenna without and with MS (MCFAMS) for X - Band Applications.

4.3.1 The input reflection coefficient of the Modified Cross Fractal Shape without MS.

Initially, the modified cross fractal antenna was implemented independently to calculate the gain, bandwidth, and directivity. Figure 4.17 shows the input reflection coefficient for this antenna, where the resonance frequency is 8.77 GHz and the obtained bandwidth is ranging from (8.68 to 8.87) GHz which is about 190 MHz, with the input reflection coefficient less than -10 dB located at -24.6 dB.

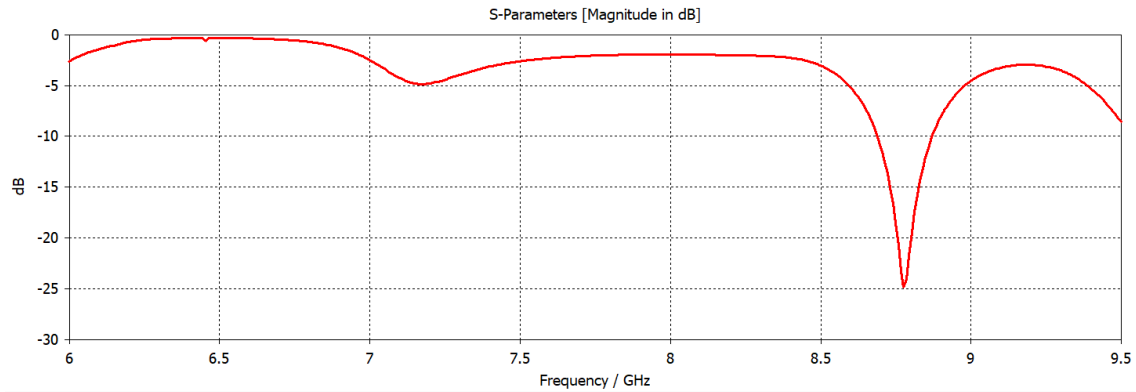
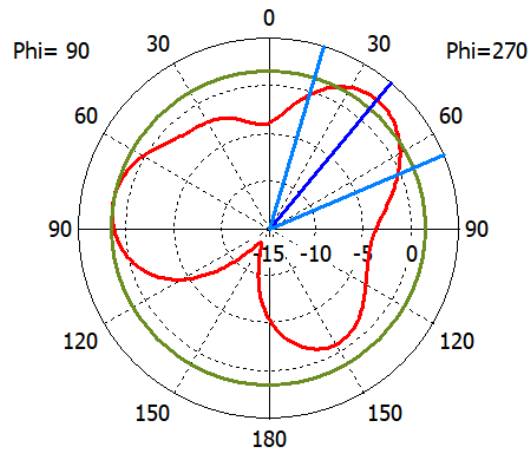


Fig.4.17: The input reflection coefficient of modified cross fractal antenna

4.3.2 The Gain and Directivity of Modified Cross Fractal Shape without MS

The gain achieved by the modified cross shape fractal antenna before applying metasurface is 2.66 dB at the center frequency of 8.7 GHz, while the value of directivity at the center frequency 8.7 GHz is 2.7 dBi. Figure 4.18 (a and b) shows the simulated gain and directivity.



(a)

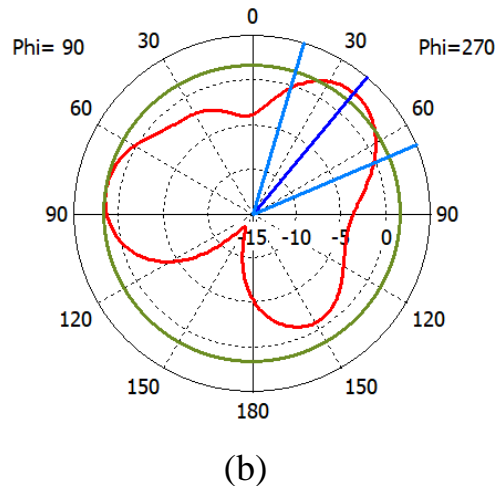


Fig.4.18: Simulated values of (a) the gain at 8.77 GHz, (b) the directivity at 8.77 GHz

4.3.3 The input reflection coefficient of the Modified Cross Fractal Shape with Metasurface

Now let us display the comparison between the simulated results of the only cross and cross integrated with the MS layer. After applying (4×4) unit cells, the resonance frequency is small shifted to 8.9 GHz and the bandwidth is ranging from (8.7 to 9.1) GHz which is about 400 MHz. The impedance bandwidth is improved but this increase is not sufficient so increasing a number of unit cells to (5×5) . The obtained results shows the improvement in the bandwidth to 414.35 MHz owing to the capacitance effects, generated by the space between the antenna which in turn

cancel the inductance influence of the antenna feedline. Figure 4.19 shows that the impedance bandwidth has been widened.

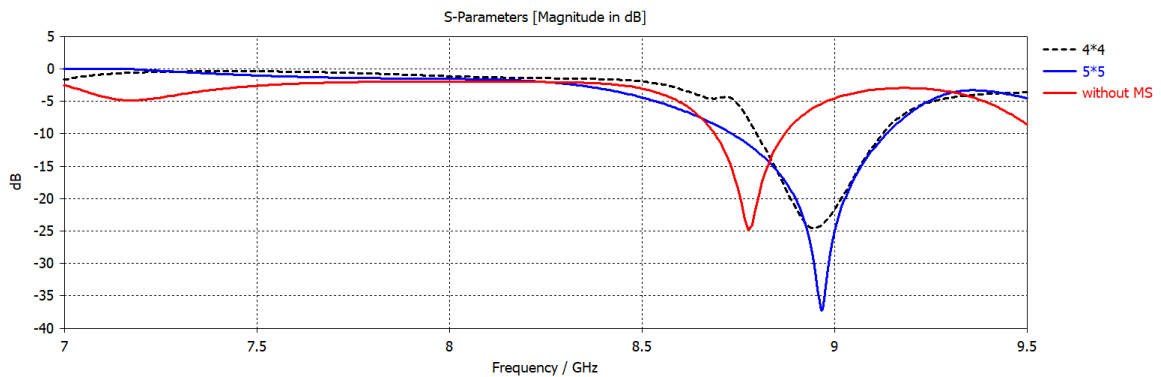


Fig.4.19: The states of simulated input reflection coefficient

4.3.4 The Gain and Directivity of Modified Cross Shape Fractal Antenna with MS

The gain achieved by the modified cross fractal shape after placing the (4×4) unit cells MS layer, (as shown in figure 3.6), is 6.3 dB at a frequency of 8.9 GHz. Then increasing a number of unit cells to (5×5) the gain is improved to 9 dB. The previous-mentioned enhancement is promising to avoid using arrays with multiple antennas to increase the gain. The directivity is also improved from (2.7 to 4.46) dBi at (4×4) unit cells and from (4.46 to 9.04) dBi at (5×5) unit cells. The proposed antenna achieves a good enhancement in the gain, so there is no need to apply another layer of MS. Fig.4.20 portrays the gain over frequency. The efficiency of the proposed antenna is after applying the MS is 99% according to (A.4).

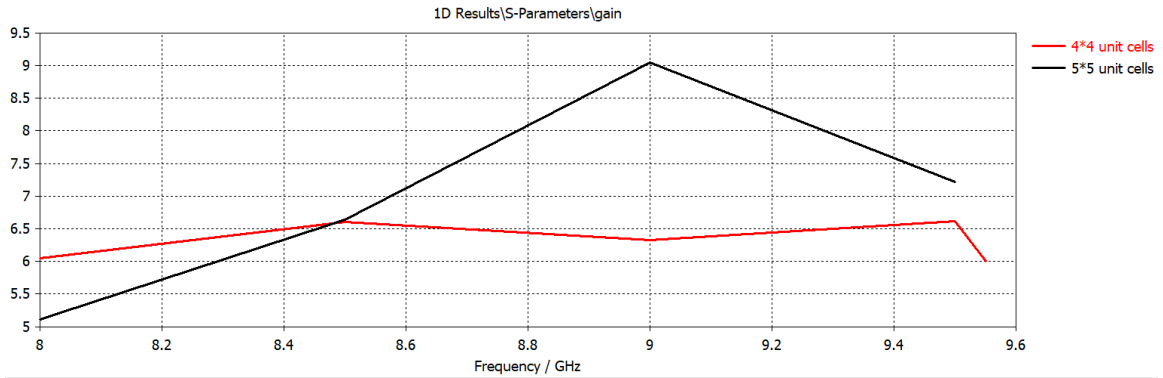


Fig.4.20: The gain over the frequency with different numbers of unit cells

The effect of distance separating between unit cells has been studied taking into account but do not exceed a quarter of the wavelength. It starts from 0.1 mm to 0.3 mm with increasing step of 0.1 mm. We have observed the first state that has the bandwidth of 461.54MHz and the gain of 8.1 dB, while the second state at the distance 0.2 mm has the bandwidth of 322.36 MHz and the gain of 7.8 dB. The case with the distance 0.3 mm has the bandwidth of 414.35 MHz and the gain of 9 dB. Finally, from the results mentioned above, the distance 0.3 mm has the best results according to the gain enhancements. Figure 4.21 shows the comparison between all distances and figure 4.22 presents the gain at each distance.

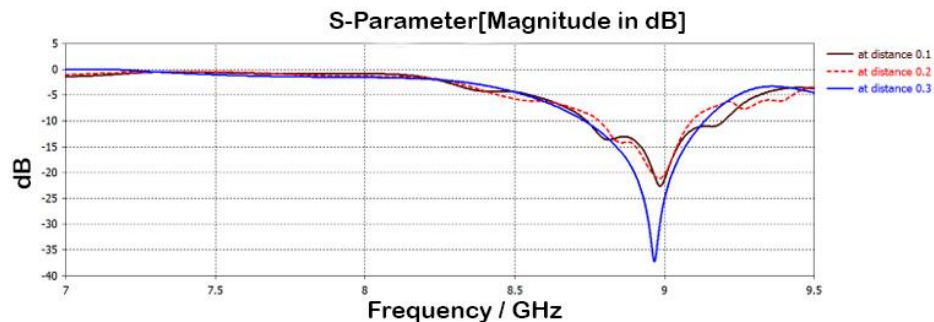


Fig.4.21: The parametric study of the distance between cells

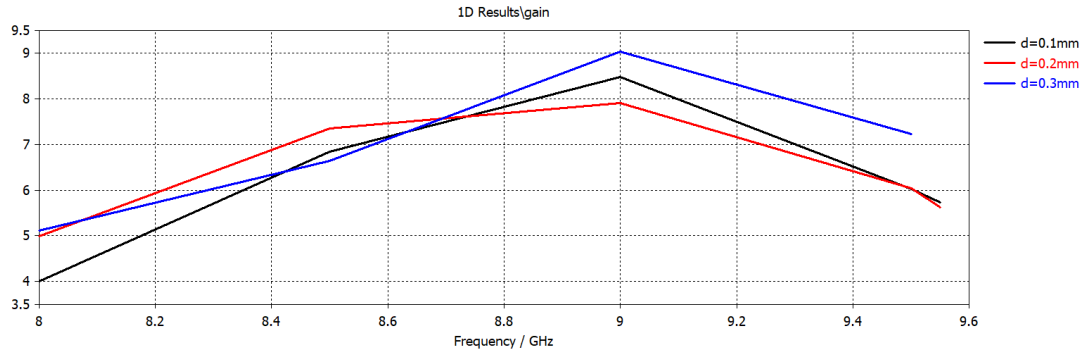


Fig.4.22: The relation between gain and frequency foreach distance

Figure 4.23 (a) illustrates the surface current distribution at the lower layer (modified cross fractal antenna) at a frequency of 8.96 GHz while figure (4-23b) shows the current distribution at the higher layer (MS plate). From the figures, the current is distributed around the antenna side when simulated the fractal antenna without MS. After adding the metasurface, the current is distributed to different areas of the cells.

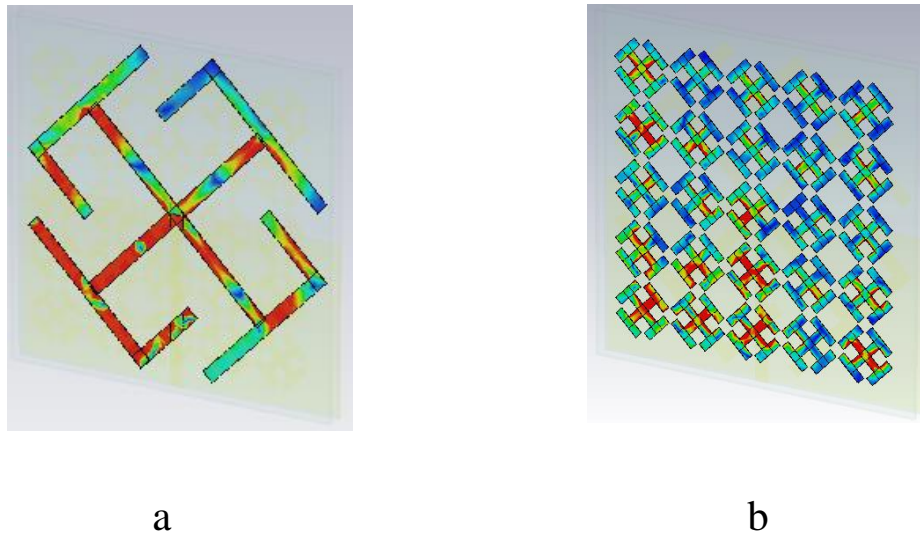
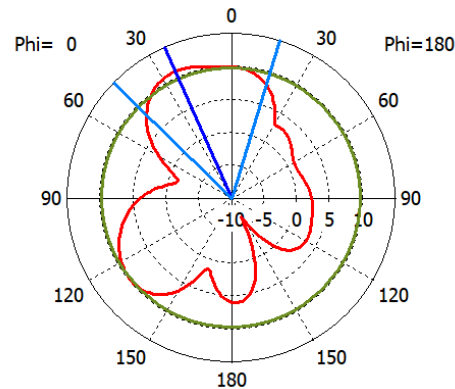
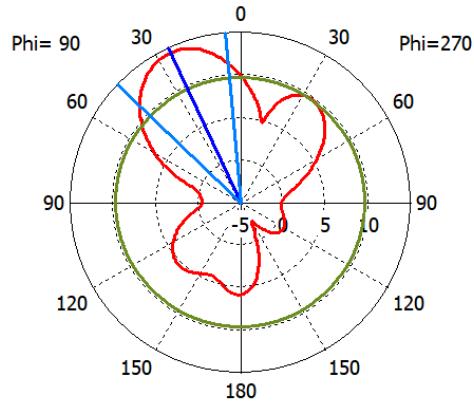


Fig.4.23: The current distribution at the center frequency of 8.9 GHz (a) fractal antenna layer (b) MS layer

The radiation pattern is the graphic representation of radiated energy as a function of direction from the antenna. The radiation pattern is analyzed in this part to understand the radiation activity of the antenna. The (x-z) plane and (y-z) plane are shown in figure 4.24.



a

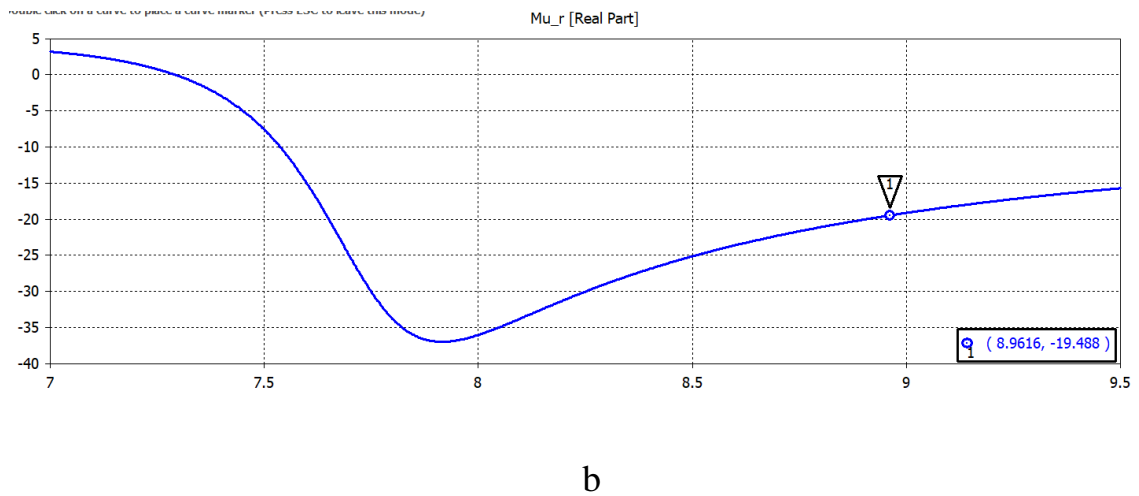
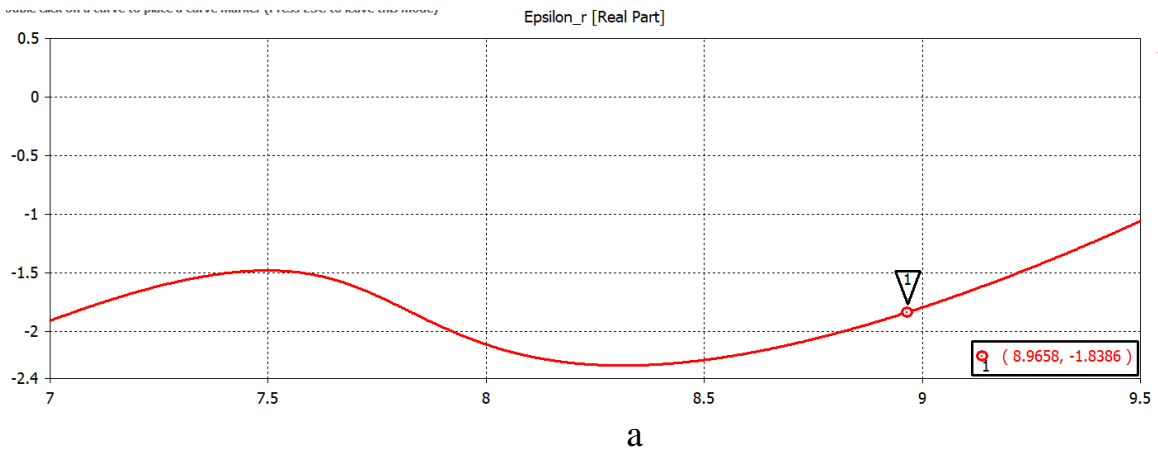


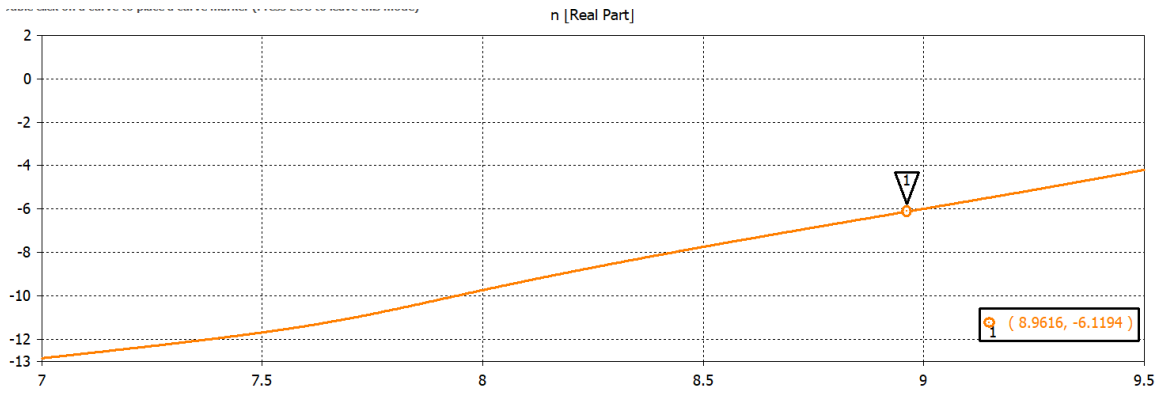
b

Fig.4.24: The radiation pattern at the center frequency (a) (x-z) plane (b) (y-z) plane

To clarify the exceptional properties of the metasurface, the final shape of a single unit cell has been studied to achieve negative values of permittivity,

permeability and refraction index. The waveguide is utilized to analyze the unit cell that is modified cross designed on a substrate layer with dimension of (9×9) mm² and the thickness is 1.6 mm as shown in figure 3.6. One unit cell is analyzed to reduce the time of simulation. The boundary conditions are set as PEC/PMC with two ports. The results obtained shows in figure 4.25 (a, b and c) with negative values of ϵ , μ and n.



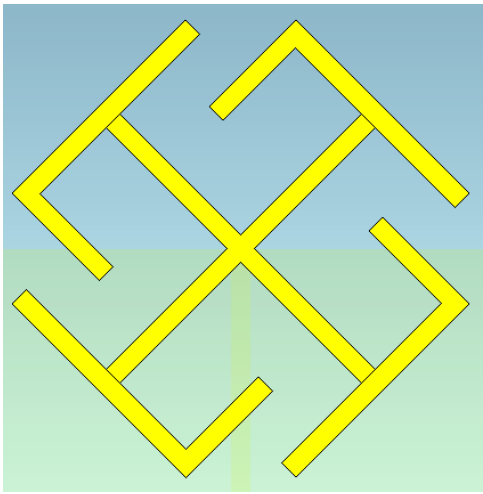


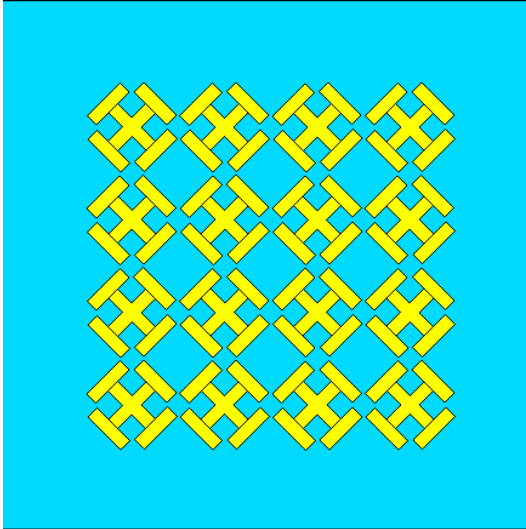
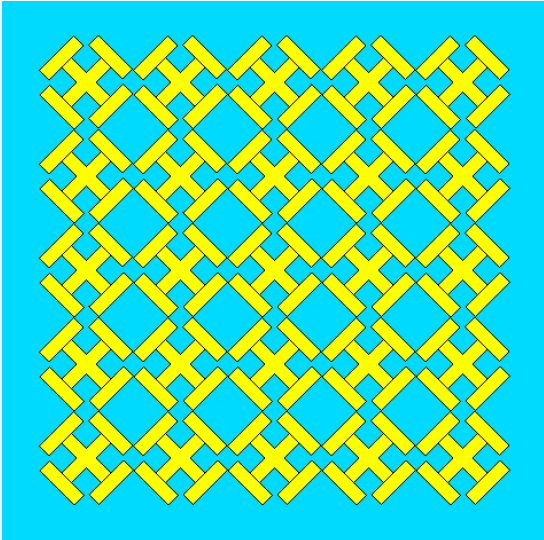
c

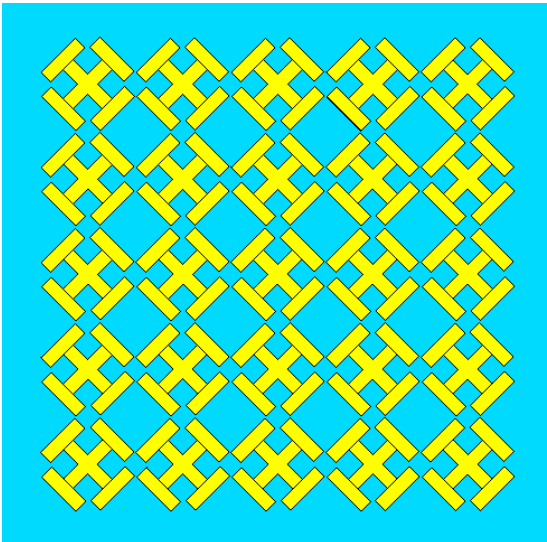
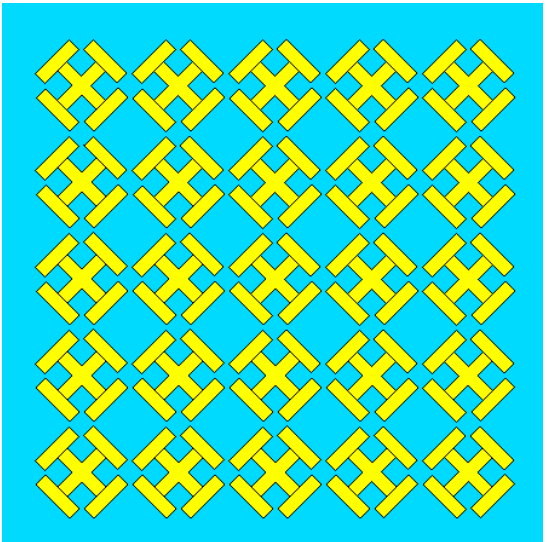
Fig.4.25: The dispersion parameters of MS (a) the real part of ϵ (b) the real part of μ (c) the real part of n

Table 4.2 shows all results for the proposed antenna before and after applying the MS layer at each distance.

Table-4.2: Present the Comparison of all Results of the Second Proposed Antenna

	Gain(dB)	BW(MHz)	Freq.(GHz)	S11 (dB)
 <p>Single cross</p>	2.66	190 MHz	8.77	-24.6

 <p>Modified cross with (4×4)MS</p>	6.3	400 MHz	8.9	-24.5
 <p>Modified cross with (5×5)MS at distance=0.1mm</p>	8.1	461.54 MHz	8.9	-22

 <p>Modified cross with (5×5)MS at distance=0.2mm</p>	7.8	322.36 MHz	8.9	-21
 <p>Modified cross with (5×5)MS at distance=0.3mm</p>	9	414.35 MHz	8.9	-37

4.4 The Third Design: The Characteristics of Minkowski Fractal Slot Antenna without and with Metasurface (MFSAMS) for C-Band Applications.

4.4.1 The input reflection coefficient of Minkowski Fractal Slot antenna without MS

When the fractal shape is simulated without the metasurface, the antenna covers the range of frequencies from (4.5448) to (5.5139) GHz and has resonance frequency at 5.1 GHz. The bandwidth is about 969.1 MHz and the S-parameter is (-16) dB. Figure 4.26 shows input reflection coefficient of the proposed antenna without MS.

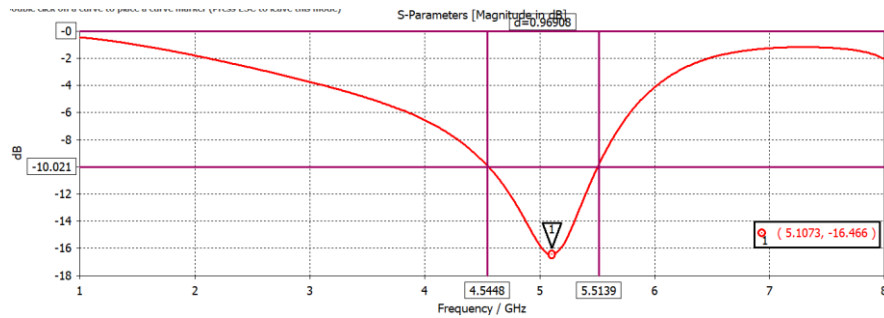
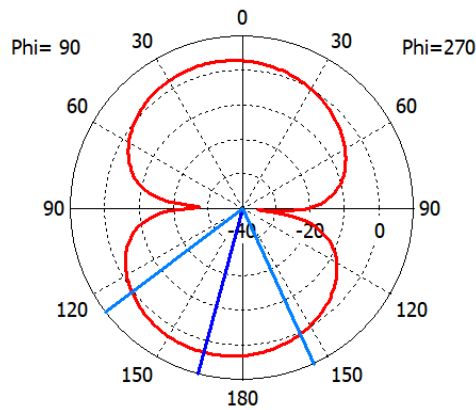


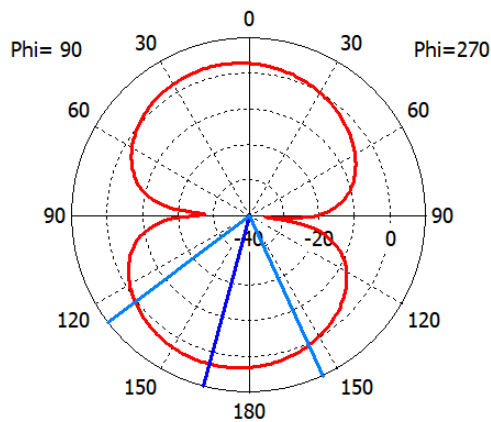
Fig.4.26: The input reflection coefficient of the Minkowski fractal slot antenna without MS

4.4.2 The Gain and Directivity of Fractal Shaped Minkowski Slotted without MS

Figure 4.27 (a, b) illustrates the gain and directivity of the proposed antenna at the resonance frequency before adding the MS layer, where the value of gain is about (3.32) dB and the directivity is about (3.4) dBi at 5.1 GHz.



(a)



(b)

Fig.4.27: The gain and directivity (a) the gain at (5.1) GHz (b) the directivity at (5.1) GHz

4.4.3 The Input Reflection Coefficient of Minkowski Fractal Slot Antenna with MS

The metasurface layer is applied to the Minkowski fractal slot antenna with a different number of rectangular closed ring resonators to improve the gain and bandwidth. The states that were studied (3×3), (4×4), (5×5) and (6×6) unit cells. The simulated results show the best state with (6×6) unit cells because the bandwidth is

enhanced from 969.1 to 1,670 MHz ranging from (3.8 to 5.47) GHz. The matching is also improved from (-16 to -27) dB. Figure 4.28 shows the response of the antenna when adding MS.

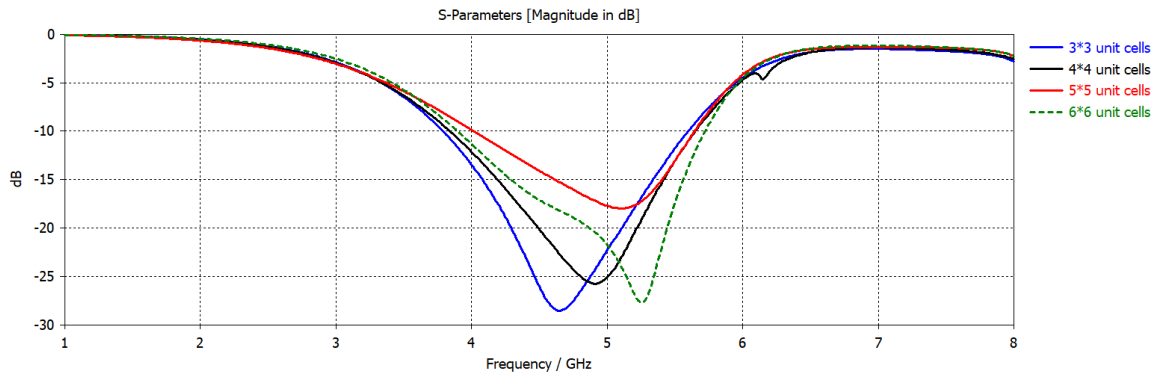


Fig.4.28: The input reflection coefficient when adding MS to the proposed antenna

4.4.4 The Gain and Directivity of Minkowski Fractal Slot Antenna with MS

According to the results shown in figure 4.29, the increase in a number of cells leads to high gain because the electromagnetic waves when they leave the antenna will be focused due to the MS layer and consequently propagate with narrow beams, which leads to increased gain and directivity. At (6×6) unit cell the gain is increased from 3.32 dB to 4.89 dB at the resonance frequency of (5.25). The main purpose of using MS is to improve the gain by 1.58 dB. Figure 4.29 shows the gain in each case.

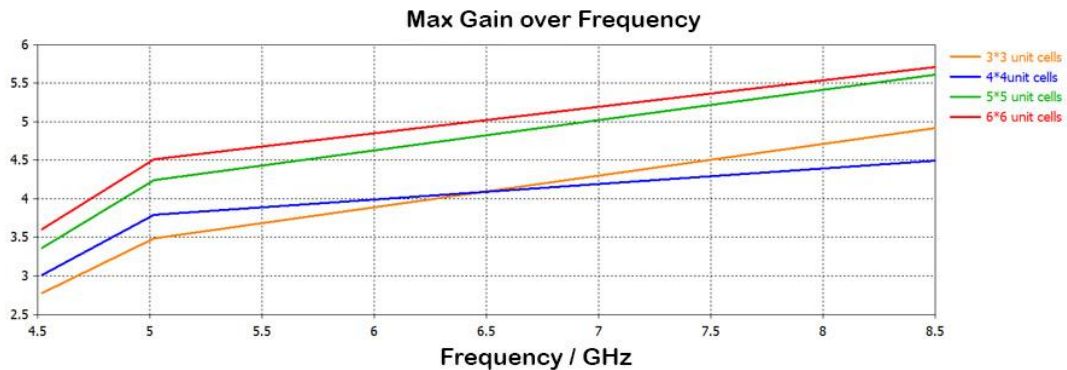


Fig.4.29: The gain of the proposed antenna

The directivity of the Minkowski fractal slot antenna when applying MS is 4.9 dBi at the resonance frequency (5.25) GHz. As shown in Figure 4.30. Thus the efficiency is 99% at 5.25 GHz according to (A.4).

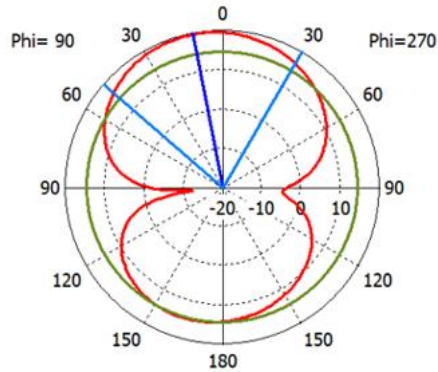


Fig.4.30: The directivity at the (5.25) GHz

Another case was studied when placing the radiator part above the metasurface layer and observing the bandwidth which is decreased to 990.9 MHz because a bandwidth of the antenna system is relied on the bandwidth of the MS structure. Figure 4.31 and figure 4.32 show the bandwidth and gain for this case.

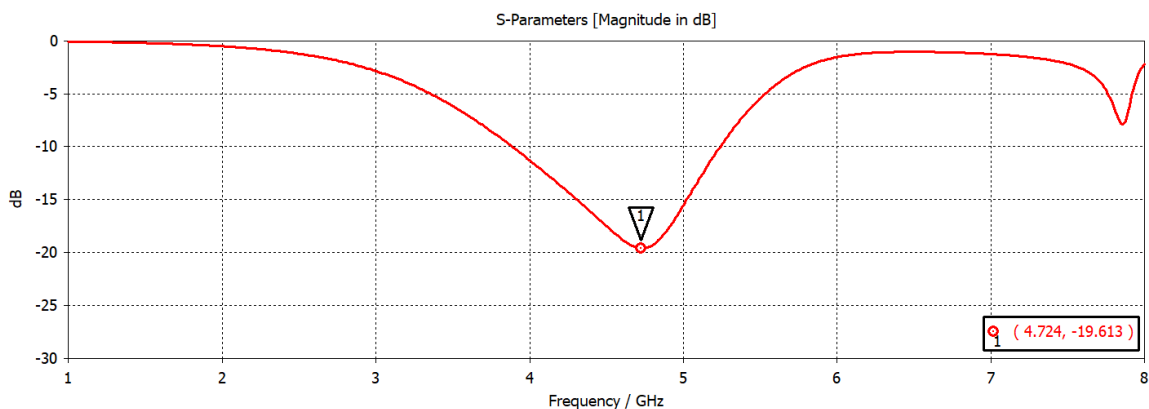


Fig.4.31: The simulated input reflection coefficient when placing the radiator part above the MS

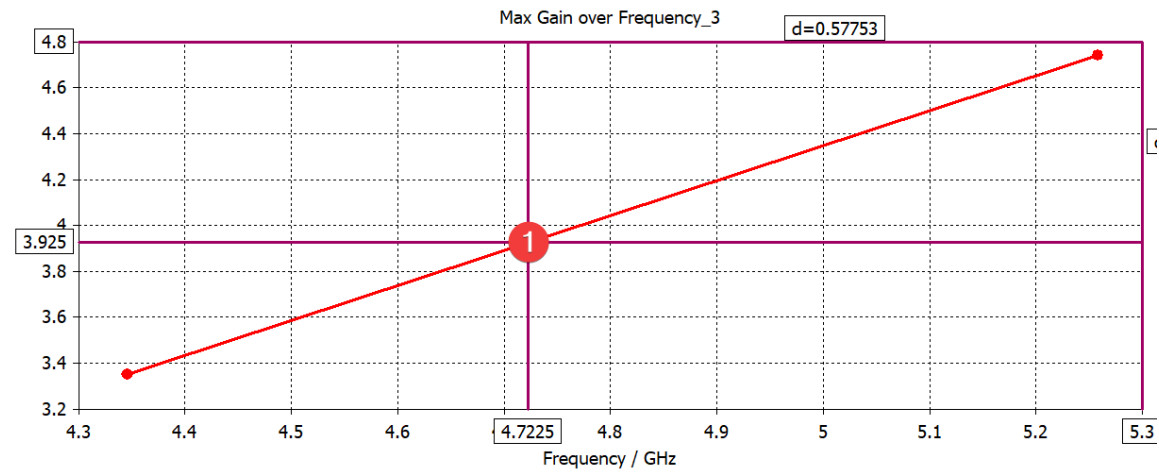


Fig.4.32: The relationship between the gain and frequency when placing the radiator part above MS

The addition of another layer of metasurface to the design is analyzed and its impact on the antenna gain is observed. An increase in gain from the one-layer state by is 1.11 dB according to the same reasons mentioned when adding one layer of MS, but its effect increases when adding another layer. Figure 4.33 displays the magnitude of gain after adding a second layer of MS.

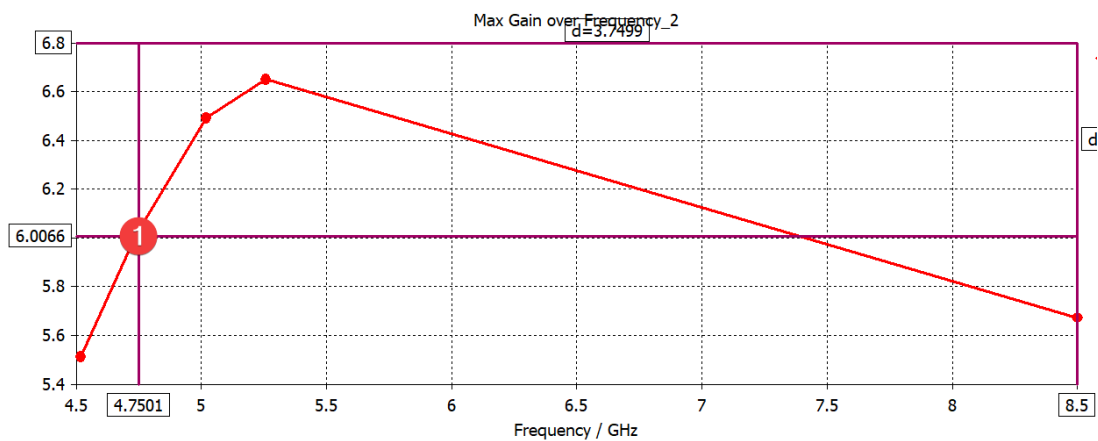


Fig.4.33: The gain over frequency when using double layers of MS

Figure 4.34 shows the current distribution before and after adding MS plate and we have that noticed the current was distributed around the slots and feeding line.

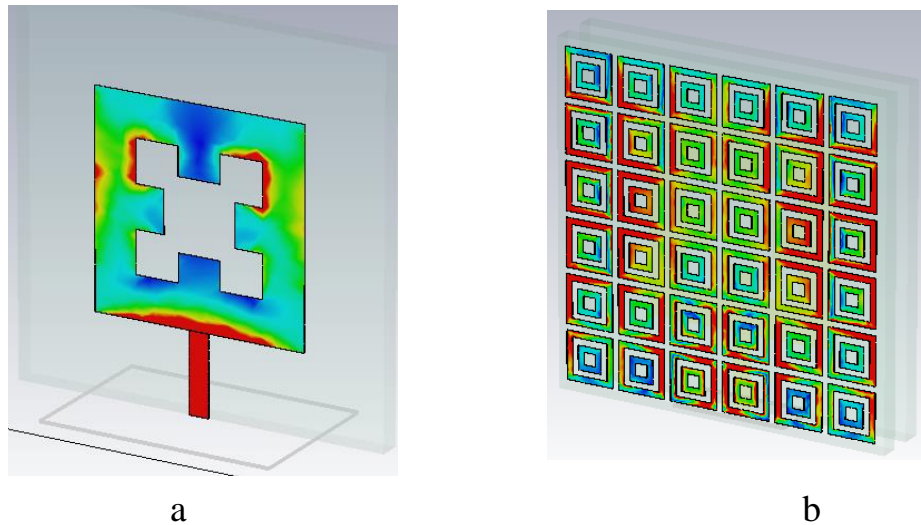
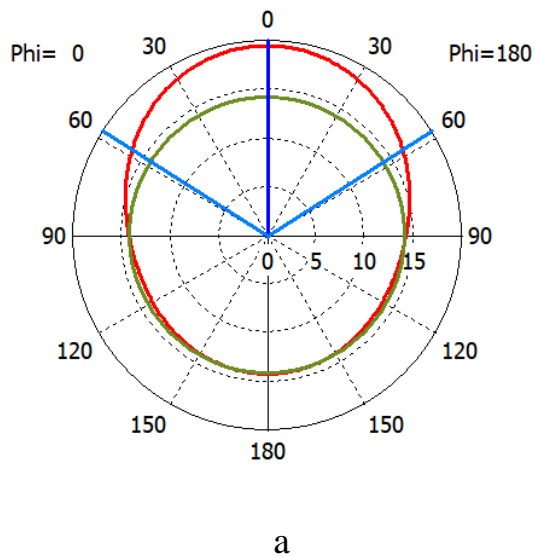


Fig.4.34: The current distribution (a) before adding MS (b) after adding MS

Figure 4.35 shows the radiation pattern of the Minkowski fractal slot antenna with MS at the resonance frequency of (5.25) GHz. The antenna has the unidirectional pattern in (x-z) plane and a bidirectional pattern in (y-z) plane.



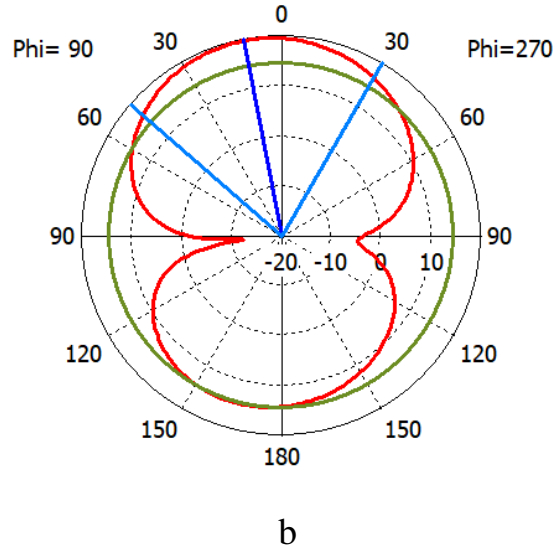


Fig.4.35: The radiation pattern of the antenna at (5.25) GHz (a) (x-z) plane
(b) (y-z) plane

The analysis of the metasurface plate is carried out. The generation of double closed rectangular ring resonator is explained in chapter three. The dimensions of this cell shown in fig.3.9. The boundary conditions are set as PEC/PMC and open space in the z-axis.

From figures (4.36-4.38), one can notice that the permittivity (ϵ), permeability (μ) and refractive index (n) are negative values at the resonance frequency of 5.25 GHz. Due to these negative values, the propagation of the wave is in the reverse direction. The Minkowski fractal slot antenna with MS achieves left-handed behaviour when simulating single unit cell.

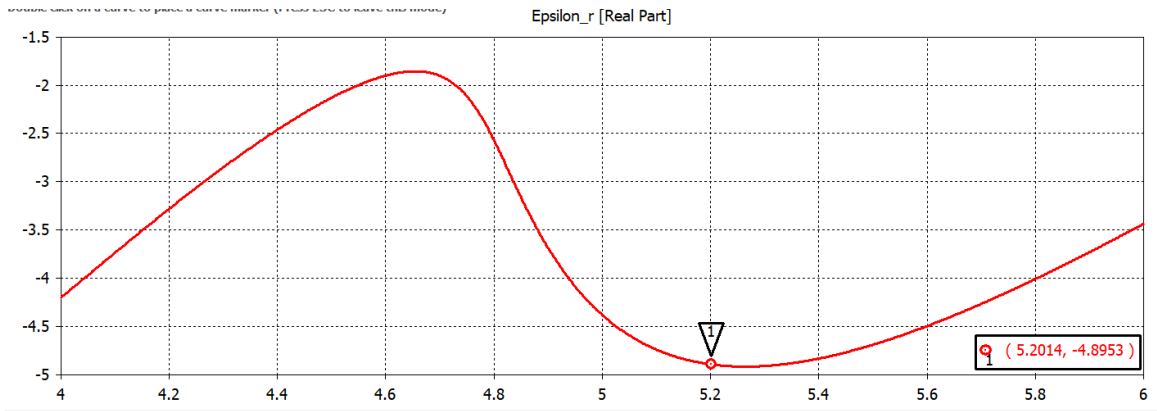


Fig.4.36: The permittivity response

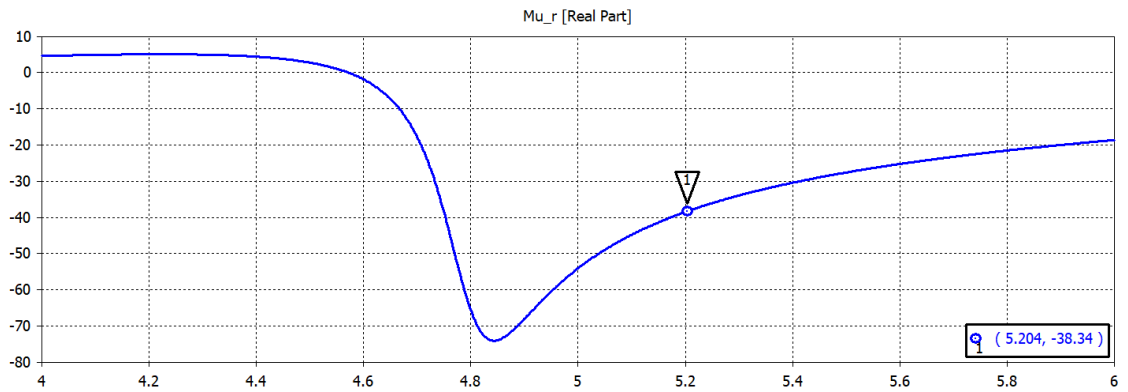


Fig.4.37: The permeability response

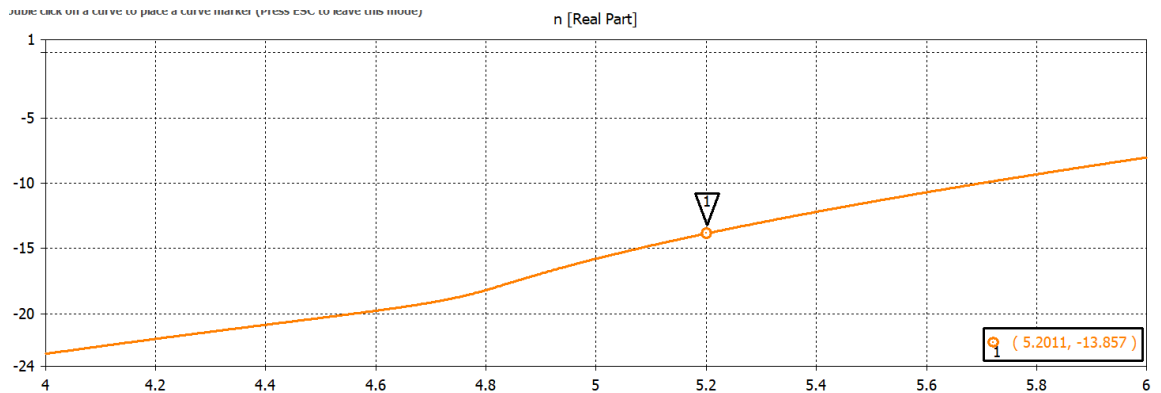
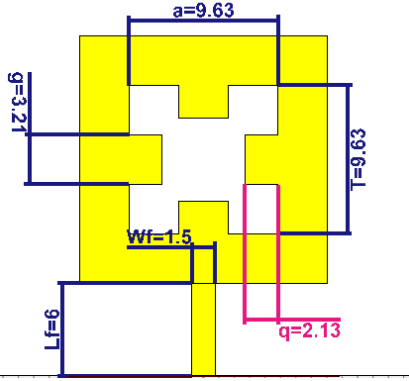
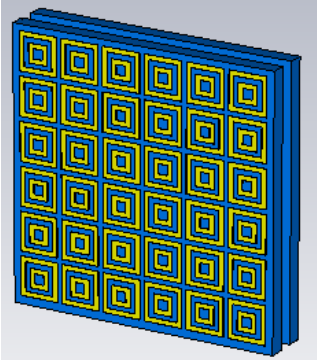
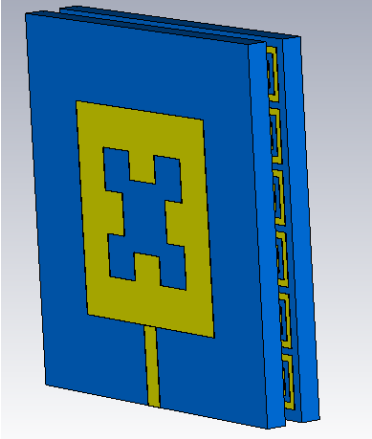
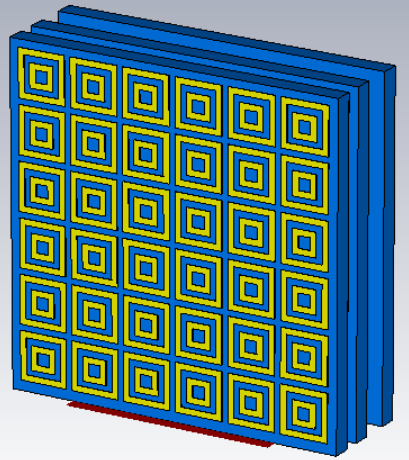


Fig.4.38: The refractive index response

Table 4.3 shows and compares all the results obtained for the antenna before and after adding the MS layer to it.

Table-4.3: Comparison between the Proposed Antenna at Four Cases

	Directivity	Gain dB	BW(MHz)	Resonance frequency	S11 dB
 <p>This work without MS</p>	3.4 dBi	3.32 dB	969.1	5.1 GHz	-16
 <p>This work with 6×6 unit cells the MS above the radiator element</p>	4.9 dBi	4.89 dB	1670	5.2 GHz	-27

 <p>This work with 6×6 unit cells the radiator element above the MS</p>	4.05 dBi	3.925 dB	990.9	4.7 GHz	-19
 <p>This work with double MS layer</p>	6.02 dBi	6 dB	1224.5	4.7 GHz	-11

4.5 The Fourth Design: The Characteristics Multiband Compact Microstrip Circular Slot Fractal MS Antenna (MCMCSFMS) for C and S – Band Applications.

4.5.1 The input reflection coefficient of Multiband Compact Microstrip Circular Slot Fractal MS Antenna

The antenna response is studied from the initial state to the third iteration where the following is observed. In the initial case, the antenna has three resonance frequencies at (3.03, 4.1 and 5.9) GHz with bandwidth is (406.16, 162.08 and 739.56) MHz, respectively. In the first iteration, it is noticed that the three resonance frequencies have shifted to (2.8, 3.9 and 5.5) GHz and the bandwidth is (721.08, 448.51 and 388.45) MHz, respectively. After repeating the procedure to make the second iteration, it is also noticed that there are three resonance frequencies at (2.8, 3.9 and 5.5) GHz with the bandwidth (734.94, 439.27 and 351.49) MHz. Finally, after making the third iteration it is observed that there are three resonance frequencies at (2.6, 3.9 and 5.7) GHz with bandwidth (790.38, 236 and 522.43) MHz. From the results of the first band, one can deduce that when increasing the order of the iteration, the bandwidth and matching are improved. The resonance frequency is shifted to a lower value. Figure 4.39 shows the input reflection coefficient at each iteration. As can be seen, it is noticed that the antenna is suitable for C & S bands applications.

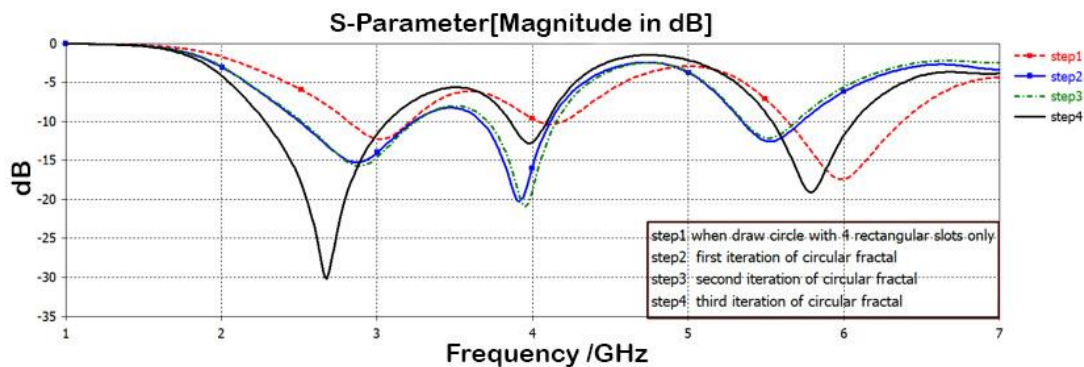


Fig.4.39: The input reflection coefficient of the proposed antenna at each state

4.5.2 The Gain and Directivity of Fractal Shaped Circular Slot Antenna with MS

The simulated results shows that the 3-dimensional values of gain at frequencies of (2.6, 3.9 and 5.7) GHz are (2.42, 4.27 and 6) dB respectively, as shown in figure 4.40.

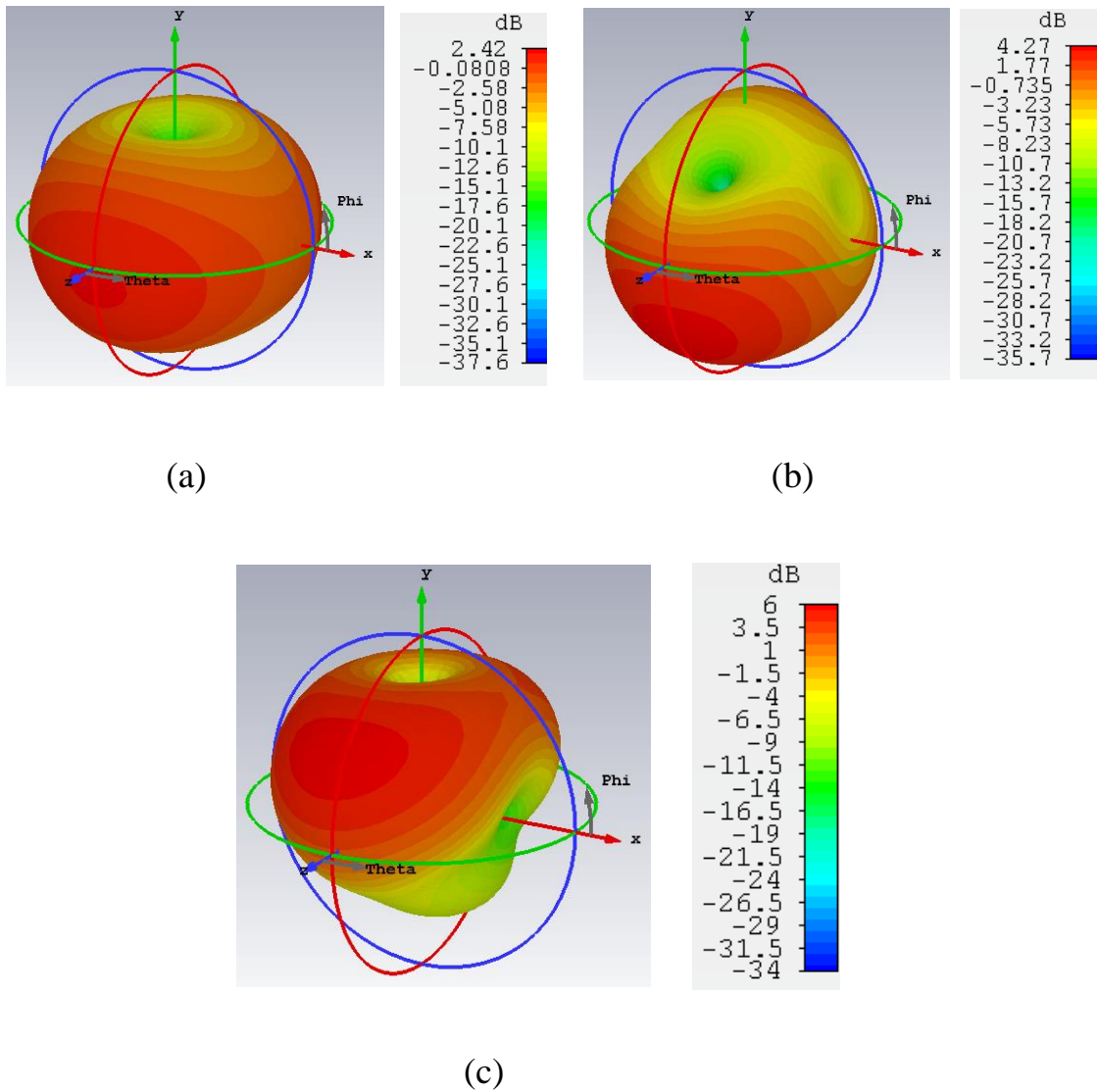


Fig.4.40: The 3D patterns of gain at a (2.6) GHz, b (3.9) GHz c (5.7) GHz

Figure 4.41 shows the 3-dimensional pattern of directivity at three resonances frequencies.

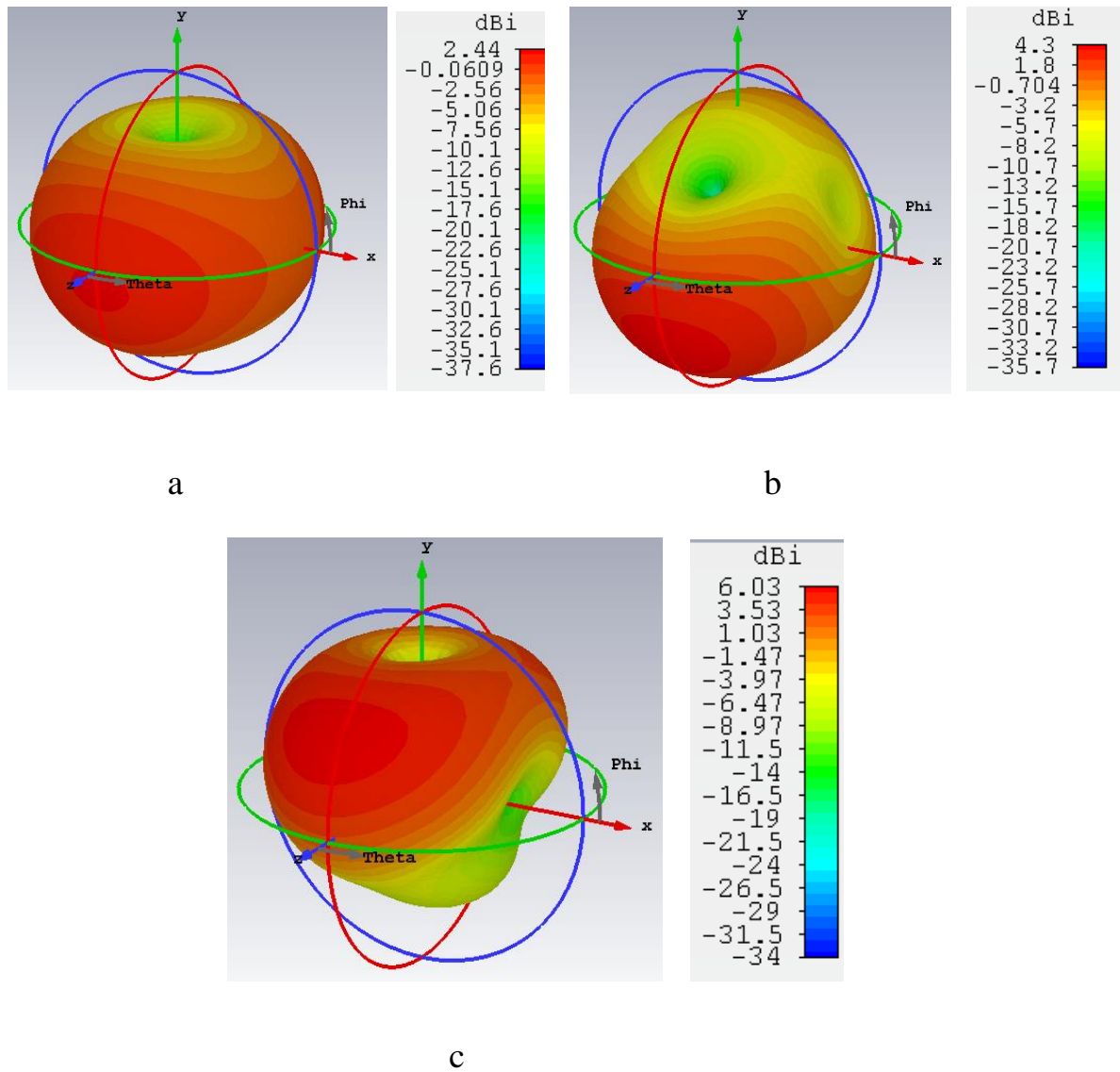


Fig.4.41: The 3D simulated patterns of directivity at a (2.6) GHz b (3.9) GHz c (5.7) GHz

The parametric study of the impacts of the width of the feeding line on the antenna performance is investigated. The simulated results shows that the antenna has three bands at the range of frequencies from (1 to 7) GHz as shown in figure 4.42. At various values, it is observed that the lower width of the feeding line has achieved narrower bandwidth and lower response, while the higher-values have realized wider bandwidth.

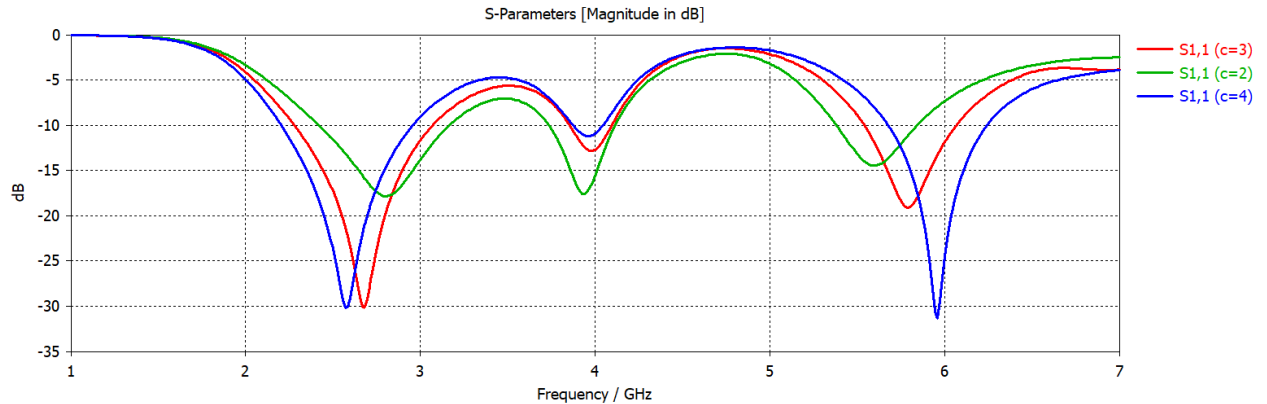


Fig.4.42: The input reflection coefficient for different widths of the feeding line

The value of the thickness of a substrate layer was also studied at (1.2, 1.4 and 1.6) mm. The results shows that the smaller thickness offers dual-band. The higher values of the thickness provide triple bands with similar values of bandwidth and some different in the response. Figure 4.43 displays the reflection coefficient for each state.

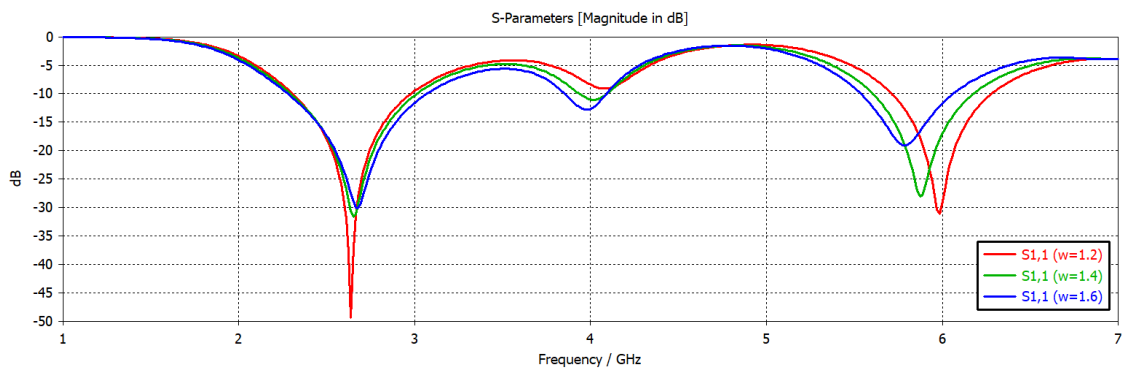
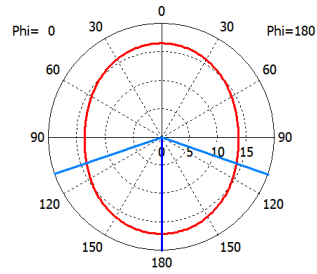
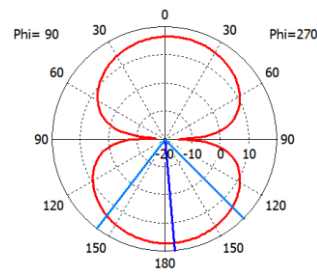


Fig.4.43: The input reflection coefficient at each thickness

Figure 4.44 shows the 2D radiation patterns of the proposed antenna at the center frequencies.

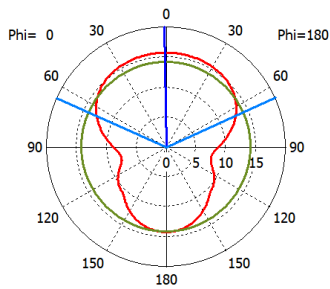


(x-z) plane

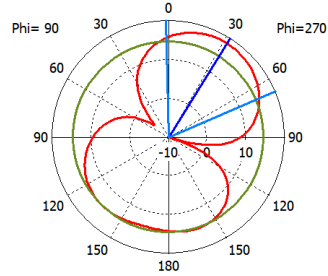


(y-z) plane

a

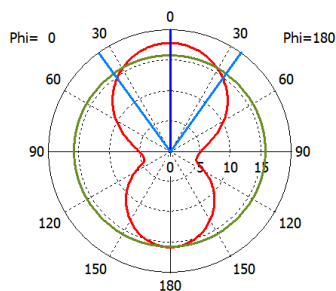


(x-z) plane

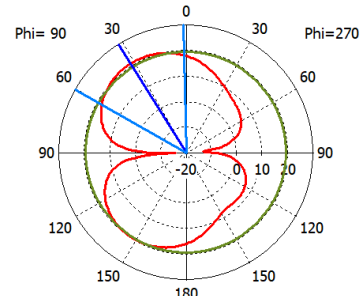


(y-z) plane

b



(x-z) plane



(y-z) plane

c

Fig.4.44: The 2D radiation patterns of the proposed antenna at a (2.6) GHz b (3.9) GHz c (5.7) GHz

Figure 4.45 offers the simulated current distribution at each resonance frequency of the proposed antenna.

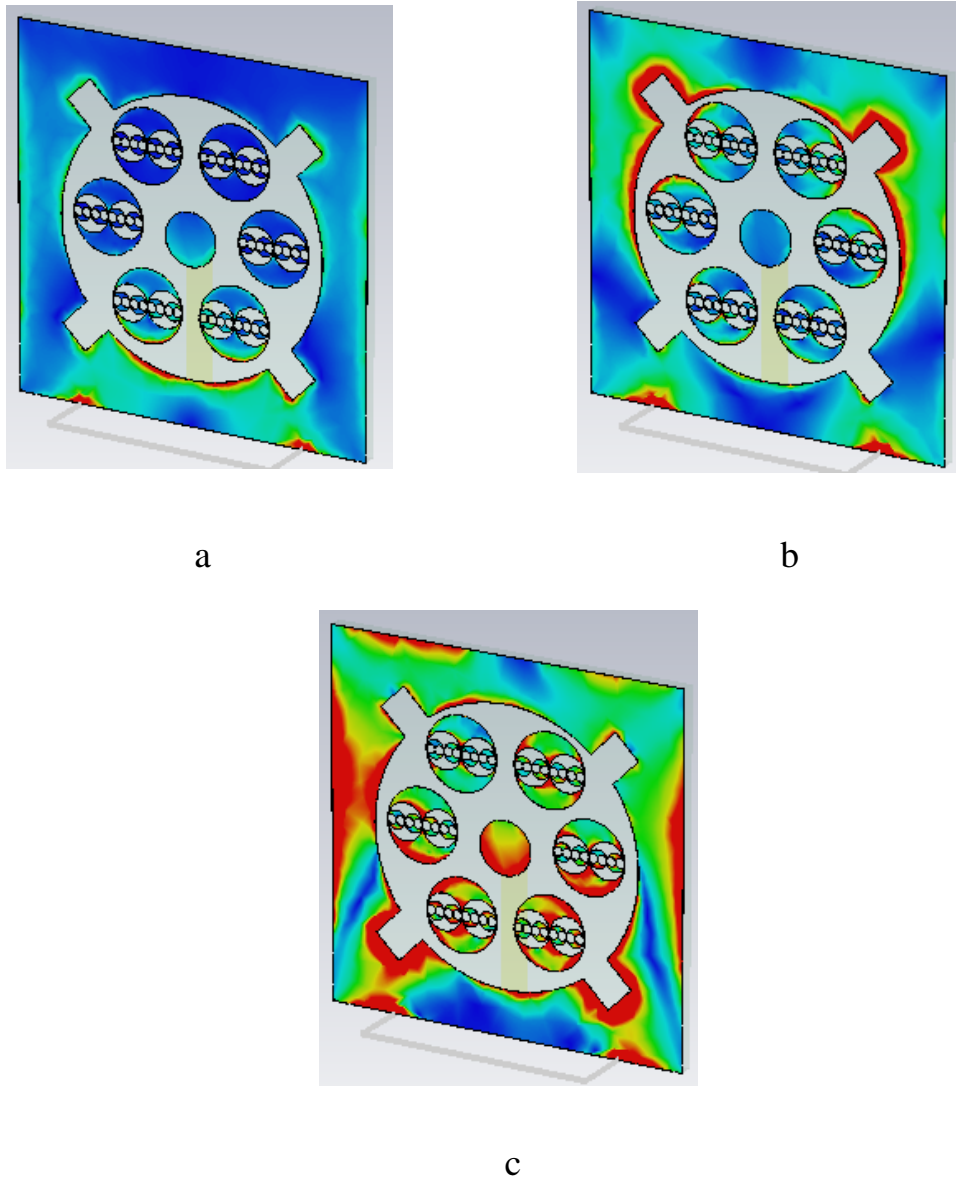


Fig.4.45: The current distribution for each frequency a (2.6) GHz b (3.9) GHz c (5.7) GHz

Table-4.4: The comparison between (MCMCSFMS) and other References

No.	Gain(dB)	Bandwidth
MCMCSFMS	6	Three bands
Ref [4]	3.5	Wide band
Ref [19]	4.5	Dual bands
Ref [22]	3.6	Wide band

Table 4.5 highlights the most prominent results that were obtained through the to show which proposed antenna design can offer the best results. The modified cross shape fractal antenna with MS is the best in the gain enhancement and the Minkowski fractal slot antenna with MS has the widest bandwidth.

Table-4.5: The comparison among all results obtained from the proposed designs

The Design Name	Center frequency(GHz)	Gain (dB)	Directivity(dB)	BW(MHz)
CFSAMS Without MS	11.18	4.55	5.76	190
CFSAMS WithMS	11.14 12.3	7.6 8	8 dB 8.6 dB	400 300
MCFAMS Without MS	8.77	2.66	2.7	190
MCFAMS With MS	8.9	9	9.04	414.35
MFSAMS Without MS	5.1	3.32	3.4	969.1

MFSAMS With MS	5.2	4.89	4.9	1,670
MFSAMS With double layers of MS	4.7	6	6.02	1224.5
MCMCSFMS	2.6	2.42	2.44	790.38
	3.9	4.27	4.3	236
	5.7	6	6.03	522.43

CHAPTER FIVE

CONCLUSIONS AND FUTURE WORKS

5.1 Conclusion

During the study of metasurface and fractal antennas following conclusions were obtained:

There are four models of metasurface which are designed and simulated with three different shapes of the fractal antenna. The main characteristic of these models is achieving negative (permittivity, permeability and refractive index). These designs vary in the magnitudes of permittivity, and permeability, number of bands, the frequencies that cover. Also, the unit element is modeled and simulated with three fractal forms: Circular fractal, modified cross, and Minkowski slot with double rectangular closed ring resonator of MS.

The circular fractal shape offered multiband behavior while the modified cross fractal antenna achieved fractional bandwidth which is 4.655% and Minkowski fractal slot antenna is offered wideband behavior and compact circular fractal shape with MS achieved three bands. The simulated results display that the fractal form of the unit cell provided the capability to have a negative value of refraction index for a high range of frequencies. Generally, the MS has enhanced the gain of the proposed antennas. A large number of attempts were used to obtain the best-separated distance between the MS and radiated elements. When used two layers of MS achieved more enhancement in the gain but this case has one drawback that is increasing the antenna size.

The circular fractal shape has two resonance frequencies and enhancement of the gain and bandwidth in two bands is a challenge so to overcome it is using the

fractal geometry with (5×5) unit cells of the metasurface. Below is a detailed illustration of the improvements obtained in gain and bandwidth:

The circular fractal slot antenna with MS has improved the gain from the 4.55 dB at 11.18 GHz to 7.6 dB at 11.14 GHz and the gain of the second band is 8 dB at 12.3 GHz after adding the MS layer. The bandwidth is improved from 190 MHz at 11.18 GHz to 400 MHz at 11.14 GHz and the bandwidth at the second band is 300 MHz at 12.3 GHz after studying three cases of the proposed antenna before and after adding MS and used a different number of unit cells to find the best enhancement at (5×5) unit cells. Also studied the air separated gap between the radiating element and the MS and found the lower distance is the best.

The modified cross fractal antenna with MS has enhanced the gain from 2.66 dB at 8.7 GHz to 9 dB at 8.9 GHz. The gain is increased by approximately 6 dB when adding MS. While the bandwidth is 190 MHz before adding MS and improved to 414.35 MHz so the fractional bandwidth is 4.655%. The matching is also improved from (-24 to -37) dB when adding MS. The parametric study investigated to study the effect of varying distance between cells at three cases from (0.1 to 0.3) mm and followed the results at each case and observed the distance 0.3 mm have best results in a gain.

The wideband Minkowski fractal slot antenna with MS has also enhanced the gain from 3.32 dB at 5.1 GHz to 4.89 dB at 5.2 GHz when used one layer of the double rectangular closed ring resonator. An additional layer of MS is used and enhanced the gain to 6 dB at 4.7 GHz. The bandwidth is also improved when adding MS where the bandwidth is increased from 969.1 MHz at 5.1 GHz to 1670 MHz at 5.25 GHz. The magnitude of improvement in the value of the gain is 2.7 dB and the bandwidth is improved by 32.11% so the antenna is suitable for wideband applications.

The compact circular fractal shape with MS offered three bands for C & S band applications. The achieved gain is (2.42, 4.27, 6) dB at (2.6, 3.9, 5.7) GHz respectively. This antenna has an efficiency above 90% and good performance with compact size. The parametric study was implemented to choose the best value of the thickness of the dielectric layer and the width of the feed line.

From the previous results obtained, it can be concluded that cells in fractal types with MS are more effective in gain enhancement and miniaturization.

5.2 Future Works

- 1- It is possible to study the addition of more than two layers of metasurface and the effect of this on improving the antenna gain.
- 2- The proposed designs can be studied at optical and terahertz frequencies.
- 3- It is possible to study the design of other forms of fractal shapes which may add another feature to the design.
- 4- It is possible to manufacture the mentioned models.
- 5- Mathematical analysis can be studied for the MS plate.

REFERENCES

- [1] C. A. Balanis, *Antenna theory: analysis and design*. John Wiley & sons, 2016.
- [2] A. N. Shareef, "Simulation of Fractal Antenna Properties Composed of Metamaterials," no. May, pp. 1–222, 2015.
- [3] G. M. Hatem, "Wearable RFID Textile Antenna Design," no. October, 2014.
- [4] M. Rahimi, M. Maleki, M. Soltani, A. S. Arezomand, and F. B. Zarrabi, "Wide band SRR-inspired slot antenna with circular polarization for wireless application," *AEU-International J. Electron. Commun.*, vol. 70, no. 9, pp. 1199–1204, 2016.
- [5] D. H. Werner and D. H. Kwon, *Transformation electromagnetics and metamaterials: Fundamental principles and applications*, vol. 9781447149965. 2014.
- [6] F. Capasso and N. Yu, "Flat optics with designer metasurfaces," *Nature Materials*, vol. 13. pp. 139–150, 2014.
- [7] F. Falcone et al., "Babinet principle applied to the design of metasurfaces and metamaterials," *Phys. Rev. Lett.*, vol. 93, no. 19, pp. 2–5, 2004.
- [8] K. Konstantinidis, "Multi-Layer Periodic Surfaces and Metasurfaces for High-Gain Antennas," no. May, 2015.
- [9] X. Li, J. Yang, Z. Chen, P. Ren, and M. Huang, "Design and Characterization of a Miniaturized Antenna Based on Palisade-Shaped Metasurface," *Int. J. Antennas Propag.*, vol. 2018, 2018.
- [10] Crnojevic-Bengin, Vesna, Vasa Radonic, and Branka Jokanovic. "Fractal geometries of complementary split-ring resonators." *IEEE Transactions on Microwave Theory and Techniques* 56.10 (2008): 2312-2321
- [11] Yahiaoui, Riad, et al. "Metasurfaces: characterization and application as

Partially Reflecting Surfaces for directivity enhancement of patch antennas." META'12-3rd International Conference on Metamaterials, Photonic crystals and Plasmonics. 2012.

[12] H. X. Xu, G. M. Wang, M. Q. Qi, L. Li, and T. J. Cui, "Three-Dimensional Super Lens Composed of Fractal Left-Handed Materials," *Adv. Opt. Mater.*, vol. 1, no. 7, pp. 495–502, 2013.

[13] Y. Li, L. Li, Y. Zhang, and C. Zhao, "Design and synthesis of multilayer frequency selective surface based on antenna-filter-antenna using minkowski fractal structures," *IEEE Trans. Antennas Propag.*, vol. 63, no. 1, pp. 133–141, 2013.

[14] H. X. Xu, G. M. Wang, J. G. Liang, M. Q. Qi, and X. Gao, "Compact circularly polarized antennas combining meta-surfaces and strong space-filling meta-resonators," *IEEE Trans. Antennas Propag.*, vol. 61, no. 7, pp. 3442–3450, 2013.

[15] T. Hongnara, S. Chaimool, and P. Akkaraekthalin, "Metasurface characteristic of fractal fishnet structure and closed ring resonator," *Proc. 20th Asia-Pacific Conf. Commun. APCC 2014*, pp. 429–433, 2015.

[16] T. Cai, G. M. Wang, J. F. Zhao, and M. Yao, "Two-dimensional fractal metasurface and its application to low profile circularly polarized antennas," *J. Electromagn. Waves Appl.*, vol. 29, no. 3, pp. 410–423, 2015.

[17] T. Hongnara, S. Chaimool, and P. Akkaraekthalin, "Anisotropic fractal metasurface-based antenna with contrary beams," *Microw. Opt. Technol. Lett.*, vol. 59, no. 3, pp. 715–720, 2016.

[18] R. Kubacki, S. Lamari, M. Czyzewski, and D. Laskowski, "A Broadband Left-Handed Metamaterial Microstrip Antenna with Double-Fractal Layers," *Int. J. Antennas Propag.*, vol. 2017, 2017.

- [19] G. Varamini, A. Keshtkar, N. Daryasafar, and M. Naser-Moghadasi, "Microstrip Sierpinski fractal carpet for slot antenna with metamaterial loads for dual-band wireless application," *AEU - Int. J. Electron. Commun.*, vol. 84, no. November 2018
- [20] J. Su, Y. Cui, Z. Li, Y. Yang, Y. Che, and H. Yin, "Metasurface base on uneven layered fractal elements for ultra-wideband RCS reduction," *AIP Adv.*, vol. 8, no. 3, 2018.
- [21] M. R. I. Faruque, M. M. Hasan, and M. T. Islam, "Tree-shaped fractal metasurface with left-handed characteristics for absorption application," *Appl. Phys. A Mater. Sci. Process.*, vol. 124, no. 2, p. 0, 2018.
- [22] M. A. Rad, M. R. Soheilifar, and F. B. Zarrabi, "Compact microstrip antenna based on fractal metasurface with low radar cross section and wide bandwidth," *AEU - Int. J. Electron. Commun.*, vol. 98, pp. 74–79, 2018.
- [23] D. Samantaray, S. Bhattacharyya, and K. V. Srinivas, "A modified fractal-shaped slotted patch antenna with defected ground using metasurface for dual band applications," *Int. J. RF Microw. Comput. Eng.*, vol. 29, no. 12, pp. 1–9, 2019.
- [24] P. Iyampalam and I. Ganesan, "Low profile antenna based on a fractal shaped metasurface for public safety applications," *Int. J. RF Microw. Comput. Eng.*, vol. 30, no. 2, pp. 1–12, 2019.
- [25] S. J. Li et al., "Multifunctional and Multiband Fractal Metasurface Based on Inter-Metamolecular Coupling Interaction," *Adv. Theory Simulations*, vol. 2, no. 8, p. 1900105, 2019.
- [26] Costanzo, Sandra, and Francesca Venneri. "Polarization-Insensitive Fractal Metamaterial Surface for Energy Harvesting in IoT Applications." *Electronics* 9.6 (2020)

- [27] B. B. Mandelbrot, *The fractal geometry of nature*, vol. 173. WH freeman New York, 1983.
- [28] P. Gupta and J. P. S. Raina, "Miniaturization of Antenna Using Fractals," *Fractals An Interdiscip. J. Complex Geom. Nat.*, vol. 1, no. 2, pp. 437–440, 2010.
- [29] D. Sornette, *Critical phenomena in natural sciences: chaos, fractals, selforganization and disorder: concepts and tools*. Springer Science & Business Media, 2006.
- [30] K. Falconer, *Fractal geometry: mathematical foundations and applications*. John Wiley & Sons, 2004.
- [31] G. Khanna and N. Sharma, "Fractal antenna geometries: A review," *Int. J. Comput. Appl.*, vol. 153, no. 7, 2016.
- [32] Ye, Xiu Bin, Guo Peng Kou, and Yi Juan Ji. "The Design of Ceramic Minkowski Fractal Antenna." *Advanced Materials Research*. Vol. 1006. Trans Tech Publications Ltd, 2014.
- [33] Ali, Jawad K., and Seevan F. Abdulkareem. "A circle-based fractal slot antenna for dual-band wireless applications." *13th IEEE Mediterranean Microwave Symposium, MMS*. Vol. 13. 2013.
- [34] S. Heydari, I. Rastan, A. Parvin, A. Pirooj, and F. B. Zarrabi, "Investigation of novel fractal shape of the nano-aperture as a metasurface for bio sensing application," *Phys. Lett. A*, vol. 381, no. 3, pp. 140–144, 2017.
- [35] R. Marqués, F. Martin, and M. Sorolla, *Metamaterials with negative parameters: theory, design, and microwave applications*, vol. 183. John Wiley & Sons, 2011.

- [36] L. Solymar and E. Shamonina, *Waves in metamaterials*. Oxford University Press, 2009.
- [37] V. G. Veselago, “Electrodynamics of substances with simultaneously negative and,” *Usp. Fiz. Nauk*, vol. 92, p. 517, 1967.
- [38] J. B. Pendry, A. J. Holden, D. J. Robbins, and W. J. Stewart, “Low frequency plasmons in thin-wire structures,” *J. Phys. Condens. Matter*, vol. 10, no. 22, p. 4785, 1998.
- [39] J. B. Pendry, A. J. Holden, D. J. Robbins, and W. J. Stewart, “Magnetism from conductors and enhanced nonlinear phenomena,” *IEEE Trans. Microw. Theory Tech.*, vol. 47, no. 11, pp. 2075–2084, 1999.
- [40] D. R. Smith, W. J. Padilla, D. C. Vier, S. C. Nemat-Nasser, and S. Schultz, “Composite medium with simultaneously negative permeability and permittivity,” *Phys. Rev. Lett.*, vol. 84, no. 18, p. 4184, 2000.
- [41] S. Tretyakov, P. Barois, T. Scharf, V. Kruglay, and I. Bergmair, *Nanostructured Metamaterials*. 2010.
- [42] X. Chen, T. M. Grzegorzcyk, B.-I. Wu, J. Pacheco Jr, and J. A. Kong, “Robust method to retrieve the constitutive effective parameters of metamaterials,” *Phys. Rev. E*, vol. 70, no. 1, p. 16608, 2004.
- [43] N. Engheta and R. W. Ziolkowski, *Metamaterials: physics and engineering explorations*. John Wiley & Sons, 2006.
- [44] J. B. Pendry, “Negative refraction makes a perfect lens,” *Phys. Rev. Lett.*, vol. 85, no. 18, p. 3966, 2000.
- [45] S. A. Ramakrishna and T. M. Grzegorzcyk, *Physics and applications of negative refractive index materials*. CRC press, 2008.

- [46] R. W. Ziolkowski and E. Heyman, "Wave propagation in media having negative permittivity and permeability," *Phys. Rev. E*, vol. 64, no. 5, p. 56625, 2001.
- [47] D. R. Smith, W. J. Padilla, D. C. Vier, S. C. Nemat-Nasser, and S. Schultz, "Composite Medium with Simultaneously Negative Permeability and Permittivity", *Phys. Rev. Lett.* 84, pp. 4184-4187 (2000).
- [48] J. B. Pendry, "Negative refraction," *Contemp. Phys.*, vol. 45, no. 3, pp. 191–202, 2004.
- [49] S. A. Ramakrishna and T. M. Grzegorzczak, *Physics and applications of negative refractive index materials*. CRC press, 2008.
- [50] B. A. Munk, *Metamaterials: critique and alternatives*. John Wiley & Sons, 2009.
- [51] X. Chen, T. M. Grzegorzczak, B.-I. Wu, J. Pacheco Jr, and J. A. Kong, "Robust method to retrieve the constitutive effective parameters of metamaterials," *Phys. Rev. E*, vol. 70, no. 1, p. 16608, 2004.
- [52] A. B. Numan and M. S. Sharawi, "Extraction of material parameters for metamaterials using a full-wave simulator [education column]," *IEEE Antennas Propag. Mag.*, vol. 55, no. 5, pp. 202–211, 2013.
- [53] I. Park, "Application of metasurfaces in the design of performance-enhanced low-profile antennas," *EPJ Appl. Metamaterials*, vol. 5, p. 11, 2018.
- [54] H. L. Zhu, S. W. Cheung, X. H. Liu, and T. I. Yuk, "Design of polarization reconfigurable antenna using metasurface," *IEEE Trans. Antennas Propag.*, vol. 62, no. 6, pp. 2891–2898, 2014.
- [55] CST MWS - CST Studio Suite 3D EM simulation Software Version:
2018

Appendix

(A-1) Antenna Parameters

(A.1.1) Reflection coefficients

S-parameters represent the relationship between input-output ports in the electrical system. S_{AB} performs the power transport from Port B to Port A in the multi-port system. A port is known as any area can transfer current and voltage. Generally, S-parameters are varying with frequency so it is the function of frequency. In action, the S_{11} parameter is the most commonly used for antennas. It means that if $S_{11}=0$ dB, no radiated power in this case and all power are reflected. If ($S_{11}=-10$ dB) means that if 3dB of energy is applied to the antenna, so -7 dB is a reflected power. The residuum of the power is "acceptable," or delivered to an antenna. The acceptable power is either radiated power or absorbed losses inside the antenna. ideally, the antenna is preferably radiated with a majority of the power supplied [A1].

(A.1.2) Gain

Gain is a parameter that is very critical and associated with the directivity. The tendency of an antenna to focus energy in a certain direction in comparison to other directions is understood. When an antenna has an ideal efficiency (100%), the gain and directive are equal, but only for isotropic antennas [A2]. As all antennas are radiated more in one direction than in the other, again is a measure of an antenna's capability to transform the input power into radiating energy in a particular direction, the gain is also known as “the amount of the energy that transported in the direction of top radiation in comparison of the isotropic source” [A3][A4].

Omni antennas typically radiate with a gain of 2.1 dB over an isotropic antenna. For a vertically oriented omni antenna, this gain in transmission horizontal distance from the antenna is at the expense of transmission above and below it [A5].

Directional antennas can be configured with gains up to more than 20 dB. These carve a significant part out of the omnidirectional pattern of an omni antenna and can significantly extend its projection distance. A disadvantage of extreme gain antennas is that they can be very sensitive to improper position displacement due to wind conditions. There are a variety of configurations that can result in good directional RF signal transmission, including Yagi antennas, dish antennas, Luneberg lenses, and phased arrays[A5].

The mathematical formula for gain is as follows:

$$G = \frac{4\pi U}{p_{in}} \quad (\text{A.1}), \text{ dimensionless}$$

$$P_{in}: \text{ input power, or } G = ecd D \quad (\text{A.2})$$

G: Gain ecd: The efficiency D: Directivity

(A.1.3) Directivity

The antenna directivity can be defined as "the ratio of transferred radiation intensity into the specific direction from the antenna to the radiation intensity averaged in all directions [A3].

$$D = \frac{U}{U_i} = \frac{4\pi U}{Prad}; \quad (\text{A.3})$$

D = directivity

U= radiation intensity

U_i= radiation intensity of isotropic antenna

Prad=total power radiated

(A.1.4) Radiation pattern

One of the essential characteristics of antennas is the pattern of radiation. It can be defined as the "the graphic exemplification of the antenna radiation field as space coordinate function", or it can be defined as a 3diementioal-Plot that displays a spatial coordinate distribution of the real electromagnetic field intensity [A3]. The divergence over an antenna-centric sphere with a fixed radius (r) is the radiation pattern, and there are only two components differences are θ and φ .

(A.1.5) Efficiency

The radiation efficiency of the antenna can be obtained by the ratio of the gain to the directivity and can be determined by equation (A.4):

$$E = \frac{G}{D} \times 100\% \quad (\text{A.4})$$

When most of the input energy is radiate, an antenna has a high output efficiency, when the most power of the antenna is dispensed because of a difference or absorbed as loss so the antenna has small efficiency.

(A.1.6) Bandwidth

Describes the frequency range in which the antenna can work properly. Often one of the decision criteria for evaluating an antenna is the desired bandwidth. You can find a BW of an antenna by calculating S11. The BW is the range of frequency at which $S_{11} < -10$ dB.

The BW is often given according to its FBW (Fractional Bandwidth). The FBW is the ratio of the value of BW is divided on the resonance frequency [A3].

(A.1.7) VSWR

The VSWR stands for (voltage standing wave ratio) which shows how much power is reflected from the antenna. It is a function of the reflection coefficient. The VSWR is defined by the following formula[A6]:

$$\text{VSWR} = \frac{1+\Gamma}{1-\Gamma} \quad (\text{A.5})$$

The input reflection coefficient is also known as S11 or return loss.

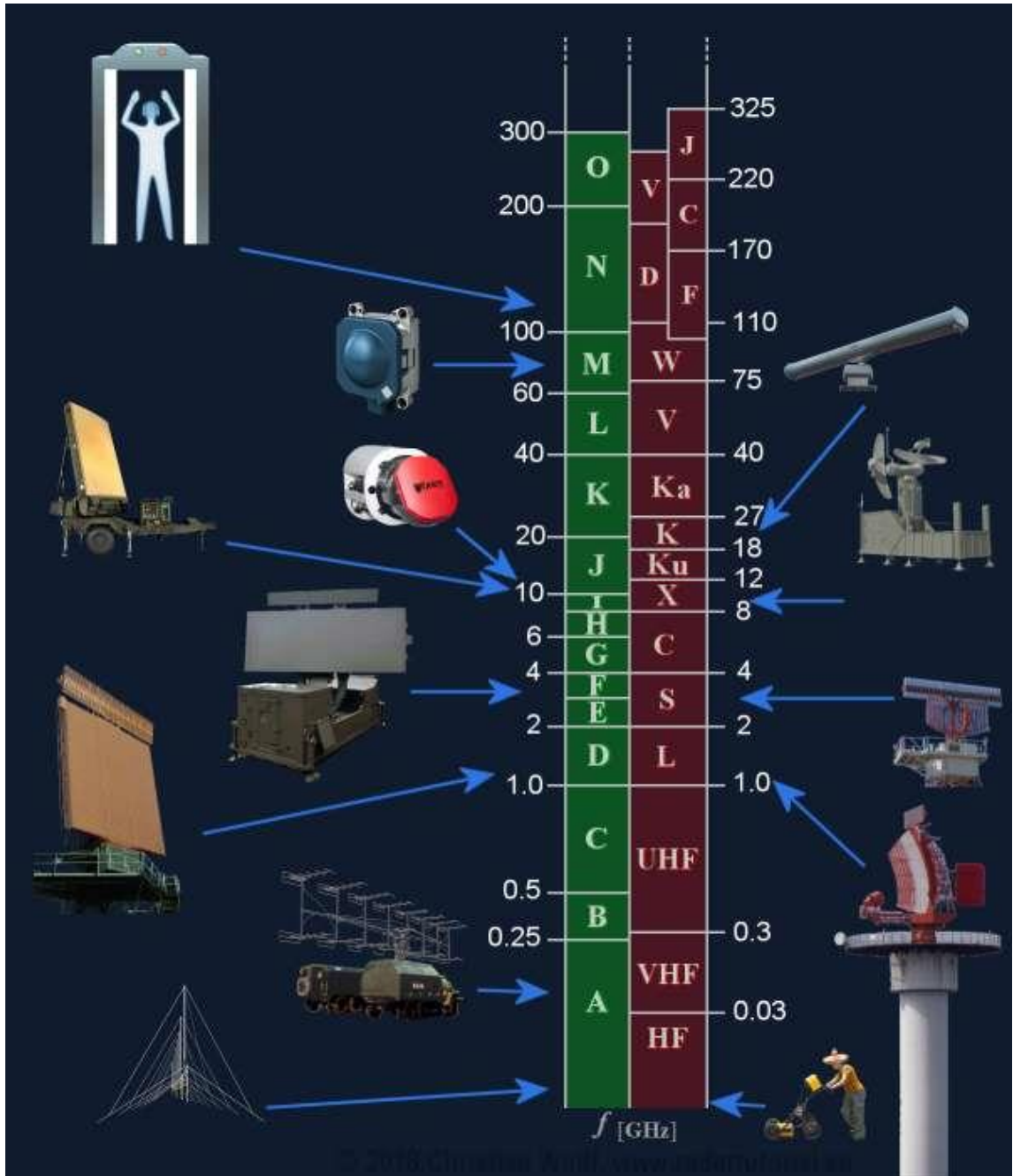


Fig. (A.1): The frequency bands with some applications

References

- [A1] Stutzman, Warren L., and Gary A. Thiele. Antenna theory and design. John Wiley & Sons, 2012.
- [A2] Visser, Hubregt J. Antenna theory and applications. John Wiley & Sons, 2012.
- [A3] Ren, Yu-Jiun, and Chieh-Ping Lai. "Wideband antennas for modern radar systems." Radar Technology (2010).
- [A4] Bansal, Rajeev. Fundamentals of engineering electromagnetics. CRC press, 2018.
- [A5] Norman, Thomas L. Integrated Security Systems Design: A Complete Reference for Building Enterprise-wide Digital Security Systems. Butterworth-Heinemann, 2014.
- [A6] Zakariyya, Sikiru Olayinka. Modeling of Miniaturized, Multiband and Ultra-Wideband Fractal Antenna. MS thesis. Eastern Mediterranean University (EMU)-Doğu Akdeniz Üniversitesi (DAÜ), 2015.

List of Publications

1- Noor Fadhel Habib, Ahmed Ghanim Wadday, and Faris Mohammed Ali. "Design Multiband Compact Microstrip Circular Slot Fractal Meta-Surface Antenna." *Al-Furat Journal of Innovations in Electronics and Computer Engineering*, <https://dx.doi.org/10.46649/110420-04>.

2- "Circular Fractal Slot Antenna with Metasurface for Satellite Communications " Has been accepted in the 8th International Conference of Applied Science and Technology ICAST 2020 Conference Proceeding. The accepted manuscripts will be published in the AIP conference proceedings which is Scopus indexed and have an impact factor.

3- "Design of Modified Cross Fractal Shape with metasurface Antenna for Satellite Communications".

Under review in *Nano Hybrids and Composites (NHC)* which is Clarivate indexed.

الخلاصة

الميتاسيرفس هو نوع ثنائي الأبعاد من الميتامتيريال التي تم إنشاؤها من الهياكل الدورية ولكنها أخف وزناً. قدمت الميتاسيرفس خصائص استثنائية مثل معامل الانكسار السالب الناتج عن مزج النفاذية السلبية والسماحية السلبية عند نفس التردد. المواد بهذه الخصائص غير موجودة في الطبيعة ولكن يمكن هندستها صناعياً.

في هذه الرسالة، تم تصميم أربعة أشكال كسورية مع طبقة الميتاسيرفس وثلاثة تصاميم لوحات الخلية وحساب معلماتها باستخدام برنامج المحاكاة الكهرومغناطيسية CST Microwave Studio . وقد أظهرت هذه التصاميم سلوكاً مشابهاً لسلوك المواد اليسارية.

تضمن دراسة تأثير خلايا الوحدة للميتاسيرفس والتقنية الكسورية في ثلاثة جوانب هي تحسين معامل الكسب، زيادة عرض النطاق الترددي وتقليل حجم الهوائي. غطاء الميتاسيرفس المتكون من خلايا كسورية الشكل تم وضعه فوق التصاميم المقترحة. التصميم الأول هو الشكل الكسوري الدائري مع لوحة الميتاسيرفس حيث بينت النتائج ان للهوائي ترددين للرنين وتحسين عامل الكسب حيث وصل الى ٨ ديسيبل وتحسين عرض النطاق الترددي بمقدار ٣,٥٩%. التصميم الثاني هو الكروس الكسوري المعدل مع لوحة الميتاسيرفس حيث تم تحسين معامل الكسب ب مقدار ٦ ديسيبل وتحسين عرض النطاق الترددي بنسبة ٤,٦٥٥%. التصميم الثالث هو حفر مانكاوسكي كسوري على رقعة الهوائي ويوفر تحسناً جيداً في عرض النطاق الترددي بنسبة ٣٢,١١% وتحسين معامل الكسب بمقدار ٣ ديسيبل تقريباً. التصميم الرابع يتكون من شكل دائري كسوري محفور على الطبقة الارضية للهوائي وحقق ٣ ترددات رنين مع معامل كسب ٦ ديسيبل بحجم مضغوط. وأخيراً، يقدم هذا العمل حلاً جديداً مثيراً للاهتمام للهوائيات المستوية منخفضة التكلفة ذات الكسب المرتفع وهو بسيط جداً مقارنة بالمصفوفات (array) لأسباب عديدة مثل مطابقة العناصر، تعقيد دائرة التغذية، المساحة الكبيرة والكلفة العالية.



جمهورية العراق
وزارة التعليم العالي والبحث العلمي
جامعة الفرات الأوسط التقنية
الكلية التقنية الهندسية - نجف

تحسين الهوائيات المطبوعة باستخدام الميٹاسرفس الكسورية

رسالة مقدمة الى

قسم هندسة تقنيات الاتصالات

كجزء من متطلبات نيل درجة ماجستير تقني في هندسة الاتصالات

تقدمت بها

نور فاضل حبيب

بكالوريوس في هندسة تقنيات الاتصالات

إشراف

الأستاذ المساعد الدكتور أحمد غانم وداي

أيلول ٢٠٢٠